İSTANBUL TECHNICAL UNIVERSITY ★ INSTITUTE OF SCIENCE AND TECHNOLOGY

MICRO-ARC OXIDATION OF COMMERCIALLY PURE TITANIUM FOR DENTAL APPLICATIONS

M.Sc. Thesis by
Cemil IŞIKSAÇAN

Department : Advanced Technologies in Engineering

Programme : Materials Science and Engineering

JANUARY 2009

İSTANBUL TECHNICAL UNIVERSITY ★ INSTITUTE OF SCIENCE AND TECHNOLOGY

MICRO-ARC OXIDATION OF COMMERCIALLY PURE TITANIUM FOR DENTAL APPLICATIONS

M.Sc. Thesis by
Cemil IŞIKSAÇAN
(521061017)

Date of Submission : 29 December 2008
Date of Defence Examination : 23 January 2009

Supervisor (Chairman): Prof. Dr. Hüseyin ÇİMENOĞLU
Members of the Examining Committe: Prof. Dr. E. Sabri KAYALI (İTÜ)
Assoc. Prof. Dr. Hakan BERMEK (İTÜ)

JANUARY 2009

İSTANBUL TEKNİK ÜNİVERSİTESİ ★ FEN BİLİMLERİ ENSTİTÜSÜ

DENTAL UYGULAMALARDA KULLANILAN TİCARİ SAFLIKTAKİ TİTANYUMUN MİKRO-ARK OKSİDASYON İŞLEMİ

YÜKSEK LİSANS TEZİ
Cemil IŞIKSAÇAN
(521061017)

Tezin Enstitüye Verildiği Tarih : 29 Aralık 2008
Tezin Savunulduğu Tarih : 23 Ocak 2009

Tez Danışmanı : Prof. Dr. Hüseyin ÇİMENOĞLU
Diğer Jüri Üyeleri : Prof. Dr. E. Sabri KAYALI (İTÜ)
Doç. Dr. Hakan BERMEK (İTÜ)

OCAK 2009

FOREWORD

I wish to thank to my supervisor Prof. Dr. Hüseyin ÇİMENOĞLU, whose suggestions, guidance and encouragement helped me in the carrying out and writing of this thesis. I would also like to thank to Prof. Dr. Eyüp Sabri KAYALI, Asst. Prof. Dr. Murat BAYDOĞAN and Assoc. Prof. Dr. Hakan BERMEK for their precious guidance and elaborate critics on my experimental work. I am also indebted to Research Asst. Mert GÜNYÜZ, Research Asst. Özgür ÇELİK, Research Asst. Onur MEYDANOĞLU and my colleague, İsa Metin ÖZKARA for their supportive attitude and courteous help.

I thank to TUBITAK (The Scientific and Technological Research Council of Turkey) for the scholarship, with which they supported me financially during my studies.

I would also like to express my deep thanks to Özge ÖZDEMİR for her continuous support and invaluable friendship.

And last but not least, thanks to my family, who backed me up under any circumstances for all my life.

January 2009

Cemil IŞIKSAÇAN

Metallurgical Engineer

TABLE OF CONTENTS

Page

ABBREVIATIONS

HA	**:** Hydroxyapatite
MAO	**:** Micro-arc Oxidation
UV	**:** Ultra Violet
CP	**:** Commercially Pure
PEO	**:** Plasma Electrolytic Oxidation
MPO	**:** Micro Plasma Oxidation
ASD	**:** Anodic Spark Deposition
TCP	**:** Tricalcium Phosphate
TTCP	**:** Tetracalcium Phosphate
ACP	**:** Amorphous Calcium Phosphate
CVD	**:** Chemical Vapor Deposition
PVD	: Physical Vapor Deposition
PBS	**:** Phosphate Buffered Saline Solution
HBSS	**:** Hank's Balanced Salt Solution
SBF	**:** Simulated Body Fluid
ALP	**:** Alkaline Phosphatase Activity
CA	**:** Calcium Acetate
GP	**:** Glycerophosphate Disodium Salt Pentahydrate
CHA	**:** Carbonated Hydroxyapatite
SSD	**:** Silver Sulfadiazine
CFU	**:** Colony Forming Unit

LIST OF TABLES

Page

LIST OF FIGURES

Page

MICRO-ARC OXIDATION OF COMMERCIALLY PURE TITANIUM FOR DENTAL APPLICATIONS

SUMMARY

Titanium and its alloys are preferred materials for biomedical applications due to their high mechanical properties, excellent corrosion resistance, low density and biocompatibility. However, titanium is a bio-inert material because of the protective, thin oxide layer present on it and can not make a connection with the bone in short periods after the implantation. For this reason, a bio-active surface layer such as hydroxyapatite has to be produced on titanium. One of the techniques performed for obtaining a bio-active surface layer is micro-arc oxidation (MAO) process, which is a new-developing and promising technique. MAO, performed in calcium and phosphorus containing electrolytes, leads to a porous, rough and strongly adhesive oxide layer on titanium. As a result, mechanical and biological bonding ability of titanium with the bone increases, due to the enhanced average surface roughness and incorporation of Ca and P into the oxide layer. But, especially for pure titanium utilized in dental applications, the probability of bacterial infection increases, because of the enhanced surface roughness.

In this study, $AgNO_3$ addition into the electrolyte was performed to investigate its effect on biological and anti-bacterial activity of pure titanium. It was concluded that, $AgNO_3$ addition into the electrolyte provided a remarkable anti-bacterial activity, which developed with increasing process voltage. Also, $AgNO_3$ addition altered the surface morphology of the oxide layer and increased the surface roughness along with wettability.

Oxidized samples were immersed in a simulated body fluid for 30 days. Carbonated hydroxyapatite phases were detected on the sample oxidized without silver nitrate; however there were not any calcium-phosphate phases on the sample oxidized in the presence of silver nitrate. UV irradiation of the oxidized samples was performed in order to shorten the apatite induction time and enhance the bio-activity. In a short period such as 14^{th} day of immersion, calcium phosphate layers were observed to form on both samples. The phases, which were formed on the surface of the sample oxidized in the presence of silver nitrate, were α-$Ca_2P_2O_7$ and β-$Ca_2P_2O_7$.

DENTAL UYGULAMALARDA KULLANILAN TİCARİ SAFLIKTAKİ TİTANYUMUN MİKRO-ARK OKSİDASYON İŞLEMİ

ÖZET

Titanyum ve alaşımları, yüksek mekanik özellikleri, mükemmel korozyon direnci, hafifliği ve biyo-uyumluluğu nedeni ile biyomedikal uygulamalarda tercih edilen bir malzeme grubudur. Fakat titanyum biyo-inert bir malzemedir ve yüzeyindeki koruyucu ince oksit film tabakası sebebiyle implantasyon sonrası kemik doku ile kısa vadede bir bağlanma gerçekleştiremez. Bu nedenle titanyumun yüzeyinde hidroksiapatit (HA) gibi biyo-aktif bir kaplama oluşturulmalıdır. Bunun için kullanılan yöntemlerden biri son yıllarda hızlıca gelişmekte olan mikro-ark oksidasyon (MAO) işlemidir. Kalsiyum ve fosfor içeren çözeltiler içerisinde gerçekleştirilen mikro-ark oksidasyon işlemi sonucunda titanyumun yüzeyinde poroz, oldukça pürüzlü ve altlık malzemeye kuvvetlice yapışan bir oksit tabakası oluşur. İşlem neticesinde artan yüzey pürüzlülüğü ve oksit tabakaya ilave olan Ca, P gibi elementlerden dolayı, titanyumun kemik doku ile mekanik ve biyolojik olarak bağ yapma kabiliyeti artar. Ancak, artan yüzey pürüzlülüğü neticesinde, özellikle dental uygulamalarda kullanılan saf titanyumun yüzeyinde bakteri birikimine bağlı enfeksiyon oluşma riski artar.

Bu çalışmada, mikro-ark oksidasyon işleminin gerçekleştirildiği çözelti içerisine yapılan $AgNO_3$ ilavesinin, saf titanyumun biyolojik ve anti-bakteriyel aktivitesi üzerindeki etkisi araştırılmıştır. Gerçekleştirilen bakteri testleri neticesinde, çözeltiye yapılan gümüş nitrat ilavesinin çok yüksek anti-bakteriyel aktivite sağladığı ve artan işlem voltajı ile anti-bakteriyel aktivitenin arttığı görülmüştür. Ayrıca gümüş nitrat ilavesinin oksit tabakanın yüzey morfolojisini tamamen değiştirdiği ve malzemenin yüzey pürüzlülüğü ile ıslanabilirliğini oldukça arttırdığı gözlemlenmiştir.

Çalışmada ayrıca, gümüş nitratsız ve gümüş nitratlı çözeltiler içerisinde oksitlenen numuneler 30 gün boyunca yapay vücut sıvısı içerisinde bekletilmiştir. X-ışını analizleri neticesinde, gümüşsüz numune yüzeyinde karbona-hidroksiapatit fazları görülse de gümüş nitrat varlığında oksitlenen numune yüzeyinde herhangi bir kalsiyum-fosfat tabakası oluşumu gözlemlenmemiştir. Yapay vücut sıvısı içerisinde apatit oluşum süresini erkene çekmek ve biyo-aktiviteyi artırmak amacıyla gümüş nitratlı ve gümüş nitratsız çözeltiler içerisinde oksitlenen numuneler, işlem sonrasında UV radyasyona maruz bırakılmıştır. Bu numunelerde, yapay vücut sıvısı içerisinde 14. gün gibi kısa bir sürede yüzeyde kalsiyum fosfat tabakaları oluşumu gözlemlenmiştir. Gümüş nitratlı çözeltide oksitlenen numune yüzeyinde oluşan fazların α-$Ca_2P_2O_7$ ve β-$Ca_2P_2O_7$ fazları olduğu tespit edilmiştir.

INTRODUCTION

Titanium and its alloys are preferred metallic materials for implants used in dentistry and orthopedics due to their good mechanical properties, high corrosion resistance and excellent biocompatibility. However, further improvement in bioactivity of titanium surfaces attracts scientific interest to induce direct growth of the bone tissue, and good bone fixation in short time period after implantation. Modifications of metal surfaces are often employed in order to control tissue-titanium interactions. For example, application of hydroxyapatite (HA) coatings on metallic implants offers the possibility of combining the strength of the metals with the bioactivity of the ceramics [1].

Hydroxyapatite ($Ca_{10}(PO_4)_6(OH)_2$) is an important material for bone and tooth implants, not only because its chemical composition is similar to that of bone tissues, but also it chemically bonds to bones [2].

There are lots of reports affirming the positive effects of the HA coatings on implants, such as more rapid and stable fixation of the implant to the bone, stronger bonding between the bone and the implant, increased uniform bone in-growth at the bone/implant interface and decreased release of metal ions from the implant to the body [1]. Using HA, with its osteoconductive properties, can decrease the healing period to about 20 days, and the bone is stimulated to bridge the gap to the implant by the formation of chemical bonding to the HA [3].

Many surface treatment techniques, such as plasma spraying, immersion in physiological fluid, sol-gel method, electrophoretic deposition, cathodic deposition, ion-beam techniques and sputtering techniques have been used to coat HA on the surface of titanium alloys [1].

Micro-arc oxidation (MAO), which uses plasma arc discharge in an electrolyte solution under high voltage, is an advanced coating process for producing a porous, relatively rough and firmly adherent inorganic glass-ceramic-like coatings on metal

surfaces such as titanium, aluminum, magnesium, tantalum, niobium or zirconium. Another advantage of this MAO process is the possibility of incorporating Ca and P ions into the surface layer, by controlling the composition and concentration of the electrolyte. For biomedical applications, Ca^{2+} and PO_4^{3-} ions in the electrolyte enter the ceramic layer during the MAO process, so that the bioactivity potential of titanium or its alloy increases [1].

However, in some case, MAO treated surfaces may encourage formation of amorphous films with low contents of Ca and P ions. Thus, they may not induce formation of crystalline HA owing to the insufficient concentration of Ti-OH groups, which serve as the sites for the nucleation of HA crystals. Recently, some other techniques including hydrothermal treatment or ultraviolet light (UV) exposure have been proposed after micro-arc oxidation in order to enhance the bioactivity and the cell response of the titania surfaces [4-5].

The techniques like MAO, hydrothermal treatment and UV exposure also modify the physico-chemical surface properties of the biomaterial, such as hydrophobicity, surface tension and electrical surface potential. Surface characteristics of materials, such as chemistry and surface energy, play an essential role in cell adhesion to biomaterials [6].

Micro-arc oxidation produces porous surfaces, which result in increasing the surface roughness. Although, increased roughness is preferred for stronger fixation between bone and the implant, it also leads to bacterial infection due to the increased surface area, which enables the retention of bacteria. Bacterial infection, which is the consequence of bacterial attachment to the implant surface and the subsequent development of a biofilm, is one of the major causes of implant failure such as loosening or bone loss at the bone-implant interface [7].

The most antibacterial inorganic materials are the ceramics, containing antibacterial metals, such as silver and copper. The cation exchange rate of HA with silver ions is very high. Thus, silver ions substituted HA is produced to provide anti-microbial effects against bacteria. Silver, known as a disinfectant for many years, has a broad spectrum of anti-bacterial activity and exhibits low toxicity towards mammalian cells [8].

The main objective of this study was to investigate the anti-bacterial activity of commercially pure titanium (CP-Ti) oxidized via micro-arc oxidation (MAO) process in a silver nitrate ($AgNO_3$) containing electrolyte and evaluate the effect of silver nitrate addition on surface morphology and bioactivity of CP-Ti. Secondly, the effect of UV irradiation on the ability of hydroxyapatite nucleation on TiO_2 surface, was researched.

2. TITANIUM IN BIOMEDICAL APPLICATIONS

Pure titanium and titanium alloys are frequently used as dental and orthopedic implant materials (Figure 2.1) because of their excellent mechanical strength, chemical stability, and biocompatibility. The biocompatibility of titanium is closely related to the properties of the surface oxide layer, in terms of its structure, morphology and composition. Various physical and chemical treatments of the Ti surface have been proposed with a view to obtain the most biocompatible implant surface. Among the techniques, which have been found to be beneficial to the biological performance of the implants, are increasing the surface roughness, the oxidation of Ti to form a TiO_2 layer on the surface. The incorporation of Ca or P ions into the surface layer, and the validity of these results has been confirmed by several different researchers [9].

Titanium is a biocompatible and a corrosion resistant material due to the native oxide film present on its surface. But, healing process is slower than bioglass or hydroxyapatite, which is the primary inorganic phase of hard tissues, due to the fact that titanium is bioinert, and seldom forms a direct chemical bond to bone tissue [10-11]. Along with these, its outstanding strength to weight ratio and excellent fatigue behaviour make titanium a great material for biomedical applications. Also, its low elasticity modulus compared to other biomaterials is very suitable by means of minimizing stress shielding factor [3].

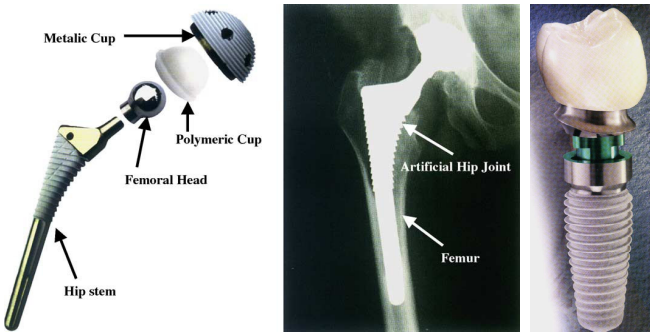

(a) (b)

Figure 2.1: Schematic diagram of (a) an artificial hip joint (b) a dental implant [12].

Until the ends of 1980's, the popular titanium alloy used in manufacturing of load bearing implants applications was Ti-6Al-4V along, while commercially pure titanium (Cp-Ti) is still an attractive material for dental applications. However, in the course of the discussion around the toxicity of the element vanadium, V-free alloys were specifically developed for medical applications. In these alloys, Fe, Nb, Ta and Mo replaces Vanadium. At the same time, orthopedic alloys gradually shifted from $\alpha+\beta$ alloys to metastable β alloys since they have a lower Young's modulus, which comes closer to that of human bone (10-30 GPa) [3].

Titanium has proven to be a mature material for dental implants. A major advantage of titanium in comparison with gold based alloys is that titanium comes as a pure element, thus avoiding chemiophysical reactions in the mouth and excluding the danger of a metal allergy. Titanium is totally biocompatible. It can be combined with other dental materials like amalgam or gold, without the risk of electrochemical reactions from contact with these alloys in mouth. Because of its high affinity for oxygen, titanium immediately forms an oxide film in the mouth, which creates this neutrality. Since the dielectric constant of titanium oxide is similar to that of water, titanium is also neutral in taste. Furthermore, its very low thermal conductivity, which is more than an order of magnitude below that of gold based alloys, is an important advantage of titanium. Teeth that are equipped with titanium react less sensitively to the fast temperature changes from hot or cold food and drinks, and this reduces the possibility of thermal irritation of the pulp. Titanium's lower density is another advantage for large dental restorations like crowns, bridges and removable partial dentures, where four times heavier gold implants may feel like a foreign body. Also, titanium implant introducted into the jawbone favors a faster and a better osseointegration. Today, titanium is successfully used in prosthetic dentistry for implant screws, crowns, bridges, dental posts, inlays and removable partial dentures. Since titanium is the only dental metal that can be easily X-rayed, a proper diagnosis of caries can be made without removing crowns or bridges [3].

The featues of titanium and its alloys are introduced below, in terms of corrosion resistance, biocompatibility, osseointegration, mechanical properties, processability and availability.

2.1 Corrosion Resistance

Titanium and its alloys belong to that group of metals which, in the body fluid, cannot undergo a breakdown of passivity. Nevertheless, in all materials, the passive layer can be mechanically damaged, for example, by fretting of metal against metal (plate/screw system) or by the instruments used during surgery. Therefore, the repassivation time is very important for these materials. Compared to other metals like 316L and Co-Cr alloys, the oxide growth rate of titanium is accelerated [3].

2.2 Biocompatibility

The cell attachment, spreading and growth are important criteria to judge the biocompatibility of a biomaterial. This process is influenced by many properties of biomaterials, including composition, the surface chemical states and morphology [1].

Titanium is reported to be biocompatible because it forms a protective surface layer of semi or nonconductive oxides. Because of the isolating effect of this oxide film, it is able to prevent a flow of ions to the surrounding tissue and a flow of electrons in the implant metal. Also, because of its corrosion resistance, it inhibits the accumulation of corrosion products on the organs or the tissues thus, preventing any hypersensitive effects occuring if the limit of toxicity for a certain metal is exceeded. And it does not cause any allergy or inflammation [3].

2.3 Osseointegration

Osseointegration is the ability of a biomaterial to make a structural and functional connection with the surrounding tissues. Experiments show that new bone formation in close contact with the surface of titanium is much more abundant and better than other materials. No loosening of the implant takes place, furthermore, the detaching moment for titanium screws increases steadily with exposure time. As the surface roughness of titanium is enhanced, the adhesion strength between metal and the bone increases. Also, it is known that in a pH region from 2.9 to 12.7, the titanium oxide is hydroxylated, at the surface OH^- groups exist which are able to react chemically with biomolecules. Therefore, in the oxide layer mineral ions from the biosystem, e.g calcium and phosphorus, are incorporated. These Ca and P deposits are able to bridge

the gap between the collagen fibrils and the oxide surface layer with a maximum mechanical stability [3].

2.4 Mechanical Properties

For a useful biomaterial, in addition to a Young's Modulus similar to that of the bone (10-30MPa), adequate fatigue strength and elongation at fracture are required. Ti, Ti alloys and Nb have an elastic modulus of about 100-120 GPa. This value is among all metalic biomaterials the closest to that of bone. In fatigue strength, titanium and its alloys are equal or even superior to other commercially pure materials and alloys. With regard to their biofunctionality value, which is given by the quotient of the fatigue strength and Young's Modulus in Table 2.1, titanium and its alloys demonstrate their superiority to other biomaterials. The lower Young's Modulus, the better the functional load on the implant can be transmitted whereby the formation of new bone is stimulated. A further decrease of Young's Modulus can be achieved by the use of porous implants or implants with a porous surface layer [3].

Table 2.1: Characteristic mechanical properties of various metalic biomaterials [3].

	E(GPa)	**YS(MPa)**	**FS(MPa)**	**%El**	**BF*10^{-3}**
316L	210	450	250	40	1.2
CoCr (as cast)	200	500	300	8	1.5
CoNiCr (as wrought)	220	850	500	20	2.3
Ti6Al4V	105	900	550	13	5.2
Ti5Al2.5Fe	105	900	550	15	5.2
Cp-Ti	100	300	200	40	1.8
Cp-Ta	200	300	200	40	1.3
Cp-Nb	120	250	150	70	1.3

BF : Biofunctionality (FS/E) E : elasticity modulus, YS : yield strength FS : fatigue strength

2.5 Processability and Availability

All current processing procedures are possible for Ti and its alloys and are used for the fabrication of implants. Among them, techniques like forging, CNC machining and precision casting via the lost wax process are present [3]. Concerning the cost of semi products, Ti and its alloys belong to the same group as stainless steels, while CoCr alloys, niobium and especially tantalum are more expensive. The processability of Ti and its alloys is unrestricted, and for the economic aspects, the volume price is lower than that of CoCr alloys, niobium and tantalum [3].

3. SURFACE MODIFICATIONS OF TITANIUM AND ITS ALLOYS FOR BIOMEDICAL APPLICATIONS

3.1 Oxidation Techniques

Although titanium and its alloys offer many attractive properties, their use is largely restricted to non-tribological applications, owing to high friction and wear and a strong tendency to galling. On the other hand, there has been increasing interest in titanium alloys in many fields, in which wear resistance, anti-scuffing, load-bearing capacity and biocompatibility are frequently of major concern. In recent years, some attempts have been made to overcome the problem by means of many surface engineering techniques such as anodic oxidation, thermal oxidation and micro-arc oxidation (MAO) [13].

Thermal oxidation can produce a 15–30μm thick oxide layer of the rutile-type TiO_2 phase. Unfortunately, due to the long-term high temperature action, thermal diffusion processes lead to the formation of an oxygen solid solution in titanium substrate, and development of phase segregation and coalescence, which may cause substrate embrittlement and worsened mechanical and corrosion performance [13]. During the thermal oxidation of Ti; at low temperature, anatase is formed, and at higher temperatures, the rutile phase becomes more stable than the anatase phase. This oxidation behavior reflects the varying thermodynamic stability of TiO_2 depending on the treatment temperature [9].

Anodic oxidation of titanium implants demonstrates changes of various oxide properties, not only oxide thickness, but also surface morphology, pore configuration, crystallinity, chemical composition, and surface roughness. Electrochemically oxidized implants of 200 nm or less oxide thickness prepared in acetic acid showed no significant differences in bone response in comparison to untreated titanium but implants with 600 nm or more oxide thickness showed a significantly enhanced bone response in a rabbit model. Phosphoric/sulphuric acid

electrolyte systems have been extensively investigated and found to form thicker anodic oxide up to a few tens of microns. Four-micron thick porous anodic oxide on the titanium implants formed in H_3PO_4–H_2SO_4 electrolyte showed strong bone reactions as evaluated by push-out test compared with control implants. More recently published animal studies of a clinical implant system with 2–10μm thick porous anodic oxide formed in H_3PO_4–H_2SO_4 electrolyte demonstrated a significantly enhanced bone response in comparison to control implants [11].

Microarc oxidation (MAO) is an enhanced electrochemical technology using a plasma arc discharge within an electrolyte solution under high voltage [10]. It is attracting increasing interest in fabricating ceramic like coatings on titanium alloys, with the purpose of providing corrosion and wear resistance or various functional properties. In addition, this technique is economic efficiency, ecological friendly and characterized by high productivity. It is also called "plasma electrolytic oxidation (PEO)", "microplasma oxidation (MPO)" and "anodic spark deposition (ASD)" in modern scientific literatures [14].

MAO is based on the conventional anodic oxidation of processing metals in aqueous electrolyte solutions under the additional condition of plasma discharge at exceeding the critical values of the polarization potential. And the fact that, discharge leading to localized high temperature and high pressure, allows forming coatings composed of not only predominant substrate oxides but also of more complex oxides containing compounds which involve the components presented in the electrolyte [14]. In Figure 3.1, the resulting natural porous structure of oxide layer on Ti6Al4V after micro-arc oxidation process is presented.

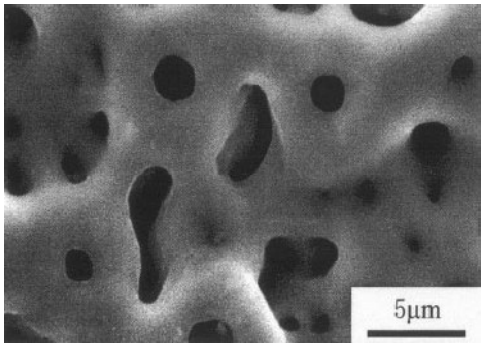

Figure 3.1: Morphology of MAO layer on Ti6Al4V [15].

Both intrinsic factors (electrolyte compositions and pH) and extrinsic factors (electrical parameters and electrolyte temperature) affect the formation and microstructure of microarc oxidation coatings. The composition and the concentration of electrolyte and electrical parameters during the process play a crucial role in obtaining the desired coatings of special phase component and microstructure. Among them, it is assumed that the intrinsical effects of electrolytes may be summarized as follows [14]:

1. Transmitting the essential energy needed for anode oxidizing, occurring in the interface of metal and electrolyte, as the medium of current conduct.
2. Providing the oxygen source in the form of oxysalt needed for oxidation.
3. Components presenting in the electrolyte incorporated into the coatings can further modify or improve the properties of microarc oxidation coatings.

In Figure 3.2 below, a classical MAO process unit is shown schematically.

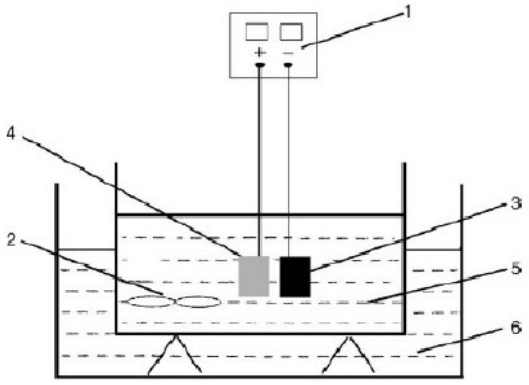

Figure 3.2: Schematic diagram of micro-arc anodizing apparatus 1) power supply 2) mixer 3)anode 4) cathode 5) electrolyte 6) cooling water [16].

Various specially selected electrolytes and their combinations have been successfully developed in order to provide protective coatings of corrosion and wear resistance and diverse functional coatings, such as biocidal or catalytic, biomedical, ferroelectric and semiconducting properties, on titanium alloys [14].

3.2 Coating Techniques other than Oxidation

The coating of hydroxyapatite (HA: $Ca_{10}(PO_4)_6(OH)_2$) on the metal surface has been suggested as the most effective way to provide biocompatibility and osseoconductivity. Up to now, several techniques of HA coating on titanium such as plasma spray coating, sputtering, electron beam deposition, chemical vapor

deposition, electrophoresis, electrochemical deposition, and dip coating, have been explored, and among them, plasma spray coating has mostly been highlighted for the applications [4].

Although plasma spray coatings exhibit a very good biocompatibility, their use presents several problems including HA porosity and low crystallinity, a low fatigue strength, degradation, a weak adherence to metallic substrates and delamination during a long-term implantation [2]. Due to the high-temperature melting and the subsequent rapid cooling during plasma spray coating, amorphous and/or secondary phases such as tricalcium phosphate (TCP) and tetracalcium phosphate (TTCP) appear, and these phases are highly bioresorbable [4]. Also it is difficult to coat complex shaped implants by this technique.

An important prerequisite for an implant with bioactive coating to be clinically used is its stability. Easy peeling off the layer from the substrate results in decrease in bonding strength of the implant to the host tissue. In addition, the layer may be accidentally scratched during operation, or dissolved after implantation by contacting with surrounding body fluids [17].

Electron beam evaporation with ion beam bombardments is one of the important techniques to produce high quality film, in which a film is deposited on a substrate while being simultaneously bombarded with ion beam. The reason for formation of strong adherent films provided by this method is that the interface between substrate and film is mixed by ion bombarding. Besides the coating-to-substrate bond strength, the chemistry and crystallinity of coating could be the key factors affecting the stability of the coating. Coatings deposited by electron beam evaporation usually contain HA, TCP, tetracalcium phosphate (TTCP), CaO and amorphous calcium phosphate (ACP) even the evaporant used was highly crystalline HA because of the extreme heat flame. Although other impurities except for ACP have a crystalline structure, all of these components are more soluble in physiological fluids than crystalline HA [17].

Ion implantation and ion beam assisted/enhanced deposition are promising techniques for enhanced biocompatibility of metal implants, even though there are difficulties in obtaining surface homogeneity of implanted ion concentration on complex shaped samples like clinical screw implants. Bone tissue reactions have

mostly depended on the implanted ion chemistry and the experimental parameters used. Nitrogen-ion implantation showed no difference in bone reactions compared to non-treated implants. However, titanium implants (plate and cylinder types) using calcium ion-implantation and a calcium ion-mixing process resulted in improved bone response [11].

There are disadvantages like weak bond strengths of biomimetic deposited and sol-gel formed Ca-P coatings to titanium substrate [18]. On the other hand, conventional-sol-gel-derived coatings are usually provided by a dip-coating method, which consists of several coating-heating cycles to obtain the necessary thickness for apatite deposition, and thus, is quite time-consuming [2]. Table 3.1 shows the surface modifications applied to Ti implants with the resulting modified layer properties.

Table 3.1: Overview of surface modifications for titanium implants [12].

Surface modification method	Modified layer	Objective
Mechanical methods		
Grinding, Polishing, Blasting	Rough or smooth surface formed by subtraction process	Produce specific surface topographies; clean and roughened surface; improve adhesion in bonding
Chemical methods		
Chemical treatment		
Acidic treatment	<10 nm of surface oxide layer	Remove oxide scales and contamination, Improve biocompatibility, bioactivity or bone conductivity
Alkaline treatment	1 μm of sodium titanate gel	
H_2O_2 treatment	5 nm of dense inner oxide and porous outer layer	Improving biocompatibility, bioactivity or bone conductivity
Sol–gel	10 μm of thin film such as calcium phosphate, TiO_2 and silica	Improve biocompatibility, bioactivity or bone conductivity
Anodic oxidation	10 nm to 40 μm of TiO_2 layer, adsorption and incorporation of electrolyte anion	Produce specific surface topographies; improved corrosion resistance; improve biocompatibility, bioactivity or bone conductivity
CVD	1 μm of TiN, TiC, TiCN, diamond and diamond-like carbon thin film	Improve wear resistance, corrosion resistance and blood compatibility
Biochemical methods	Modification through silanized titania, photochemistry, self-assembled monolayers, protein-resistance, etc.	Induce specific cell and tissue response by means of surface-immobilized peptides, proteins, or growth factors
Physical methods		
Thermal spray		
Flame spray, Plasma spray, HVOF	30 to 200 μm of coatings, such as titanium, HA, calcium silicate, Al_2O_3, ZrO_2, TiO_2	Improve wear resistance, corrosion resistance and biological properties
PVD		
Evaporation, Ion plating, Sputtering	1 μm of TiN, TiC, TiCN, diamond and diamond-like carbon thin film	Improve wear resistance, corrosion resistance and blood compatibility
Ion implantation and deposition	10 nm of surface modified layer and/or μm of thin film	Modify surface composition; improve wear, corrosion resistance, and biocompatibility
Glow discharge plasma treatment	1 nm to 100 nm of surface modified layer	Sterilize, oxide, nitride surface; remove native oxide layer

4. LITERATURE SURVEY ON MICRO-ARC OXIDATION OF TITANIUM FOR BIOMEDICAL APPLICATIONS

There are lots of studies in literature in order to make the titania, micro-arc oxidized in Ca and P containing electrolytes, more bioactive by utilizing some treatments such as hydrothermal treatment and UV exposure. This section is focused not only on these treatments but also on the MAO process parameters affecting the mechanical, chemical and biological performances of the coatings.

As mentioned in Chapter 2, titanium and its alloys are currently used as an implant material due to its good mechanical properties and excellent biocompatibility. However, titanium together with its natural oxide thin film is known to be bio-inert. It is difficult to achieve chemical bond with bone and form new bone on its surface at an early stage after implantation. To overcome this drawback, hydroxyapatite (HA) coatings are used as bioactive surfaces of titanium implants, of which many processing techniques have been developed [19].

All the efforts in both construction and processing are expected to endow the bioactive coatings or layers with firm adhesion and structural stability for long-term clinical use. Although such coatings and layers are to a great extent successful, it is difficult to make them porous and on implants with complex surface geometry, such as dental root implants with screw [19].

In recent years, micro-arc oxidation technique is gaining increasing interest in preparing rough and bioactive coatings on titanium surfaces. These coatings are primarily known by their high biocompatibility, high adhesion strength on substrate and porous morphology, which is an important factor in making a strong connection between the metal and the bone. The rough nature of this oxide layer influences the interactions between cell and material and is also beneficial to enhance osseointegration. Figure 4.1 depicts the porous oxide layers produced by in different electrolytes by MAO process.

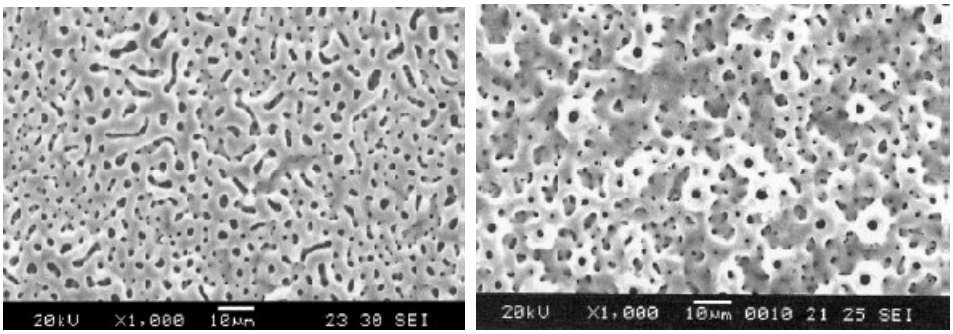

(a) (b)

Figure 4.1: Micro-arc oxidized Ti samples at 350V (a) Na_2CO_3 (b) calcium acetate containing electrolyte [19].

If we look at the mechanism of this oxidation technique, dielectric breakdown of oxide film on titanium takes place under high voltage and leads to spark or micro-arc discharge. In the initial stage of oxidation, the voltage between the titanium specimen (anode) and the cathode increases gradually, and a thin anodic film on titanium is formed in aqueous solution. That is actually an anodizing stage. When the voltage is over a critical value of about 100V, the dielectric breakdown in the oxide film takes place, and then spark or microarc discharges appear on the surface of titanium anode. If this higher voltage is held, many visible sparks or microarcs cover the whole surface and move rapidly. It is suggested that the instantaneous temperature in these discharge channels can be over 7000 K, where the plasma atmosphere is generated. Under such a high temperature, the oxide coating on titanium may be locally and temporarily molten, as shown in Figure 4.2 [13].

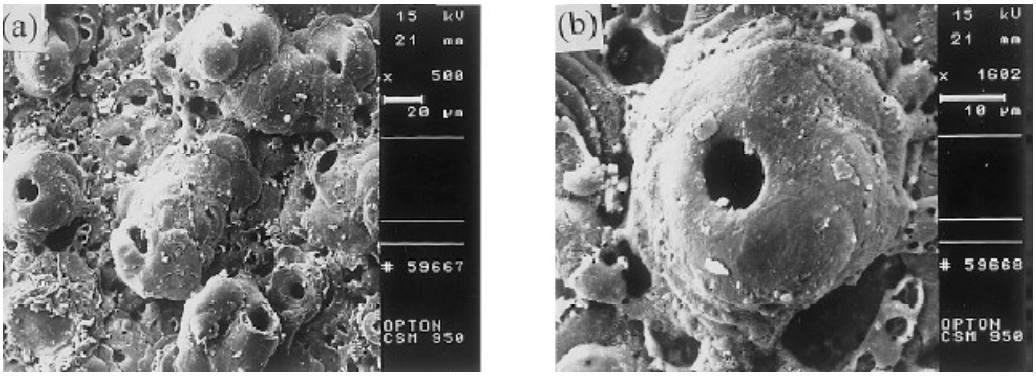

(a) (b)

Figure 4.2: Surface morphology of the microarc oxidation coating on pure titanium (a) low magnification (b) high magnification [13].

It is found that the coating surface contains many grains with various sizes. Microarc discharge over many times at the same position of specimen would result in one

large grain due to the deposition of erupted melt from the discharge channel. One crater-like pore of several micron is remained at the center of grain as shown in Figure 4.2. When the spark or microarc quenches, the melting in the microplasma discharge zone rapidly solidifies due to the aqueous solution cooling. Thus, both the coating thickness and insulation property are enhanced in these previous discharge spots. Then the micorarcs move to other spots because the dielectric breakdown always occurs at a relative thin part of the coating. With increase of oxidation time, the coating thickness increases and the breakdown becomes more difficult, so the quantity of sparks or microarcs decreases gradually. While the coating grows to a certain thickness, it will not be broken down. In this stage microarcs disappear completely and the oxidation ends. The structure of the coating is rough and porous. The cracks that can be seen on the coating surface are due to the thermal stresses in the process of rapid solidification of erupted melt [13].

According to Yaming Wang et al. [14], MAO using a constant current density regime is time saving compared with a constant voltage regime. This is not surprising because the current density, which defines the intensity of sparking on the surface, is kept at the same high level through the microarc oxidation process, which facilitates the coating growth. In constant voltage oxidation, current density gradually decays and sparking intensity decreases in the process, which leads to a relatively low rate of coating growth. However, coatings formed using the constant current density regime tends to have a loose and a much more rough microstructure [14].

Coatings produced by MAO grow as a result of plasma chemical oxidation reaction of the substrate near the electrolyte, and do not contain an artificial interface as deposited coatings do. Therefore, the adhesion strength is expected to be relatively high. However, the measured adhesion strength is determined not only by the adhesion of the coating to substrate, but also partly by the cohesive strength inside the coating. Also in MAO, coatings grow towards the inside of the substrate at the cost of consuming substrate metal [14].

The advantage of MAO technique is not only simple and quick but also can prepare homogeneous thin oxidized films on the whole inner-pore wall of porous titanium. Compared with the MAO films formed on dense titanium plates, the structural characteristics of the MAO films formed on porous titanium are different. In vitro apatite-forming ability assessment shows that the MAO-treated porous titanium has a

high bioactivity, although its bioactivity is slightly lower than that of porous titanium subjected to 5.0 M NaOH treatment at 60 °C for 24 h and subsequent heat treatment at 600 °C for 1 h. This difference is due to the different apatite induction mechanisms [18].

It is known that a macro-porous surface of an implant is beneficial to bone tissue growth and enhanced anchorage of implant to bone; furthermore, a micrometer-sized porous surface has the function of an enhanced cell proliferation. On the other hand, nano-crystallized surface has been proved to be efficient in biological response. For example, compared with conventional-crystallized titania, nano-crystallized titania can promote osteoblast adhesion and proliferation, and osseointegration. Therefore, alternative approaches to make titanium implant surface bioactive, porous and nano-crystallized, are still worth exploring [19].

Cell adhesion is a fundamental process, which will directly affect cell proliferation, migration, and differentiation. It is involved in many biological behaviors including the biomaterial tissue integration. Osteoblast adhesion and proliferation on the implant material surface is therefore essential for the success of any implant in which osteointegration is required. Surface properties of implant material have a crucial role for cell adhesion and cell proliferation. As an example, MC3T3-E1 cells are shown on oxidized titanium substrate in Figure 4.3. Several authors have well studied some of these properties including chemical composition, surface roughness, and surface energy. The surface characteristics and the mechanism that determine cell behavior on the different material surfaces and that lead to cell attachment remain unknown [20].

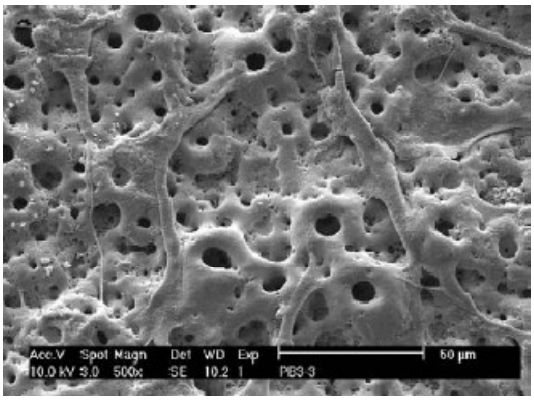

Figure 4.3: SEM image of MC3T3-E1 cells cultured on a Ti specimen treated with MAO for 2 d after inoculation [21].

The surface energy is an important parameter of the material surface. It is affected by several surface characteristics, such as chemical composition, surface charge, and microstructural topography. Several recent studies have shown that the surface energy of biomaterials strongly influences the initial cell attachment and spreading of osteoblastic cells on the biomaterial surface. Surface energy may influence protein adsorption and the structural rearrangement of the proteins on the material [20].

It is thought that surface energy might be a more important determinant of cell adhesion and proliferation, and might be more useful than surface roughness for generating cell adhesion and cell colonization on the engineered tissue scaffolds. Therefore, understanding the relationship between surface energy and cell adhesion on different biomaterials will facilitate the design of optimized implant material surfaces and subsequently the cell attachment [20].

Concerning the stability of coatings, much efforts have been devoted to determine the immersion behavior of calcium phosphate coating in solutions with ionic composition similar to the inorganic fraction of blood plasma, such as phosphate buffered saline (PBS) solution, Hank's balanced salt solution (HBSS) and Kokubo's simulated body fluid (SBF). These in vitro studies are important in a practical sense in that it could give some indication of the in vivo behavior of the coating. Consequently, these tests are practiced as a first stage to assess the bioactivity of a potential biomaterial through the formation of a bone like apatite layer [17].

4.1 MAO Process Parameters

4.1.1 Effect of Applied Voltage on Morphology

The microstructural change of the oxide layer was found to be closely related to the voltage used for the MAO treatment. Increasing the voltage resulted in an increase in both the roughness and pore size as shown in Figure 4.4, as well as in the thickness of the oxide layer [9].

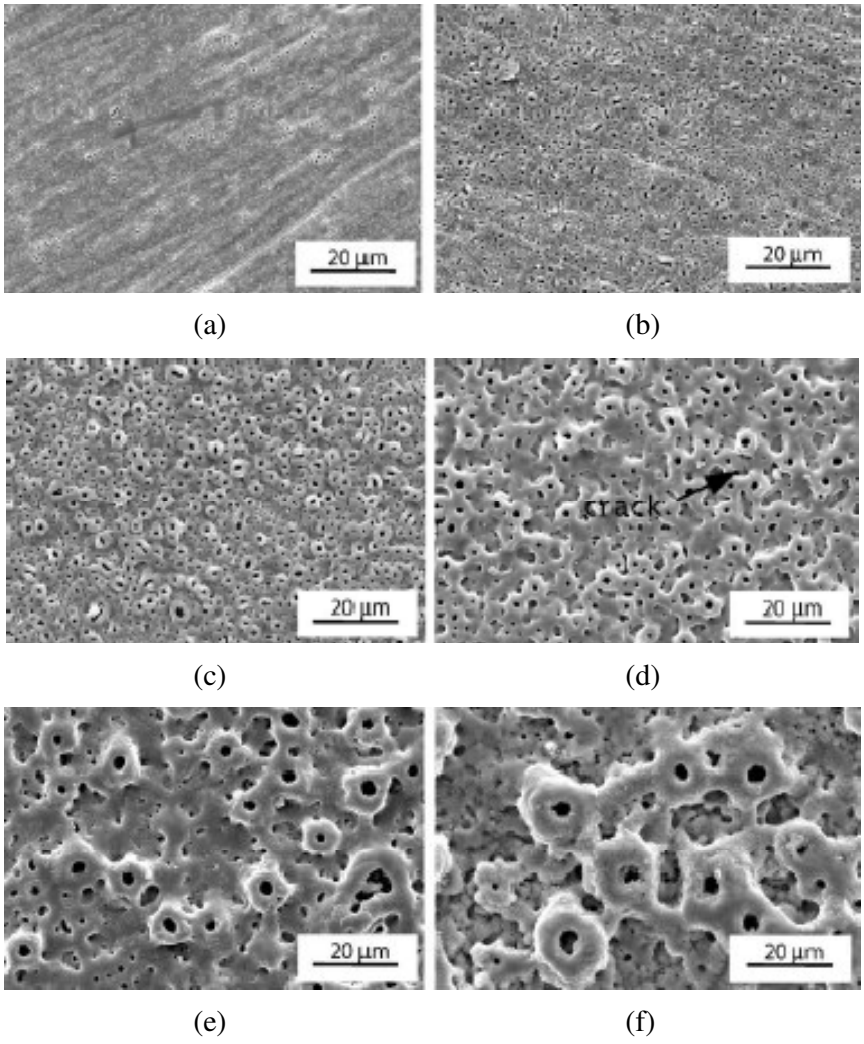

Figure 4.4: SEM surface morphologies of Ti surfaces treated with MAO at different voltages (a) 190 V (b) 230 V (c) 270 V (d) 350 V (e) 450V (f) 600 V [9].

These microstructural evolutions are attributed to the dielectric breakdown of the oxide layers. During the MAO process, as the TiO_2 layer becomes thicker, micro-arc discharges occur on the local area of the substrate, that break down the surface dielectric layer to form micropores. At the same time, the oxide layer becomes thicker due to the increased extent of the electrochemical reaction. As the oxide layer becomes thicker, the resistance of the oxide layer increases and a higher potential energy is required to break down the dielectric layer. As a result of this series of reactions, the pore size and the roughness of the oxide layer increase rapidly [9]. In Figure 4.5, the effect of voltage on oxide thickness is shown.

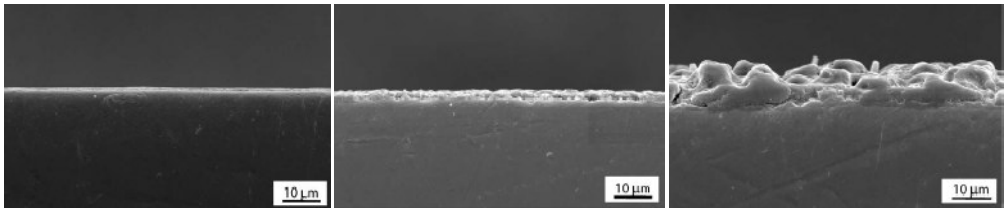

(a) (b) (c)

Figure 4.5: SEM cross-sectional views of Ti specimens treated with MAO at different voltages (a) 230V (b) 270V (c) 450V [9].

According to Won Hoon Song et al [22]. Ca content and morphology of the oxidized films are dependent on applied voltage. Up to 250 V, no Ca containing compounds or phases were observed. However, with further increases in voltage, $CaTiO_3$ phases, which are believed to be an apatite inducer, began to form. It is said that $CaTiO_3$ undergoes hydrolysis to form Ca^{2+}, OH^- and $TiO(OH)_2$ which yields a Ti-OH surface, acting as a nucleation site [22].

In another study of Won Hoon Song et al. [2], β-$Ca_2P_2O_7$ and α-$Ca_3(PO_4)_2$, which are well known bioresorbable phases, were obtained above 450V, having a positive effect on hydroxyapatite inducing. Until 250 V, TiO_2 was in anatase form. With increasing voltage, a rutile phase (TiO_2) began to appear. Rutile has a tetragonal lattice structure and is stable at all temperatures and pressures, while anatase is metastable and can transform to rutile by heating [13].

According to Jian Zhi Chen et al. [23], the number of calcium phosphate precipitates depends not only on the number of hydroxyl groups, but also on the structure of the oxide layer, because not all hydroxide groups present on the titanium surface are able to nucleate calcium phosphate. The highest nucleation ability is shown by anatase, less pronounced by rutile, whereas amorphous oxides do not have this ability at all. But the presence of rutile structures may possibly play a role in improving dissolution resistance of the enhanced oxide. The rutile oxide was considered to be denser and had a closer packed structure with few paths for ion diffusion as compared to anatase oxide. However, the presence of rutile oxide may also inhibit atom and ion diffusion in the oxide and have negative effects for HA formation on titanium surface [23].

They also reported that increasing voltage increased the pore sizes on oxide surface and the thickness of the coating up to 30 µm. In EDS results, they found that Ca/P ratio was unchanged up to 350 V, and increased rapidly at higher voltages with

compound formation. Then after 450 V, it decreased again and it was difficult to determine at 500 V because it varied from place to place due to compound formation and showed a changing distribution across the oxide film. They also indicated that using a more concentrated SBF (1.5 SBF) shortens apatite induction time to 14 days and decreases the voltage (350V) at which apatite forms related to the Ca and P incorporated [24].

When the apatite nuclei are formed, they spontaneously grow at the expense of calcium and phosphate ions from the metastable SBF solution. First, apatite fills the pores, then spreads over the entire surface. In addition to the apatite induction during immersion, calcium and phosphate in the SBF appear to be incorporated into the β-$Ca_2P_2O_7$ and α-$Ca_3(PO_4)_2$ phases resulting in the growth of these phases compared to the as-oxidized specimen [24].

Wang Yingjun et al. [10] also reported that, at high voltage (450 V), the oxide layers were slightly cracked and the surfaces become more irregular. With increasing applied voltage, the intensity of the two TiO_2 phases (anatase and rutile) decreased, indicating that the degree of crystallinity of the films diminished, while the thickness of the films increased following the applied voltage. They reported that P incorporation into the oxide film, with increasing voltage, had an adverse effect on crystallization of the oxide film. P/Ti is enhanced from 0.16 to 0.30 when the voltage increased from 380 V to 450 V [10].

Jifeng Sung et al. [25] stated that increasing voltage is an important effect for hydroxyapatite formation, reporting that they detected HA in XRD spectra over 430V. During the MAO process, amorphous TiOx dielectric film is formed on the surface at first, then transits into TiO_2 crystal at higher voltages. However, further increasing the voltage causes the TiO_2 dielectric to breakdown. At the same time, Ca^{2+}, HPO_4^{2-} or PO_4^{3-} and OH^- from the ionization of the electrolytes and H_2O respectively, incorporate into the coatings. Then more complex ceramics, such as $CaTiO_3$, α-TCP and Ca-deficient HA ($Ca_{10-x}(HPO_4)_x\ (PO_4)_{6-x}(OH)_{2-x}$, $0 \le x \le 1$, e. g. d-HA), are formed with reactions 4.1 and 4.2 [25].

$$TiO_2 + 2OH^- + Ca^{2+} \rightarrow CaTiO_3 + H_2O \quad \textbf{(4.1)}$$

$$(10-x)Ca^{2+} + 6PO_4^{3-} + 2(1-x)OH^- + xH_2O \rightarrow Ca_{10-x}(HPO_4)_x(PO_4)_{6-x}(OH)_{2-x} \quad \textbf{(4.2)}$$

Yong Huang et al. [1] found that, with increasing voltage, the oxide layer became thicker, and Ti content showed a decreasing trend while Ca and P content increased [1]. And according to Long Hao Li et al. [9], as the applied voltage increased, the average roughness of the surface increased, which had a positive effect on biomaterial-bone connection by mechanical interlocking between the material and the tissue [9].

After the removal torque tests, Long Hao Li et al. [9] examined the implant surfaces by a SEM. Small chips adhered to the implant surface were detected, as shown in Figure 4.6. From the EDS analyses, these chips were found to possess high concentrations of Ca and P, confirming them to be connective tissues. A greater number of adhered chips were observed in the case of the MAO treated specimens than in that of the pure Ti [9].

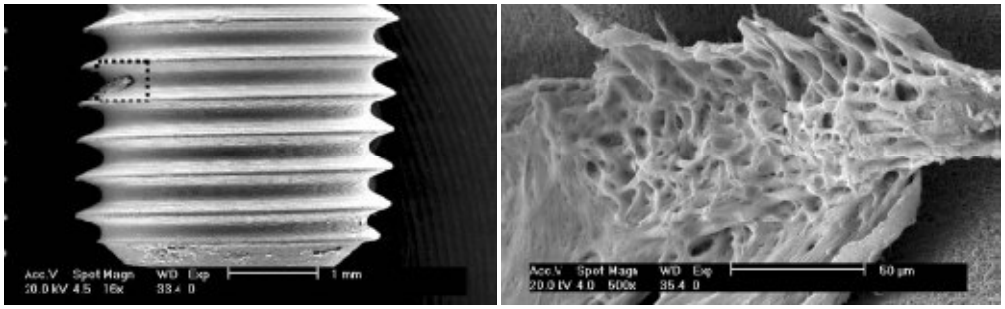

(a) (b)

Figure 4.6: (a) SEM images of Ti implants (MAO treated at 270 V) removed from the tibia of rabbits 4 weeks after their implantation and (b) high magnification (x500) micrograph of adhered chip [9].

4.1.2 Effect of Applied Voltage on Biological Performance

According to Long Hao Li et al. [9], the changes in chemical composition and roughness of the Ti surface played crucial roles in the biocompatibility of the implant. The proliferation rate was highest when the specimen was oxidized at the relatively low voltage of 190 V, and it decreased steadily with increasing voltage. Even though there was some variation depending on the applied voltage, the number of cells increased more than 10 times compared to the originally plated cells. These proliferation results simply indicate that all of the specimens offered a biologically favorable environment. In contrast to the proliferation behavior, the ALP activity of the cells increased when the applied voltage was increased. ALP activity is regarded as a marker for the early stages of cell differentiation. Generally, surface roughness

affects cell proliferation and differentiation: increasing surface roughness decreases the cell proliferation rate, but increases ALP activity. Moreover, cell differentiation is sensitive to chemical composition, but cell proliferation is not. Their result shows that the roughness and the amount of Ca and P ions incorporated into the titanium oxide layer strongly affect the cell response. Especially, the ALP activity significantly increased at higher voltages, which is deemed to be closely related to the increase in surface roughness and the increased amount of Ca and P contained in the oxide layer [9].

4.1.3 Effect of Processing Time

The structure and evolution of phase components in the coatings as a function of duration time (1–20 min) at constant 450 V were investigated in the study of Yong Han et al. [8]. At duration times up to 8 min, some additional phase components, such as HA, α-TCP and $CaCO_3$, appeared in the coatings beside rutile and $CaTiO_3$ [26].

In their experiment, it was observed that with prolonging the MAO duration time, the electrolyte adjacent to anode was heated up to 60 ^{o}C while the electrolyte far away from the anode was lower than 40 ^{o}C due to water cooling. The high temperature can promote hydrolysis of the electrolyte, generating more phosphate and carbonate ions. Once these ions in the electrolyte adjacent to anode reaches a certain concentration, they could react with the abundant Ca^{2+} ions to form HA, $Ca_3(PO_4)_2$ and $CaCO_3$ precipitates. It has been reported that biphasic calcium phosphate porous ceramics such as HA + $Ca_3(PO_4)_2$ and HA + $CaCO_3$ have higher bioactivity and osteoinduction relative to HA [26].

Yaming Wang et al. [14] reported that, with increasing treatment duration, coating growth varies from rapidness to tardiness accompanied by gradually roughening in appearance as shown in Figure 4.7. Meanwhile, phase transformation of anatase to rutile occurs. They found a lineer growth within the first 10 minutes (3μm/min), then a slowing down regime until 15 minutes and from then on, no obvious growth was observed [14].

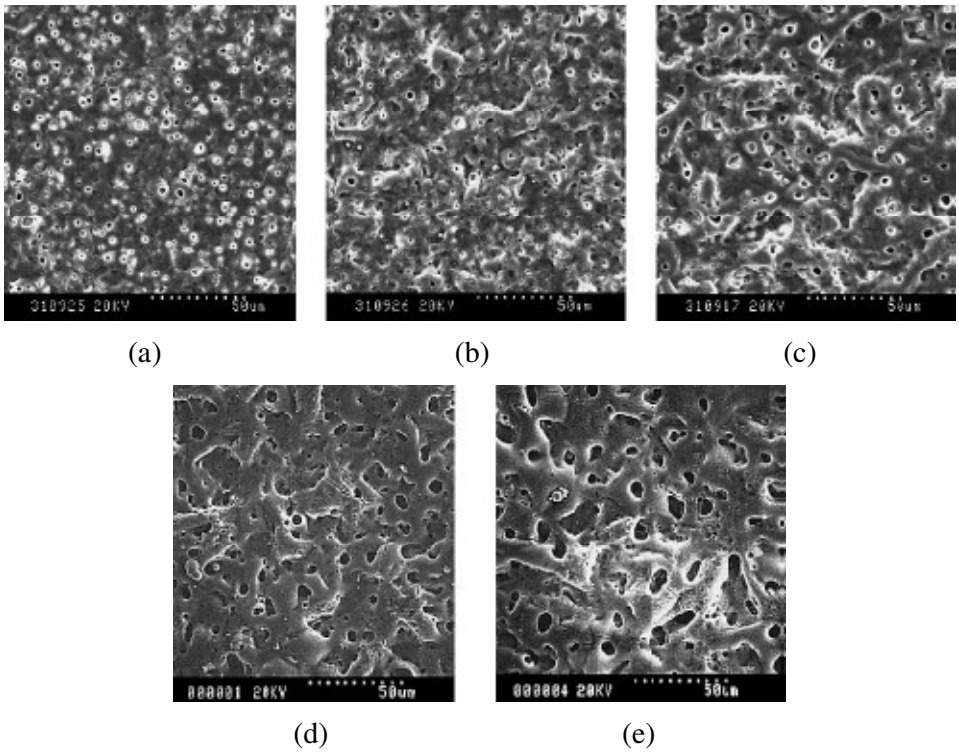

Figure 4.7: Surface morphology of microarc oxidation coatings formed on Ti6Al4V alloy in $(NaPO_3)_6$–NaF–$NaAlO_2$ solution at different treatment time periods: (a) 2 min (b) 5 min (c) 10 min (d) 15 min (e) 30 min [14].

Yaming Wang et al. [14] also concluded that at the initial oxidation stage (below 2 min), fine and uniform micropores with sizes less than 1 μm distribute randomly on the surface of the coatings. With proceeding of the oxidation, the micropores number quickly decreases in an exponential function, while micropores sizes increases strikingly. As a result, the porosity increases from 3.8% for 2 min to 11.6% for 30 min as in Figure 4.8 [14].

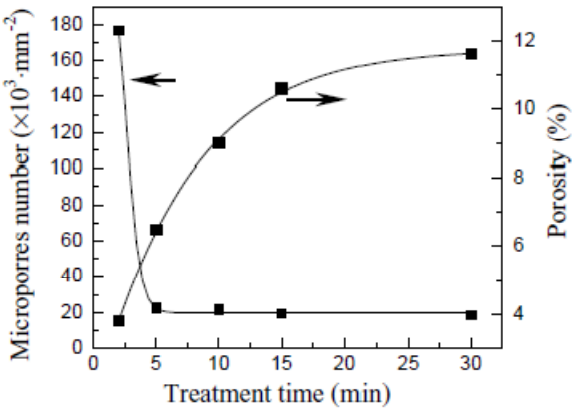

Figure 4.8: Variation of number of micropores and porosity on the surface of the coating during microarc oxidation treatment of Ti6Al4V alloy [14].

During microarc oxidation, the temperature and pressure in the discharge channels can reach about $2*10^4$ K and 102 MPa, which promote the conversion of Ti substrate into titanium oxides. Meanwhile, the incorporation of electrolyte components into coatings results from the high-temperature reactions proceeding just in discharges channels or adjacent areas. As the coatings thickness increases, the previously formed products are calcined repeatedly under the effect of the frequent microdischarge, which facilitates the anatase to rutile transformation, as well as the thermolysis process. Furthermore, the low thermal conductivity of titanium dioxide causes the underlying layer of the coatings to become heated, which also promotes the further transformation of the initially formed metastable anatase to the stable rutile phase. Thereby, the amount of rutile phase in the coatings increases with increasing oxidizing time [14].

From the XRD spectra of Jifeng Sun et al. [25], at 1.5 min, only rutile, $CaTiO_3$ and α-TCP peaks were detected on Ti6Al4V. When the treated time was extended to 3 min, HA and $CaCO_3$ peaks appeared. When the treated time varied from 1.5 min to 20 min, rutile and $CaTiO_3$ peaks reduced, α-TCP peaks had little change, however HA and $CaCO_3$ peaks gradually increased. The results indicate that, the treated time is also an important factor for the HA formation. At 20 min, there are almost only HA and $CaCO_3$ phase left, which indicates that the HA and $CaCO_3$ have covered the TiO_2 matrix, and become the predominant components of the coatings surface. Surface morphologies of the MAO coatings formed at 480 V are shown in Figure 4.9. It is found that when the treated time varies from 1.5 min to 20 min, the number of the pores on the surface gradually reduces; even the pores disappear when the treated time extends to 20 min [25].

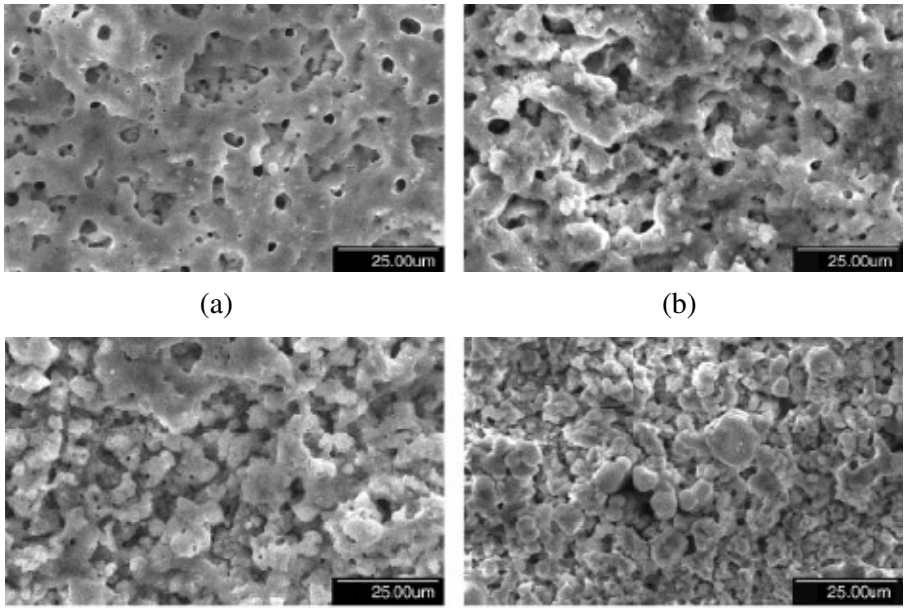

Figure 4.9: SEM of the MAO coatings formed at 480 V treated for (a)1.5 (b)3 (c)10 (d)20 min [25].

It was due to the gradual coverage of HA and $CaCO_3$ on the TiO_2 matrix, which has been testified by XRD. In combination with the XRD and SEM results, it can be inferred that HA and $CaCO_3$ are gradually formed on the TiO_2 matrix, i.e. the coatings are a kind of bi-layer HA/TiO_2 coatings, containing α-TCP and $CaCO_3$ [25].

4.1.4 Effect of Electrolytes

One of the most important parameters of MAO process is the content and the concentration of the electrolytes used. Electrolyte has a great influence on the properties of the coatings because of the decomposition of the chemicals in electrolyte via plasma occuring during oxidation process.

Won Hoon Song et al. [24] used an electrolitic solution containing 0.04 mol/L β-glycerophosphate disodium salt pentahydrate ($C_3H_7Na_2O_6P.5H_2O$, β-GP) and calcium acetate monohydrate ($(CH_3COO)_2Ca.H_2O$, CA) in order to incorporate Ca^{2+} and PO_4^{3-} ions into the coating to stimulate apatite nucleation and enhance the bioactivity potential of titanium [24].

Fu Liu et al. [2] claimed that the concentrations of Ca and P do not significantly change with the final voltage and current density in the same electrolyte concentration, but these concentrations also increase with increasing concentrations of β-GP and CA used in electrolyte [2].

Long Hao Li et al. [9] reported that the amount of Ca and P ions incorporated into the titanium oxide layer strongly affect the cell response after using a β-GP and CA as an electrolyte. Especially, the ALP activity significantly increased with the increased amount of Ca and P contained in the oxide layer [9].

However, Wang Yingjun et al. [10] used an electrolyte only comprising of sodium phosphate, so the oxide films obtained by MAO, were free of Ca ions. But they had the capability to induce apatite after 30 days by the contribution of the Ca ions present in the SBF, although they obtained a Ca-deficient hydroxyapatite [10].

Wenbin Zue et al. [13] obtained a double layered oxide by using a aluminate solution containing $NaAlO_2$. The outer layer consists of a large amount of $TiAl_2O_5$ phase and a little amount of rutile. Nevertheless, $TiAl_2O_5$ content in the inner layer is much lower than in the outer layer while the rutile content obviously increases in the inner layer [13].

An electrolyte comprising of $(NaPO_3)_6$, NaF and $NaAlO_2$ was used by Yaming Wang et al. [14]. The crystalline $AlPO_4$ is found to be involved in the coatings via high-temperature thermolysis of hydrated aluminium polyphosphates in the nearby discharging channels. NaF and $NaAlO_2$ was used to adjust the alkalinity and increase conductivity, as well as addition of $NaAlO_2$ increased growth rate of the microarc oxidation coatings. Yerokhin et al. measured the adhesion strength of coatings to the substrate, formed in different electrolytes, and found that the highest critical load was obtained in coatings formed in $KAlO_2/Na_3PO_4$ electrolyte [14].

Jifeng Sun et al. [18] treated the inner-pore wall of the porous titanium by micro-arc oxidation in the aqueous electrolytes containing 0.1 and 0.2 M NaOH. It was found that continuous thin films with pore sizes of 20–60 nm are formed in both electrolytes. The reason of the thin films was the larger contact surface areas per unit volume with the adjacent electrolyte leading to a slow electrode reaction and a weak electrical discharge intensity. The films consisted of an amorphous TiO_2 outmost layer, a coexisted intermediate layer of amorphous TiO_2 and rutile, and a Ti_2O_3 bottom layer, and tightly bond to the titanium substrate without any cracks. In vitro bioactivity assessment showed that both MAO films possess high apatite-forming abilities as seen in Figure 4.10 and 4.11. It is also found that, compared with the film formed in the 0.1 M NaOH-containing electrolyte, the film formed in the 0.2 M

NaOH-containing electrolyte had a higher roughness and more nanopores which help shortening the apatite induction time [18].

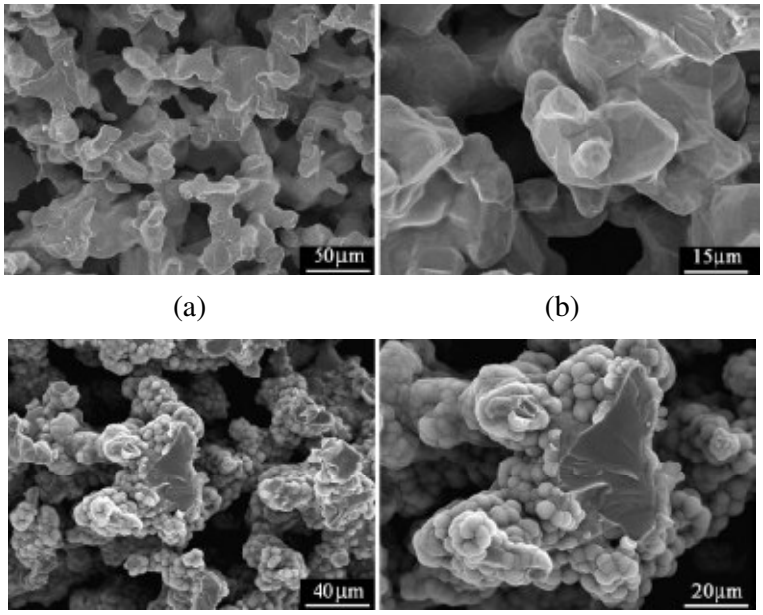

Figure 4.10: Cross-section morphologies of porous titanium oxidized in the 0.1M NaOH-containing electrolyte after immersing in SBF for (a) 7 days low mag. (b) 7 days high mag. (c) 12 days low mag. (d) 12 days high mag. [18].

Jifeng Sun et al. [18] reported that porous titanium would not only be beneficial to bone ingrowth into the porous structure, but also be beneficial to achieve a tough chemical bonding at the bone/implant interface. They stated that, because NaOH is used as the electrolyte, the oxidized films will partially be dissolved by reacting with NaOH as soon as they are formed by MAO. On one hand, the partial dissolution of oxidized films by NaOH delays the rapid increase of the thickness of the MAO-formed films. On the other hand, it improves the roughness of the MAO-formed films. The more concentrated the NaOH electrolyte is, the more the MAO-formed films are dissolved. And the film formed in 0.2 M NaOH-containing electrolyte is rougher than that formed in 0.1 M NaOH-containing electrolyte. Thus, it takes shorter time for the former film to induce apatite precipitate. From the above mentioned results, it was concluded that the porous titanium oxidized in the concentrated NaOH containing electrolytes showed a better bioactivity [18].

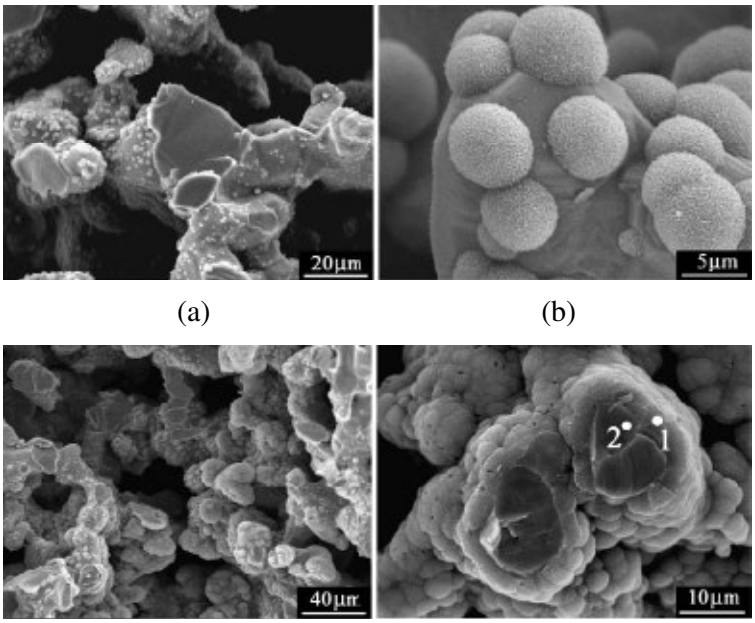

Figure 4.11: Cross-section morphologies of porous titanium oxidized in 0.2M NaOH-containing electrolyte after immersing in SBF for (a) 7 days low mag. (b) 7 days high mag. (c) 12 days low mag. (d) 12 days high mag. Point 2 indicates the fractured surface of titanium [18].

Young Taeg Sul [11] performed MAO in different electrolytes containing S, P and Ca ions. It was stated that MAO treatment in all three electrolytes enhanced the removal torques of implants, but the highest removal torque was obtained for Ca implants. The lowest torques were obtained in P implants. The reason of that was neither increased roughness nor the morphological texture but, was thought to be biochemical bondings which may be formed between bone and Ca implant by ionic bonds. The evidence for this was indirect, since no other surface property differences between the tested implants could explain the strong bone response, particularly to the Ca implant [11].

In another study, Young Taeg Sul et al [27]. oxidized CP-Ti implants in in acetic acid (TiO implant) and in a mixed electrolyte containing magnesium ions (MgTiO implant). XPS spectra indicated that the chemical composition of the outer most surface oxide of the TiO implant consisted mainly of titanium dioxide and in the case of the MgTiO implant, magnesium ions were incorporated into titanium oxide matrix, i.e. magnesium titanate and TiO_2. The oxidized layer of MgTiO implant was thicker and more porous, also the pore sizes were smaller. Bonding failure generally occurred at the bone to implant interface for the TiO implant and mainly occurred in

the bone away from the interface for the MgTiO implant as shown in Figure 4.12, although MgTiO implant had a lower roughness [27].

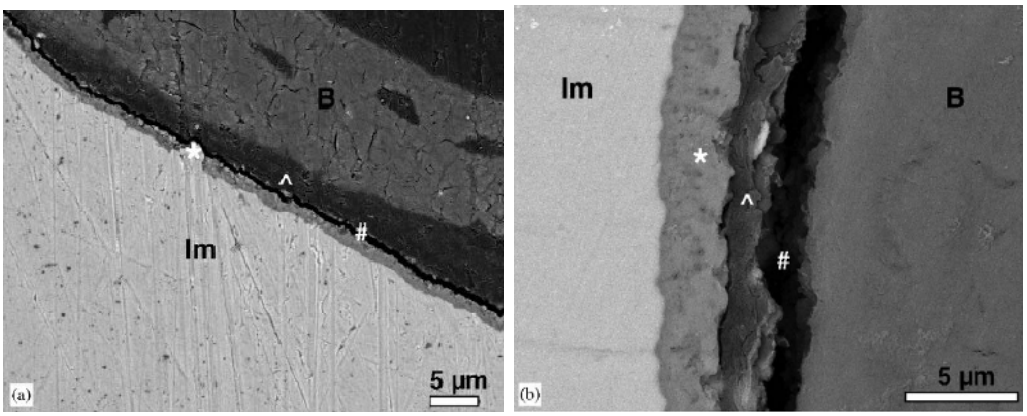

(a) (b)

Figure 4.12: SEM analysis of bond failure (a) TiO implant (b) MgTiO implant, Im = implant B = bone, * = oxide layer, # = fractured space during mechanical loads / RTQ testing, ^ = amorphous immature bone layer [27].

SEM analysis of bond failure in Figure 4.12 shows that fracture line for the TiO implant was more often observed between the surface oxide of the implant and the soft tissue/immature bone. The fracture line for the MgTiO implant more often occurred between immature and mature bone and sometimes appeared at inside the immature bone while actual interface remained. The delamination of the surface oxide of both oxidized implants was not observed [27].

Between bone and the Mg-incorporated implant surface, ionic movements and ion concentrations gradient were detected. It was indicated that Mg ions in the oxide layer moved toward the amorphous immature bone layer, whereas P and Ca ions of the tissue including body fluid moved toward the oxide layer of the implant. These movements did finally build up the ion concentration gradient. This ion exchange was said to support biochemical bonding theory, stated as previously [27].

In the study of Jian Zhi Chen et al. [23], the titanium sample was immersed in electrolytic solution containing calcium acetate monohydrate and sodium biphosphate dihydrate ($NaH_2PO_4 \cdot 2H_2O$) to make bioactive films without any alkaline or heat treatment. An uneven porous titania film structure, without apparent interface to the titanium substrates, was produced. The film consisted of anatase, rutile and hydroxyapatite. The thickness of the film was about 20 µm and the pore

sizes of the coating were in the scale of 1–5 μm. Maximum concentration of Ca and P ions was reported to be found to occur just beneath the surface of 3μm [23].

J.T. Filho et al. [28] used two kinds of solutions at 110-140 V; one consisted of $Ca(CH_3COO)_2$ (0.3M), Na_2CO_3 (0.6M) and the other was Na_2HPO_4 (0.1M) solution. The surface of the film produced with Na_2CO_3 solution showed a porous but very irregular surface with a great quantity of delaminated areas shown in Figure 4.13. It was suggested that the conditions of ionic conductivity and/or applied potential used for the 0.6 M Na_2CO_3 solution were too aggressive, causing delamination of the oxide layer during the process of titanium oxide film growing [28].

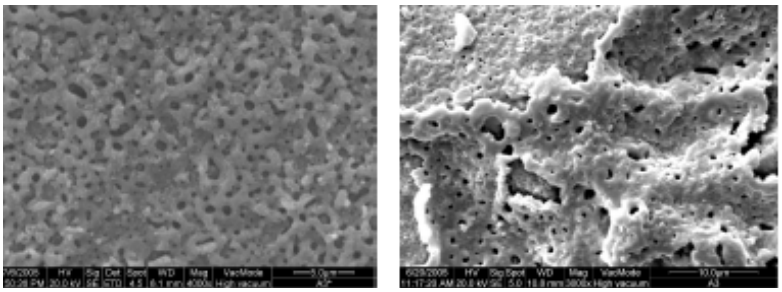

(a) (b)

Figure 4.13: SEM micrographs of TiO_2 layers produced with (a) 0.3M $Ca(CH_3COO)_2$ solution (b) 0.6M Na_2CO_3 solution [28].

Layers produced with CA (0.3M) showed the presence of calcium on the surface, while the ones produced with Na_2HPO_4 (0.1M) showed the presence of phosphorous. In the last case, a further hydrothermical treatment using a $Ca(OH)_2$ suspension was able to produce a surface enriched by phosphorous and calcium. It was stated that the presence of these elements on the surface can be extremely beneficial to the growth of osteoblast cells and osseointegration, enhancing the bioactivity of the layer. In addition, the presence of homogeneously distributed calcium on the titanium oxide surface could increase its biocompatibility properties. Low-angle X-ray diffraction revealed an anatase-rich crystallographic structure due to the low voltage applied, for all the titanium oxide layers, which is known to stimulate osseointegration [28].

Min Seok Kim et al. [4] performed micro arc oxidation with calcium chloride ($CaCl_2$) and potassium phosphate monobasic (KH_2PO_4) at constant voltage and constant KH_2PO_4 concentration. It was found that the crystallinity of HA increased with increasing concentration of $CaCl_2$. Also anatase, rutile and bioresorbable phases were not detected. An amorphous $CaTiO_3$ interlayer was obtained between HA and

the substrate as shown in Figure 4.14, having a thickness dependant on $CaCl_2$ concentration [4].

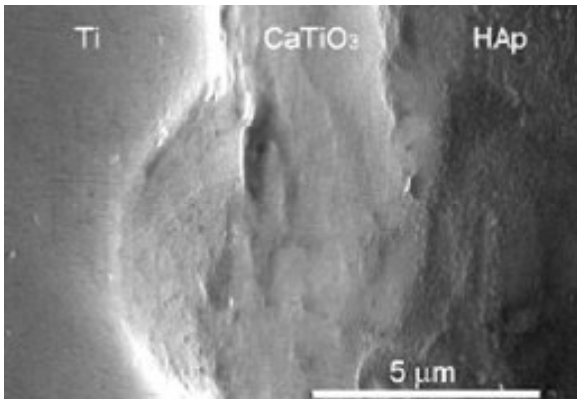

Figure 4.14: Cross-sectional view of the MAO-treated specimen prepared using 0.05M KH_2PO_4 and 0.10M $CaCl_2$ [4].

The formation mechanism of HA is as the following [4]:

As the first step, the electrolytes containing $CaCl_2$ and KH_2PO_4 produce Ca^{2+}, Cl^-, K^+, and $H_2PO_4^-$ ions. The Ca^{2+} ions incorporate with the Ti substrate to form the amorphous $CaTiO_3$ compounds. Because the Ti plate is used as an anode, it has a tendency to lose electrons to produce Ti^{4+} ions, which will react with Ca^{2+} ions to form the $CaTiO_3$ [4];

$$Ti \rightarrow Ti^{4+} + 4e^- \quad \textbf{(4.3)}$$

$$Ca^{2+} + Ti^{4+} + 3O^{2-} \rightarrow CaTiO_3 \quad \textbf{(4.4)}$$

Here, O^{2-} ions come from the dissociation of water molecules in the electrolytes, which occurs at the surface of Ti anode during the MAO. As the second step, the $H_2PO_4^-$ ions make H_3O^+ (H^+) ions, and these are combined with the $CaTiO_3$. As a result, $TiO(OH)_2$ is produced via exchange of the Ca^{2+} ions coming from $CaTiO_3$ with H_3O^+ ions [4];

$$CaTiO_3 + 2H^+ \rightarrow TiO(OH)_2 + Ca^{2+} \quad \textbf{(4.5)}$$

As the third step, the $TiO(OH)_2$ forms various Ti–OH groups at the Ti surface due to thermal energy originated from the micro-arcing, and these Ti–OH groups induce the formation of bone-like apatite. As the final step, Ti–OH groups forming right on the $CaTiO_3$/Ti attract the Ca^{2+} and PO_4^{3-} ions from the electrolytes and form the HA nuclei. The continuous supply of the Ca^{2+} and PO_4^{3-} ions from the electrolytes can cause the HA crystal growth. The thermal energy from the micro-arcing can also

assist the diffusion of ions for the nucleation and crystal growth of the HA [4]. HA formation mechanism is depicted in Figure 4.15.

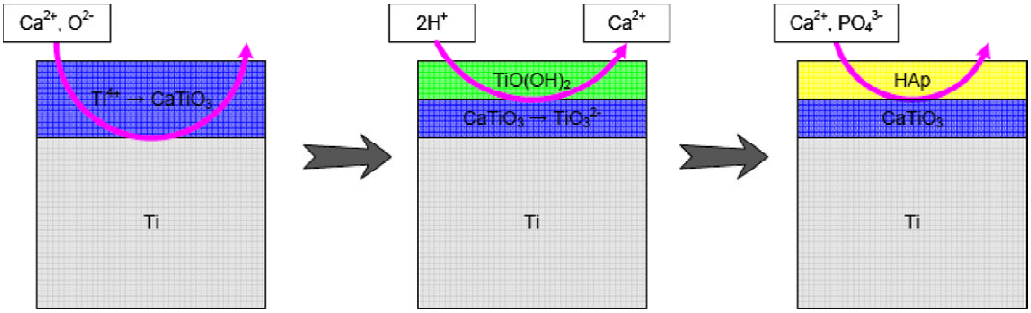

Figure 4.15: Schematic diagram showing the HA nanocrystal formation in the micro-arc oxidized (MAO) samples prepared using an electrolyte containing 0.05M KH_2PO_4 and 0.10 M $CaCl_2$ [4].

It was also found that as the concentration increases, the number of micro arcs decreases during the MAO process, leading to a coarse microstructure which can give benefit to the HA films, since it can promote the intergrowth of natural bones and accelerate interfacial bonding between the implants and the natural bones. Another interesting characteristic was that numerous nanocrystals, believed to be HA, were formed at the surface of the films, and the number of these nanocrystals gradually increased with the concentration of $CaCl_2$. All the samples showed formation of spherical-shape nanoparticles with the size distribution of 50–100 nm, and the density of the nanocrystals showed steady increase. The increase in the nanocrystal density with the $CaCl_2$ concentration was claimed to originate from the increase in the number of Ti–OH hydroxyl groups. The high density hydroxyl groups can incorporate with Ca^{2+} and PO_4^{3-} ions actively to form the crystalline HA. It was suggested as the most probable mechanism for the HA formation that, the high density hydroxyl groups of $TiO(OH)_2$, formed by the reactions between the amorphous $CaTiO_3$ interlayer and the H^+ ions from the dissolution of the KH_2PO_4, can play a key role in the nucleation and crystal growth of HA by attracting Ca^{2+} and P^{5+} ions in the electrolytes [4].

Also one interesting result was that, despite the use of the same number of moles of KH_2PO_4 and K_2HPO_4 at a fixed $CaCl_2$ concentration, the atomic % of Ca in the samples prepared using the electrolyte of KH_2PO_4 was 7.8 times higher than that of K_2HPO_4 [4].

Yong Han et al. [19] investigated the morphology, elemental composition and phase components of the films as a function of the electrolytes composition and concluded that only the film, oxidized in CA and β-GP containing electrolyte at high voltage (500 V), could compose $CaTiO_3$, β-$Ca_2P_2O_7$ and α-$Ca_3(PO_4)_2$ which could induce an apatite layer on the surface, exhibiting bioactivity [19]. The cross section of oxide film formed at 500 V is seen in Figure 4.16.

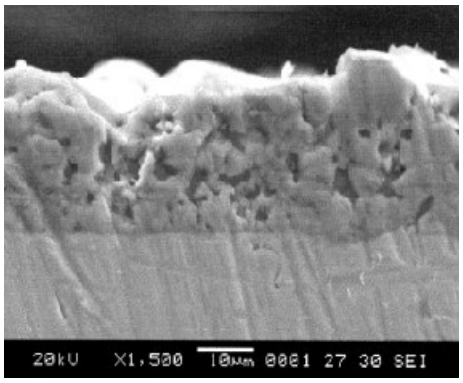

Figure 4.16: Cross-sectional view of the MAO sample formed in the CA and β-GP-containing solution at 500 V [19].

At the same voltage, the films formed in CA and β-GP containing electrolytic solution became more rough compared with the films formed in Na_2CO_3 and Na_3PO_4 containing solutions. The sample oxidized with CA and β-GP at 500 V subjected to immersion for 40 days clearly exhibited apatite. The intensity of the apatite peaks became strong after 50 days, suggesting that the thickness of the formed apatite layer increased with immersion time. Nano-crystallized characteristic of the matrix was observed in the films formed in only CA containing electrolytic solution [19].

In another study, Huang Yong et al. [21] performed a micro arc oxidation in a cerium nitrate containing electrolyte and obtained not only a high crystallinity of HA yielding higher rates of cell proliferation but also anti-bacterial effects comparable to the ones in which silver salts are used [21].

Recently, soaking the implants in supersaturated calcium phosphate solutions containing some biologically active molecules has been developed to form the coprecipitate of active molecules and apatite on the surface of the implants. When implanted, these loaded molecules will release in the body and be of great value for the integration of the implants with the host tissue [17].

As a result, the type of electrolyte, applied voltage and process time are important parameters that must be optimized for better results.

4.2 Effect of Hydrothermal Treatment

Micro arc oxidation (MAO) has been developed as a room-temperature electrochemical process suitable for the formation of native ceramic films on metals such as Al, Mg, and Ti to improve their wear and corrosion resistance. People also have tried to simply overcoat hydroxyapatite (HA) at the surface of Ti using Ca and P containing electrolytes by MAO. However, the only MAO-treated samples showed formation of amorphous films with low content of Ca and P ions, and could not form crystalline HA. They proposed that the concentration of hydroxyl groups (Ti–OH), which can play a key role in inducing bone-like apatite including HA, were insufficient in these samples. Thus, the hydrothermal treatment after the MAO was proposed as a method to increase the crystallinity of the films. There exist two main effects of the hydrothermal treatments using a high-temperature and high-pressure autoclave. One is that the hydrothermally treated samples can form sufficient Ti–OH groups at the surface, which serve as the sites for the nucleation of HA crystals, and the other is that the Ca and P ions combined with the hydroxyl groups can transform into the crystalline HA at the applied temperature and pressure. Thus, to date, no successful results have been reported on producing the highly crystalline HA films through the single step MAO process using electrolytes containing Ca and P [4].

Fu Liu et al. [2] performed a hydrothermal treatment on micro arc oxidized samples at 190^{o} C for 10h at the bottom of an autoclave, in which 20 ml of water solution whose pH was adjusted to 11.0 – 11.5 by adding NaOH. HA crystals were found to be precipitated after this treatment, and the number of precipitates increased as the pH of the water solution was raised (from 7.0 to 11.0) as depicted in Figure 4.17. Also the rough and porous surface was retained after treatment [2].

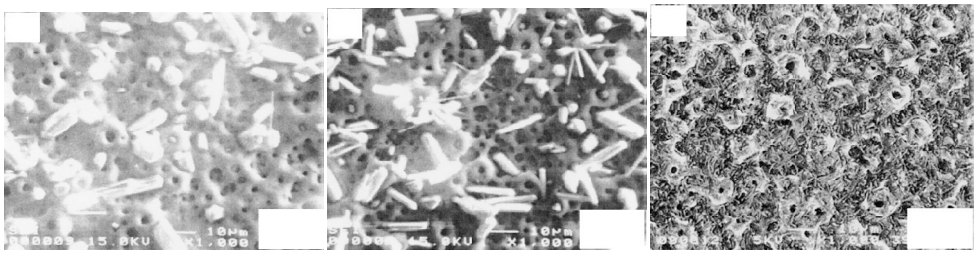

(a) (b) (c)

Figure 4.17: SEM micrographs of oxide films treated hydrothermally at 190°C for 10h (a) solution pH 7.0 (b) solution pH 9.0 (c) solution pH 11.0 [2].

The technique of forming hydroxyapatite by microarc oxidation and hydrothermal treatment has obvious advantages compared to the conventional sol-gel method used to form a hydroxyapatite coating. The bonding strength of the hydroxyapatite coating produced by this technique is higher than that of the hydroxyapatite coating produced by the sol-gel method. On the other hand, conventional-sol-gel-derived coatings are usually provided by a dip-coating method, which consists of several coating-heating cycles to obtain the necessary thickness for apatite deposition, and thus, is quite time-consuming [2]. However, Yong Han et al. [26] indicated that HA/TiO_2 coatings obtained by hydrothermal treatment, exhibited a relatively low bond strength.

The formation of HA crystals is affected by two factors [2]:

1. the nucleation of HA
2. the diffusion of Ca and P from the inner layer towards the film surface

It is well known that Ti-OH groups induce HA nucleation. When the oxide films are exposed to the water solution in an autoclave and hydrothermally treated at 190°C, Ti-OH groups are produced on the film surface. Li et al. [29] showed that porous anatase induces HA nucleation, and dense single-crystal anatase does not [29]. Yang et al. [30] also described that anatase TiO_2 with a porous structure formed by microarc oxidation induces HA formation when immersed in a simulated body fluid containing Ca^{2+} and PO_4^{3-} ions [30]. HA nuclei are formed due to the effects of Ti-OH groups and the porous structure on the surface on inducing HA nucleation, and they spontaneously grow and give rise to HA products according to the following reaction [2]:

$$10Ca^{2+} + 6PO_4^{3-} + 2OH^- \leftrightarrow Ca_{10}(PO_4)_6(OH)_2 \quad \textbf{(4.6)}$$

It is clear that a high OH^- concentration is beneficial for the formation of hydroxyapatite. As a result, the amount of hydroxyapatite crystal precipiated

gradually increases with increasing water solution pH. The reaction 4.6 occuring on the film surface, results in a deficiency of Ca and P in the surface reaction areas. Consequently, Ca and P diffuse towards the surface from the inner layer in order to compensate for the deficiency of Ca and P. Thus, the hydrothermal treatment is required to make Ca and P diffuse from the inner layer to the surface [2].

In biological means, Y. M. Zhang et al. [20] evaluated the effect of hydrothermal treatment (HT) on osteoblast behaviour. Samples oxidized at 350 V in β-GP and CA electrolyte were hydrothermally treated in an autoclave with 180°C for 4 h and cooled within the autoclave. The pH value was modified by ammonia with the rate of 1:9 (v/v) in distilled water, which resulted in the formation of HA crystals (sized several hundred nanometers) inducing roughness on the micro porous surface [20]. The crystals can be observed in Figure 4.18.

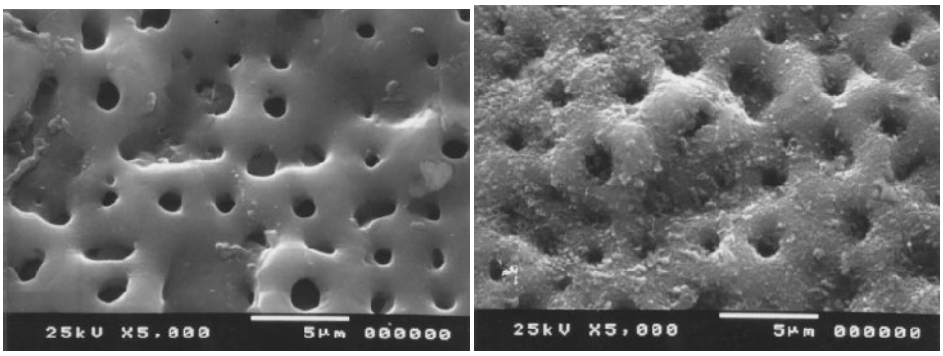

(a) (b)

Figure 4.18: Morphology of the surfaces (a) MAO (b) MAO-HT surface [20].

The contact angle of hydrothermally treated samples decreased due to porous matrix action, suggesting that the surface energy increased. Also a faster cell adhesion due to higher surface energy was observed after hydrothermal treatment, meanwhile, the cell proliferation rate on MAO–HT was significantly lower than that on MAO and untreated cp-Ti. This decrease was attributed to the different and perhaps less suitable surface texture and chemical composition of the HA crystals obtained on MAO–HT samples [20].

In another study, Won Hoon Song et al. [22] prepared titania films by micro-arc oxidation of Ti in an electrolytic solution containing calcium acetate monohydrate (CA), and evaluated their apatite inducing ability in a simulated body fluid (SBF). The $CaTiO_3$-embedded titania was obtained at higher voltages (>300 V). When

immersed in SBF, no apatite was induced in all the MAO specimens irrespective of the presence of $CaTiO_3$, which has been claimed to be an apatite inducer. However, after a hydrothermal treatment at 250°C for 2h, apatite was formed on the surfaces of the $CaTiO_3$-embedded titania after 28 days as seen in Figure 4.19, which was closely related to the formation of amorphous $Ca(OH)_2$ and presumably surface Ti–OH groups [22].

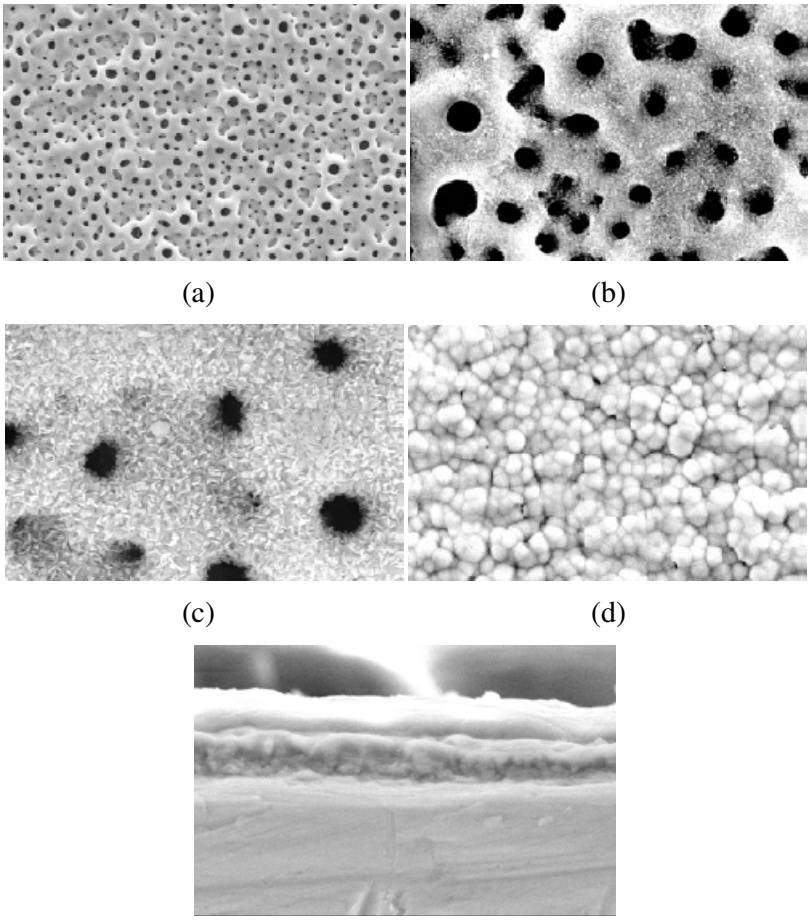

Figure 4.19: SEM micrographs of (a) MAO at 350 V (b) hydrothermally treated at 250°C for 2 h (c) hydrothermally treated MAO sample immersed in SBF for 28 days (d) for 56 days (e) cross section after 56 days in SBF [22].

Hamada et al. reported that hydrothermal modification in a CaO solution enhanced the precipitation of apatite on the titanium surface either by increase of calcium titanate or increase of calcium oxide (hydroxide) [31].

According to Won Hoon Song et al. [22], the porous microstructure was unchanged after hydrothermal treatment, but the surface became rough and numerous precipitates were formed. EDS analysis indicated that these precipitates contained a

considerable amount of Ca. Therefore, it was concluded that Ca ions in the micro-arc-oxidized layer diffused out to the surface and reacted with water, forming the amorphous calcium hydroxide ($Ca(OH)_2$), detected in FT-IR analysis. Furthermore, the micro-dissolution of Ca^{2+} ions from the oxidized layer occurred during the hydrothermal treatment. It was speculated that a large number of Ti–OH groups were formed via exchange of the Ca^{2+} ion with H_3O^+ ion during the hydrothermal treatment [22].

After 56 days of immersion in SBF, broad apatite peaks were detected and FT-IR spectrum showed the absorption bands of PO_4^{3-} and CO_3^{2-}. The broad nature of the apatite peaks was believed to be due to a defective, poorly crystalline apatite formation. The porous surface completely disappeared and the entire surface was covered with the spherical apatite grains of about 5 μm in size. As a result, it was concluded that the provision of abundant Ti–OH groups and the enrichment of calcium had triggered the apatite nucleation. The $CaTiO_3$ phase appeared to provide little contribution to the apatite induction in their study [22].

Ping Huang et al. [15] heated the micro arc oxidized titanium in high pressure steam in an autoclave at 160 and 180°C, respectively, for different time periods, and the pH of water was adjusted to 11–12 by adjustment of ammonia content. The HA crystals gradually grew in high pressure steam, consuming the Ca and P contained in the MAO layer. It is said that the quantity of the Ca and P in the layer affects the Ca/P ratio of apatite, which forms later in hydrothermal synthesis. The formed HA particles were cooled from the molten state; the HA layer thus consisted of very fine crystallites and high crystallinity, as the intensity of the HA peaks became stronger and stronger, which could prevent or slow the pace of degradation [15].

These crystals were reported to have a Ca/P ratio of about 1.2 which is lower than those of HA and Ca-deficient HA (the Ca/P ratio of which are 1.67 and 1.50 –1.67, respectively). This may be because the EDXA result was actually a combination from HA crystals and the matrix that had a Ca/P ratio about 0.8. So, if the layer has a high content of Ca/P, it is believed that the Ca/P ratio in the HA particles will possibly be near 1.67. Otherwise, Ca deficient HA will be reached [15].

The advantages of this layer obtained by this hybrid method of MAO and heat treatment, regarding the implants include the followings [15-29-32-33]:

- First, the porous surface layer can encourage bony ingrowth to provide a morphological fixation of the implant to the bone, essentially a mechanical fixation [32]. The surrounding bone could ingrow uniformly into pore space to the bottom of the porous layer and be tightly bonded to the implants.
- Second, the bony ingrowth into the porous layer is appreciably accelerated, because the bone-like apatite formed makes the surface bioactive. It has been demonstrated that the HA layer on titanium and its alloy implants enhances rapid bone formation because of improved osteoconductive properties [33].

Therefore, the above two effects would be attained soon after implantation. It is expected that immobilization time prior to mechanical fixation will be minimized.

- Third, the layer contacts with the substrate very well. It offers not only a mechanical interlocking force between the bone and the porous surface, which is necessary for a long-term clinical use, but also a chemical bonding attained by the apatite-layer, which acts on short-term fixation [29]. So, through the layer both chemical bonding and mechanical interlocking can be utilized to improve the implant surface and an the ideal interlocking attachment will be achieved.

Additionally, this method can form uniform, even layers on implants with complex surface geometries, such as screws and metal porous coatings [15].

4.3 Effect of Ultraviolet Irridation

In order to enhance the bioactivity and cell response of micro arc oxidized titania coatings, UV irridation of coated samples in distilled water were performed by Yong Han et al. [5].

Compared with the MAO coating, the UV-irradiated coatings did not exhibit any obvious change in surface roughness, morphology, grain size and phase component; however, they had more abundant basic Ti–OH groups and became more hydrophilic because the water contact angle decreased significantly from 17.9 ± 0.8^{o} to 0^{o}. In simulated body fluid (SBF), bonelike apatite forming ability was reported to be significantly stronger on the UV-irradiated coatings than the MAO coating [5].

In the analysis of UV irradiated coatings, the amount of the basic Ti-OH groups increased as the irradiation time was prolonged, from which the enhanced apatite

forming ability was thought to stem. And also, the wettability of the coating increased, although the surface roughness did not change. The reason was the abundant hydroxyl groups on the surface. On the UV irradiated coating for 2h, sphere-like particles were observed at a short immersion period of 13 days, and a dense precipitate layer fully covered the surface after immersion for 17 days as shown in Figure 4.20. On the other hand, initial cell attachment due to the higher surface energy, cell proliferation and ALP activity were reported to enhance [5].

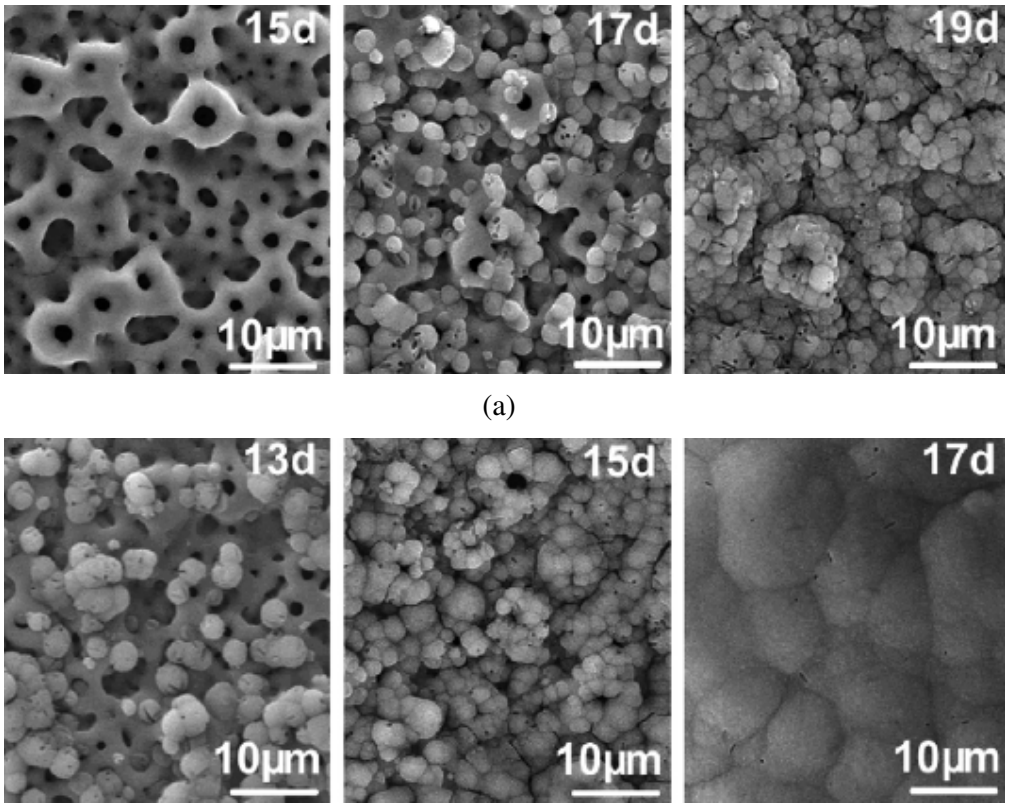

Figure 4.20: Surface morphologies of coatings after immersion in SBF for different times (a) UV-0.5h (b) UV-2h. The notifications on top right-hand corner indicates the number of days in SBF [5].

The results indicated that UV irradiated TiO_2 coatings possessed good apatite forming ability, the mechanism of which can be discussed as follows [5]:

Anatase TiO_2 is an n-type semiconductor oxide with the band gap of about 3.2 eV. It presents intrinsic light absorption when the wavelength of irradiating light is lower than 380 nm, giving rise to photo-excitation and resulting in the generation of electron-hole pairs. The electrons tend to reduce the +4 charged Ti to the +3 state, and the generated hole reacts with the bridging site oxygen, resulting in oxygen

vacancy [34]. When the surface defect is generated, water and oxygen compete to dissociatively adsorb on it [35]. UV irradiation in water facilitates more basic Ti–OH generation than in air. The amount of basic Ti–OH groups on the UV-irradiated coatings increases as the irradiation time in distilled water is prolonged. These results suggest that the oxygen vacancy (O^-) is favorable for dissociating water, resulting in abundant basic Ti–OH groups on the surface of the UV-irradiated TiO_2 coating as follows [5]:

$$(Ti^{3+} - O^-) + H_2O \longrightarrow Ti\text{-}OH + H_2 \qquad \textbf{(4.7)}$$

where Ti in the Ti–OH group is +4 charged.

The surfaces of the UV irradiated coatings contain some acidic Ti-OH groups as well as basic Ti-OH groups. The basic Ti–OH groups are believed to be negatively charged. It is believed that the enhanced apatite forming ability of the UV-irradiated TiO_2 coating is related to the abundant basic Ti-OH groups but not to the acidic Ti-OH groups. In the SBF with pH 7.4, the abundant basic Ti-OH groups make the UV irradiated TiO_2 coating surface more negatively charged. The coating then selectively combines with the positively charged Ca^{2+} ions in the SBF to form Ca-rich calcium phosphate. As the calcium ions accumulate, the surface appears positively charged, and thus combines with PO_4^{3-} and CO_3^{2-} ions in the SBF to form carbonated HA with a low Ca/P ratio (bonelike apatite) [5].

Interestingly, Amparo M. Gallardo-Moreno et al. [6] claimed that, while human cell adhesion, in other words the biocompatibility, was not altered by UV irradiation of Ti6Al4V alloy, this treatment reduced not only the initial bacterial adhesion rates but also the retention ability of them on the surface [6]. This bacterial behaviour should be examined on the micro arc oxidized titanium irradiated by UV.

Baikun Li and Bruce E. Logan [36] demonstrated that exposure of metal oxide surfaces to UV light is an effective, and non-polluting method for reducing biofouling at surfaces. The UV light treatment by itself is also effective at killing the bacteria on the surfaces. The main effect of the UV light is to decrease the surface hydrophobicity, although photocatalysis can further decrease bacterial adhesion [36].

Titania (TiO_2) coatings with nanostructural surfaces, prepared using plasma spraying technology, were irradiated via ultraviolet light in simulated body fluids for 12 and 24h to improve their bioactivity by Xuanyong Liu et al. [37]. The ability of apatite

formation on the nano TiO_2 surface was improved with the increase of UV irradiation time. The in vivo results reveal that the as-prepared TiO_2 coating with nanostructural surface can not induce the formation of new bones during the implantation period, but the UV irradiated TiO_2 coating with nanostructural surface could do so during an implantation time longer than 2 months [37].

Yong Han et al. [38] prepared macroporous and nano-crystallized monoclinic zirconia (m-ZrO_2) film by micro-arc oxidation. UV irradiation of the ZrO_2 film did not alter surface morphology, grain size and phase component, however, significantly improved hydrophilicity and bioactivity of the film as shown in Figure 4.21. The enhanced hydrophilicity and bioactivity were thought to result from the abundant basic Zr-OH groups on the UV-irradiated film, which have relative long-term stability [38].

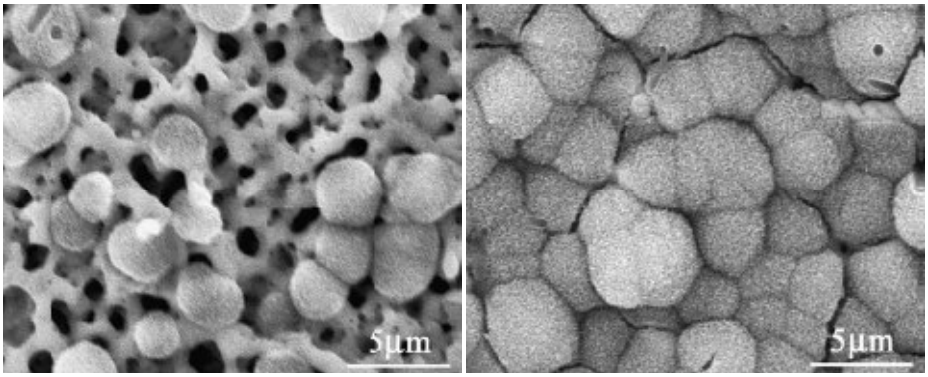

(a) (b)

Figure 4.21: Surface morphologies of the MAO-UV film after immersion in SBF for (a) 10 days (b) 15 days [38].

As a result, UV irradiation is a promising technique to produce TiO_2 films, having high hydrophilicity and high apatite forming ability. Another advantage is that, it has an anti-bacterial effect.

4.4 Anti Bacterial Effect

The moderately roughened surface of dental implant is well known to enhance osseointegration. However, rough implant surface, as compared to smooth surfaces, is thought to be a higher risk of bacterial accumulation when exposed to the oral cavity [8]. Also, the resistivity and band gap density of states of the film were also reported to have influence on bacterial adhesion and biological interactions [7].

Microbial infection is one of the most destructive complications related to implants because antimicrobial therapy usually lacks efficacy at the point when the infection process is detected. Controlled antibiotic release from the biomaterial and antibiotic loading on the biomaterial surface are strategies employed to overcome this problem, but there is concern about the increased microbial resistance to antibiotics that these procedures may induce. An alternative approach in the fight against bacterial adhesion focuses on the modification of physico-chemical surface properties of the biomaterial, such as hydrophobicity, surface tension and electrical surface potential, because they are crucial in the initial approach and further retention of bacterial cells to various surfaces. On the other hand, adequate adhesion of osteoblasts and their progenitors to the implant surface ultimately influences their capacity to proliferate and perform their specific functions. Surface characteristics of materials, such as chemistry and surface energy, play an essential role in cell adhesion to biomaterials. Thus, any modification of the surface characteristics introduced in order to diminish adhesion of microorganisms to a biomaterial should not compromise bone-forming cell adhesion [6].

It is generally believed that rapid osseointegration with titanium compared with that of other metallic implants is due to the ease with which calcium phosphates and serum proteins are adsorbed on titanium surfaces. This implies, however, that the calcium and pellicle in saliva are adsorbed and form on titanium surfaces, and then, that oral bacteria adhere and colonize on titanium surfaces. This situation leads to the probable risk of plaque formation to titanium implants exposed to the oral cavity. Therefore, it is important to provide a source of antibacterial activity as well as to inhibit the initial adhesion of oral bacteria to titanium surfaces [39].

Bacteria cells grow by a process called binary fission in which one cell doubles in size then splits in half to produce two identical daughter cells. If a bacterial population in an environment is without any growth restrictions by nutrient or metabolic products, the number of bacteria increases as an exponential function of time [40].

Microbial plaque accumulation surrounding dental implants may develop into peri-implantitis or peri-implantoclasia, which is defined as inflammation or infection around an implant, with accompanying bone loss. It is important to maintain plaque-free surfaces on both supra and sub-gingival portions of dental implants to prevent

peri-implantitis. There are at least two methods of inhibiting the formation of microbial plaque. The first method is to inhibit the initial adhesion of oral bacteria. The second method is to inhibit the colonization of oral bacteria, which involves surface antibacterial activity. Titanium itself has no antibacterial activity, but there is a probable risk of plaque formation on titanium implants. Nevertheless, few experiments have been conducted on the surface modification of titanium implants to inhibit the colonization of oral bacteria [39].

The modification of hydroxyapatite films by fluorine and zinc via sol-gel method considerably reduced the attachment of the bacteria *P. Gingivalis*, according to Y.L. Jeyachandran et al. [7].

Yoshinari et al. [39] evaluated the antibacterial effect of surface modifications to titanium on *Porphyromonas gingivalis* ATCC 33277 and *Actinobacillus actinomycetemcomitans*. Surface modifications were performed with dry processes including ion implantation (Ca, N, F), oxidation (anode oxidation, titania spraying), ion plating (TiN, alumina), and ion beam mixing (Ag, Sn, Zn, Pt) with Ar^+ on polished pure titanium plates. F^+ implanted specimens significantly inhibited the growth of both *P. Gingivalis* and *A. actinomycetemcomitans* more than the polished titanium. The other surface-modified specimens did not exhibit effective antibacterial activity against both bacteria. No release of the fluorine ion was detected from F-implanted specimens under dissolution testing. This result and the characterization of the F-implanted surfaces suggested that the possible antibacterial mechanism of the F-implanted specimen was caused by the formation of a metal fluoride complex on the surfaces. In addition, F-implanted surfaces did not inhibit the proliferation of fibroblast L929-cells. These findings indicate that surface modification by means of a dry process is useful in providing antibacterial activity of oral bacteria to titanium implants exposed to the oral cavity. Fluoride is widely used as a highly effective anticaries agent in dental fields, and fluorine ions released from fluoride can affect bacterial metabolism as an enzyme inhibitor [39].

In recent years, the use of inorganic antibacterial agents has attracted interest for control of microbes. The key advantages of inorganic antibacterial agents are improved safety and stability. The most antibacterial inorganic materials are the ceramics containing antibacterial metals, such as silver and copper. Hydroxyapatite (HA) has been widely used for bone repair and substitute because of its good

biocompatibility and the cation exchange rate of HA is very high with silver ions. Thus silver ions substituted HA was prepared to study the antimicrobial effects against bacteria. Silver, known as a disinfectant for many years, has a broad spectrum of antibacterial activity and exhibits low toxicity towards mammalian cells [8].

4.4.1 Silver

Silver has been in use since time immemorial in the form of metallic silver, silver nitrate, silver sulfadiazine for the treatment of burns, wounds and several bacterial infections [41].

Silver is effective against a broad range of aerobic, anaerobic, Gram-negative and Gram-positive bacteria, yeast, filamentous fungi and viruses. In addition to the antimicrobial properties, silver also appears to have anti inflammatory properties, as suggested by the loss of rubor in chronic wounds treated with colloidal silver [42].

The antimicrobial properties of silver were well known to the ancient Egyptians and Greeks, for example Hippocrates mentions silver as a treatment for ulcers. Since then silver has been widely used as an antimicrobial agent in applications such as wound dressings and as surface coatings for, e.g. catheters. Silver has also been incorporated into bioglass. Silver ions (Ag^+) interact strongly with electron donors and the antimicrobial activity of Ag primarily involves interactions with sulphydryl groups in proteins also reacts with other cellular components such as nucleic acids. Silver has been shown to inhibit energy production by inhibition of the respiratory chain of *E. Coli.* Indirect toxicity may also arise from salt formation with silver ions that results in a chloride or anion limitation within the cell. Nanocrystalline silver also releases Ag^0 and has been shown to rapidly kill bacteria and fungi. Although Ag^+ is rapidly inactivated by interaction with organic matter, Ag^0 is much more stable [43].

Silver composites with a tailored slow silver-release rate are currently being investigated for various applications [40]. Silver has an oligodynamic effect, that is, silver ions are capable of causing a bacteriostatic (growth inhibition) or even a bactericidal (antibacterial) impact. It has been suggested that DNA loses its replication ability once the bacteria have been treated with silver ions [40].

In a study, the composite which contains Ag^+ and nanosized hydroxyapatite with TiO_2 was deposited onto titanium via dipping method by Anchun Mo et al. [8]. And

a 99% antibacterial effect on *S. Aureus* and *E. Coli* was obtained after 24h incubation with a good bioactivity [8]. TEM and SEM images of nAg-HA/TiO_2 are displayed in Figure 4.22.

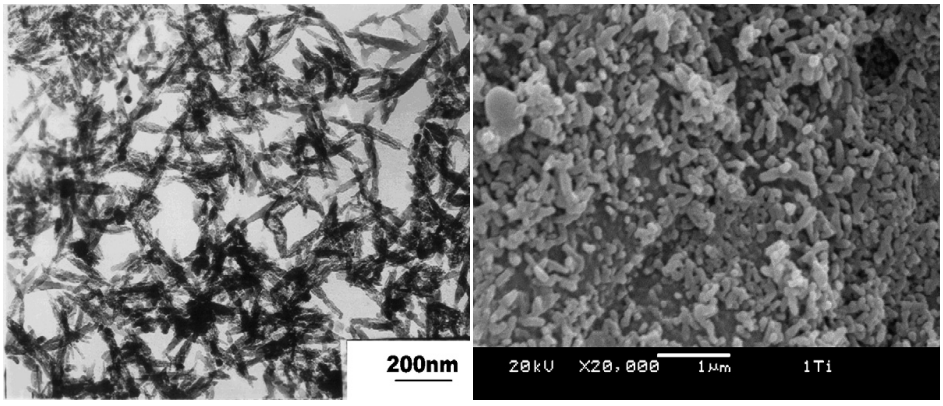

(a) (b)

Figure 4.22: (a) TEM photograph of nAg–HA/TiO_2 (b) SEM image of the surface structure of nAg–HA/TiO_2 coated plate [8].

Also, TiO_2 is said to have a positive antibacterial effect which enhance the bactericidal effect of Ag and decrease the Ag concentration as well. Ag inhibits the DNA synthesis with direct binding on the bacterial DNA. Ag also adsorbs the protein on the surface of the bacterial membrane; influencing membrane synthesis with S–Ag bonds. The Ag bactericidal effect is of great use for preventing the bacterial infection at osseointegration phases [8].

H. Q. Tang et al. [44] obtained anti-bacterial effect against *S. Aureus* and *E. Coli* on pyrolitic carbon (used as an artificial heart valve) by ion implantation of Ag^+ ions depending on the ion dose. Ag^+ implanted pyrolytic carbon did not show any cytotoxicity [44].

G. J. Chi et al. [45] also obtained antibacterial activity on aluminum by electrodeposition of Ag. By using AC electrodeposition, the Ag nanowires were prepared in pores of the anodized aluminum film, and the diameters of the nanowires were 10 or 25 nm [45].

TiO_2 photocatalytic disinfection also seems to be a promising technique. To obtain higher bactericidal activity under weak UV intensity, TiO_2 films deposited with antibacterial metals such as copper and silver have been developed [46]. Ag is capable, under the correct conditions, of improving TiO_2 photoactivity. The addition of Ag promotes the charge separation of the electron–hole pairs from TiO_2 after

photon absorption by acting as an electron sink. It has been pointed out that the addition of Ag can modify the grain sizes of the TiO_2, so increasing the surface area and hence also the photoactivity [43].

W. Chen et al. [48] examined the effect of in vitro antibacterial activity and in vitro cytotoxicity of co-sputtered silver (Ag)-containing hydroxyapatite (HA) coating and found positive results, while Yoshinari et al. [38] reached success with F-ion implantation on titanium [39].

M. Stigter et al. [47] applied carbonated hydroxyapatite (CHA) coatings onto titanium implants by using a biomimetic precipitation method. And, then incorporated different antibiotics into the CHA coatings and studied their release and efficacy against bacteria growth in vitro. Antibiotics incorporated in CHA coatings on titanium implants might be used to prevent post-surgical infections and to promote bone-bonding of orthopedic devices [47].

Silver doped titanium oxide coatings were prepared via argon ion beam assisted deposition in an oxygen atmosphere by Feng Zhang et al. [48]. Ag was found in metallic state on coating and a higher surface tension measured as the concentration of Ag increased [48].

4.4.2 Silver Nitrate

Silver has long been known to exhibit a strong toxicity to a wide range of microorganisms; for this reason silver-based compounds have been used extensively in many bactericidal applications. Silver compounds have also been used in the medical field to treat burns and a variety of infections. There are several silver salts for use as an antibacterial agent, such as silver nitrate, silver sulphadiazine (SSD), silver sulphadiazine/chlorhexidine, SSD with cerium nitrate [49-50].

In 1700, silver nitrate was used for the treatment of venereal diseases, fistulae from salivary glands, and bone and perianal abscesses. In the 19th century granulation tissues were removed using silver nitrate to allow epithelization and promote crust formation on the surface of wounds. Varying concentrations of silver nitrate was used to treat fresh burns. In 1881, Carl S.F. Crede cured opthalmia neonatorum using silver nitrate eye drops. Crede's son, B. Crede designed silver impregnated dressings for skin grafting. In the 1940s, after penicillin was introduced the use of silver for the treatment of bacterial infections minimized. Silver again came in picture in the 1960s

when Moyer introduced the use of 0.5% silver nitrate for the treatment of burns. He proposed that this solution does not interfere with epidermal proliferation and possess antibacterial property against *Staphylococcus aureus, Pseudomonas aeruginosa* and *Escherichia coli*. In 1968, silver nitrate was combined with sulfonamide to form silver sulfadazine cream, which served as a broad-spectrum antibacterial agent and was used for the treatment of burns [41].

Spacciapoli et al. (2001) demonstrated the use of silver nitrate for the treatment of periodontal pathogens. He found silver nitrate more efficient than antibiotics for the treatment of oral cavity of periodontal infections [41]. Also the solubility of silver nitrate in water is highest among all the silver salts present [51].

Chai et al. [45] synthesized silver doped titania by mixing silver nitrate and the precursor of titania. Then, examined the effects of thermal treatment and found that, the release rate of silver ion of powder treated at the relatively low temperature is larger than that of powder treated at the relatively high temperature. The antibacterial tests show that the antibacterial activity of silver-doped titania powders is excellent against *E.coli* and *S. aureus*, and the antibacterial activity of powders weakens with the increase of the calcination temperature. Composite powder exhibits stronger antibacterial activity as more silver ions are released from powder; thus, the release rate of silver ion of composite powder becomes a main factor to evaluate the antibacterial activity [52].

4.4.3 Nanosilver

Due to the emergence of several antibiotics the use of these silver compounds has been declined remarkably. Instead, nanotechnology is gaining tremendous impetus in the present century due to its capability of modulating metals into their nanosize, which drastically changes the chemical, physical and optical properties of metals. Metallic silver in the form of silver nanoparticles has made a remarkable comeback as a potential antimicrobial agent. The use of silver nanoparticles is also important, as several pathogenic bacteria have developed resistance against various antibiotics. Hence, silver nanoparticles have emerged up with diverse medical applications ranging from silver based dressings, silver coated medicinal devices, such as nanogels, nanolotions, etc. [41].

Nanosilver particles are generally smaller than 100 nm and contain 20-15,000 silver atoms. At nanoscale, silver exhibits remarkably unusual physical, chemical and biological properties. Due to its strong antibacterial activity, nanosilver coatings are used on various textiles but as well as coatings on certain implants. Further, nanosilver is used for treatment of wounds and burns or as a contraceptive and marketed as a water disinfectant and room spray. Thus, use of nanosilver is becoming more and more widespread in medicine and related applications and due to increasing exposure toxicological and environmental issues need to be raised. In sharp contrast to the attention paid to new applications of nanosilver, few studies provide only scant insights into the interaction of nanosilver particle with the human body after entering via different portals. Biodistribution, organ accumulation, degradation, possible adverse effects and toxicity are only slowly recognized and this review is focusing on major questions associated with the increased medical use of nanosilver and related nanomaterials [53].

Silver nanoparticles act primarily in three ways against Gram-negative bacteria [50]:

(1) nanoparticles mainly in the range of 1–10 nm attach to the surface of the cell membrane and drastically disturb its proper function, like permeability and respiration

(2) they are able to penetrate inside the bacteria and cause further damage by possibly interacting with sulfur and phosphorus containing compounds such as DNA

(3) nanoparticles release silver ions, which have an additional contribution to the bactericidal effect of the silver nanoparticles

Silver nanoparticles may deplete the antioxidant defense mechanism, initiating an inflammatory response and perturbation and destruction of the mitochondria take place. Cell death is a final result. Finally for silver, whether nano-sized or not, there is always the problem of argyia [53].

All in all, it is very important to develop some kind of antibacterial biomaterial which can modify the implant surface to achieve excellent antibacterial activity as well as cell compatibility [8].

5. EXPERIMENTAL

This study focuses on the biological and anti-bacterial activities of micro-arc oxidized (MAO) commercially pure titanium (CP-Ti). In this respect, MAO process was conducted in a silver nitrate ($AgNO_3$) containing electrolyte and samples were exposed to Ultra Violet (UV) light after the MAO process.

5.1 Sample Preparation

Commercially pure titanium (99.6% Ti) discs, having a thickness of 3mm, were cut from 16 mm diameter rods, having a diameter of 16 mm and were ground by #240-#1200 SiC sandpaper gradually. Then, they were cleaned with acetone and distilled water.

A group of samples were oxidized in an aqueous electrolyte containing $(CH_3COO)_2Ca.H_2O$ and Na_3PO_4 at positive voltages between 350-500 V and negative voltages between 55-83V for 5 minutes at room temperature. The micro-arc oxidation apparatus having 30 kW power supply was utilized in this study (Figure 5.1).

Another group of samples were oxidized in the same electrolyte but, $AgNO_3$ was added in different concentrations differing from 1 to 4 g/L. The pH of the solution showed a decreasing trend from 10 to 8, as the concentration of silver nitrate increased. After the treatment, samples were rinsed with distilled water and dried with hot air.

After the MAO process, some of the samples were irradiated by UV-light, with an intensity at 366 nm, in distilled water for 2h at room temperature.

Figure 5.1: Micro-arc oxidation apparatus [57].

5.2 Characterization Tests

Characterization of the samples were carried out by, macroscopic and microscopic examinations via optical microscope and scanning electron microscope (SEM), X-ray diffraction analysis, surface roughness measurements and contact angle measurements.

The surface morphologies of the coatings were examined by a SEM at different magnifications. The composition of the surface layer was analyzed with an energy dispersive spectroscope (EDS) incorporated into the SEM. Cross-section images were collected and the thickness of the oxidized layer was measured by using Leica optical microscope. Qualitative phase analysis was made with X-ray diffractometer (XRD, GBC-MMA) using Cu K_α radiation with a scan range between 20-80^o at a step of 0.020^o. The average surface roughness (Ra) of the samples was quantified using a Veeco Dectac 6M surface profilometer under 5 mg load, with a scan distance of 5000 μm. Contact angles of liquid droplets were measured using sessile drop method with KSV Cam 200 apparatus equipped with a camera. A 8 μl droplet of distilled water and SBF were dropped on the sample surfaces and images were collected with the camera. Adhesion of the oxide layer was evaluated by Rc tests by utilizing Zwick Rockwell hardness tester under 150 kg load. The imprints and their surroundings were examined by a Leica optical microscope whether any cracks or delaminations due to the applied load were developed or not.

5.3 Bioactivity Tests

In vitro biocompatibility tests were conducted in a stimulated body fluid (SBF) at 37^{o} C having a concentration shown in Table 5.1. The duration of tests differed from 14 days to 56 days. The pH of the solution was adjusted to 7,4 with hydrochloric acid. The bioactivity test apparatus is shown in Figure 5.2 below.

Figure 5.2: Bioactivity test apparatus [54].

Table 5.1: Compounds and their concentrations used in SBF [54].

Compound	Concentration (g/L)
NaCl	7,996
$NaHCO_3$	0,350
KCl	0,224
$K_2HPO_4.3H_2O$	0,228
$MgCl_2.6H_2O$	0,305
$CaCl_2$	0,278
Na_2SO_4	0,071
$H_2NC(CH_2OH)_3$	6,057

5.4 Bacteria Tests

In 50 ml Falcon tubes, 5 ml sterile distilled water was soiled with *E.coli*, *S.aureus*, *S.epidermidis* and *P.aeruginosa* bacteria, respectively to a final concentration of 8.5 million bacteria/100 ml. The samples were then placed into the tubes. At the time-points of 30, 60 and 120 minutes, water samples were taken from the tubes and following 200X, 500X and 1000X dilutions with sterile water, the samples were passed through 0.45 micron filter papers. The filter papers were inserted onto the plates containing medium with TTC tergitol and incubated for 21 h at 36^{o}C. The colony counts were then taken as colony forming unit (CFU) per ml.

5.5 Corrosion Tests

Static immersion test was used in order to test the corrosion resistance of the samples. Specimens were immersed in a lactic acid (10 g) and sodium chloride (5,85 g) containing solution (1000 ml) for 30 days. The pH of the solution was 2,3. The loss of mass was measured after immersion, and the surfaces of the samples were examined by a microscope. Corrosion tests were followed according to ISO 10271 standard.

6. RESULTS AND DISCUSSION

In this study, results of the experiments were evaluated in three sections, in order to analyse

1. The effect of the voltage (at constant $AgNO_3$ concentration)
2. The effect of $AgNO_3$ concentration present in the electrolyte of MAO process (at constant voltage)
3. The effect of the UV exposure (at constant voltage and $AgNO_3$ concentration) on bioactivity of CP-Ti

6.1 Effect of Voltage

For the examined CP-Ti, optimum positive and negative voltages were reported to be 500-83V for the MAO process conducted in $(CH_3COO)_2Ca.H_2O$ and Na_3PO_4 containing electrolyte according to Mert Gunyuz [16]. Figure 6.1 and Figure 6.2 show the stereo and SEM micrographs of the samples subjected to $AgNO_3$ free electrolyte at optimum parameters, respectively.

(a)

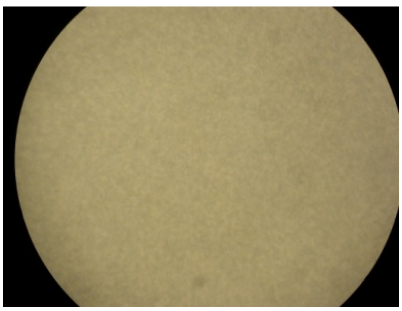

(b)

Figure 6.1: Stereo photographs of the sample oxidized in $AgNO_3$ free electrolyte at 500-83V (a) 6x (b) 50x

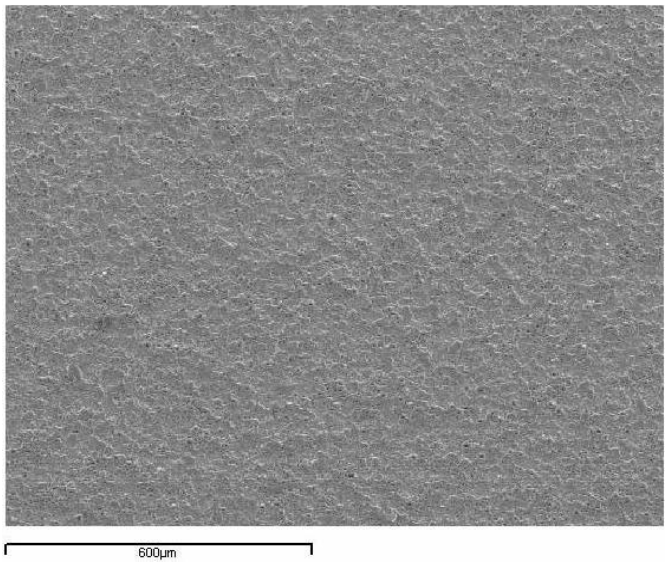

(a)

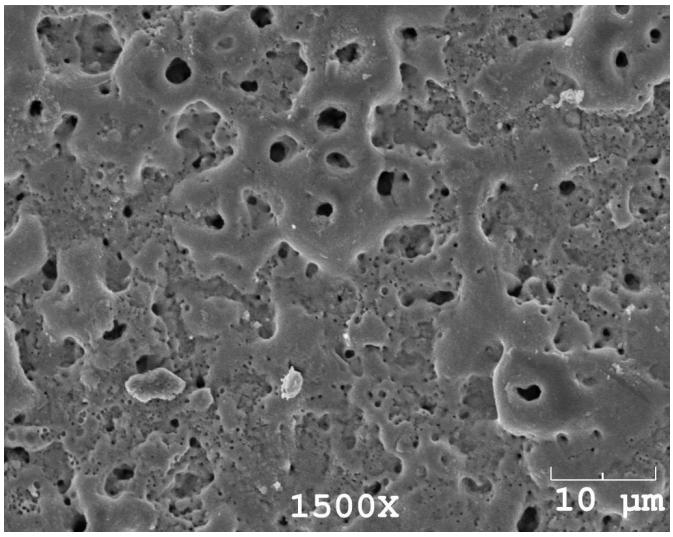

(b)

Figure 6.2: SEM micrographs of the sample oxidized in $AgNO_3$ free electrolyte at 500-83V (a) 100x (b) 1500x

In the scope of the present study, samples were oxidized at different voltages in the electrolyte containing 4 g/L silver nitrate. The positive and negative voltages were 350-55V, 400-60V, 450-70V and 500-83V, respectively. The stereo surface photographs of the samples are displayed in Table 6.1. The color of the samples oxidized with silver nitrate were completely different from the samples micro-arc oxidized in silver nitrate free electrolyte. Additionally, the increase in the surface roughness due to silver nitrate addition into the electrolyte was realized even by a naked eye. The surface morphologies detected by SEM are shown in Table 6.2. When compared to Figure 6.2, presence of silver nitrate in the electrolyte of the

MAO process, remarkably altered the morphology of the oxide layer. As the most important result, silver nitrate caused the disappearance of the classical porous structure along with a development of rough oxide layer.

Table 6.1: Stereo photographs of the samples oxidized in 4 g/L $AgNO_3$ containing electrolyte at different voltages

Voltage (V)	6x	50x
350-55	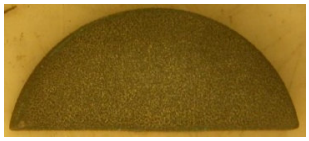	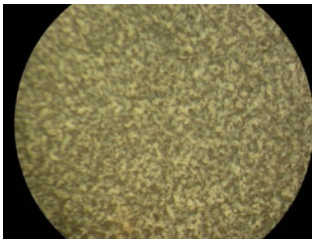
400-60		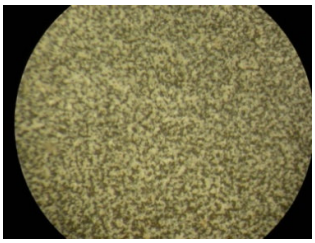
450-70		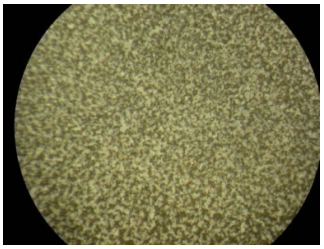
500-83	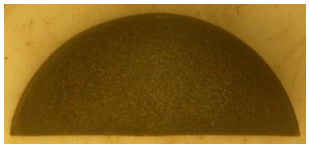	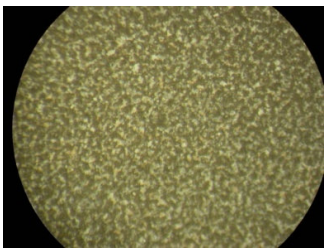

Table 6.2: SEM micrographs of the samples oxidized in 4 g/L $AgNO_3$ containing electrolyte at different voltages

Voltage (V)	50x	1500x
350-55	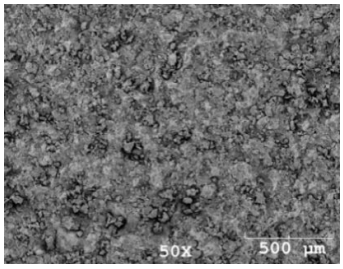	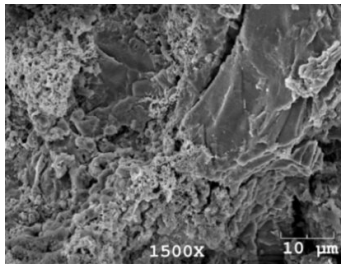
400-60	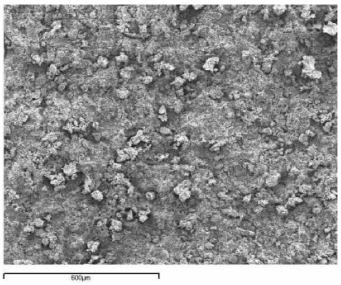	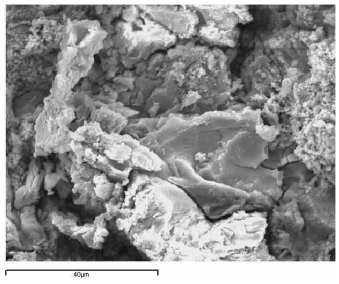
450-70	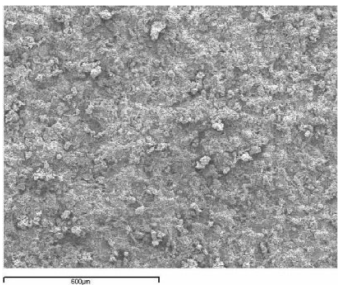	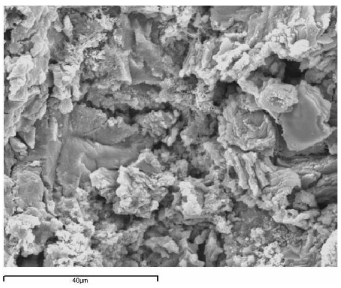
500-83	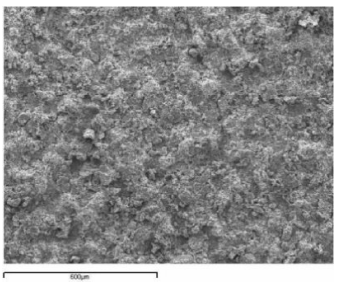	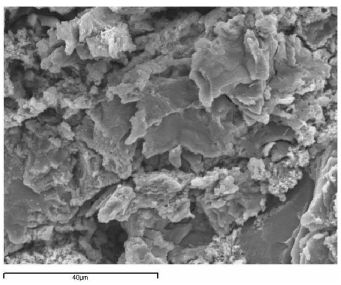

General composition of the oxide layers obtained by EDS analysis conducted during SEM studies are given in Table 6.3. As a general trend, the amount of Ti tends to decrease with increasing process voltage. According to the EDS results shown in Table 6.3, Ca/P ratio of the oxide layers was drawing near to the hydroxyapatite Ca/P ratio (1.67), as the voltage applied increased.

However, in bulk XRD patterns given in Figs. 6.3 – 6.6, no distinct apatite peaks were observed. Also the Ti/O ratio decreased when the applied voltage exceeded 400-60V. The highest Ag concentration was present at the lowest voltage. With increasing voltage, the amount of Ca, incorporated into the layer, also increased. According to Long Hao Li et al. [9], alkaline phosphatase (ALP) activity tends to be enhanced with increasing Ca content and decreasing surface roughness. The results of the present study may support this statement in accordance with anti-bacterial activity because Ca content increased and roughness decreased (Figure 6.7) with increasing voltage.

Table 6.3: General surface EDS results of samples oxidized in 4 g/L $AgNO_3$ containing electrolyte at different process voltages

Element (at.%)	**350-55V**	**400-60V**	**450-70V**	**500-83V**
Ti	40.38	21	20	21.8
O	42	59	60	62.1
Ag	10.36	4.16	3.25	7.29
Ca	2.57	2.88	3.79	4.35
P	3.58	2.13	2.63	2.60
Ca/P	0.71	1.35	1.44	1.67

In Figure 6.3, 6.4, 6.5, and 6.6, the bulk XRD patterns of the samples oxidized at 350-55V, 400-60V, 450-70V and 500-83V are shown. On the XRD patterns, silver was detected in metallic form without making any compound. Titanium peaks clearly appeared, but only a small peak of rutile form of TiO_2 was observed. There was no apparent anatase peak until the voltage was reached to 500-83V. Also, no apatite peaks were observed on the XRD pattern. On the XRD pattern of the sample oxidized at 500-83V, an additional anatase and a rutile peak appeared at 47.7^o and 54.3^o. A titanium and a silver peak were seen to coincide at 77.5^o.

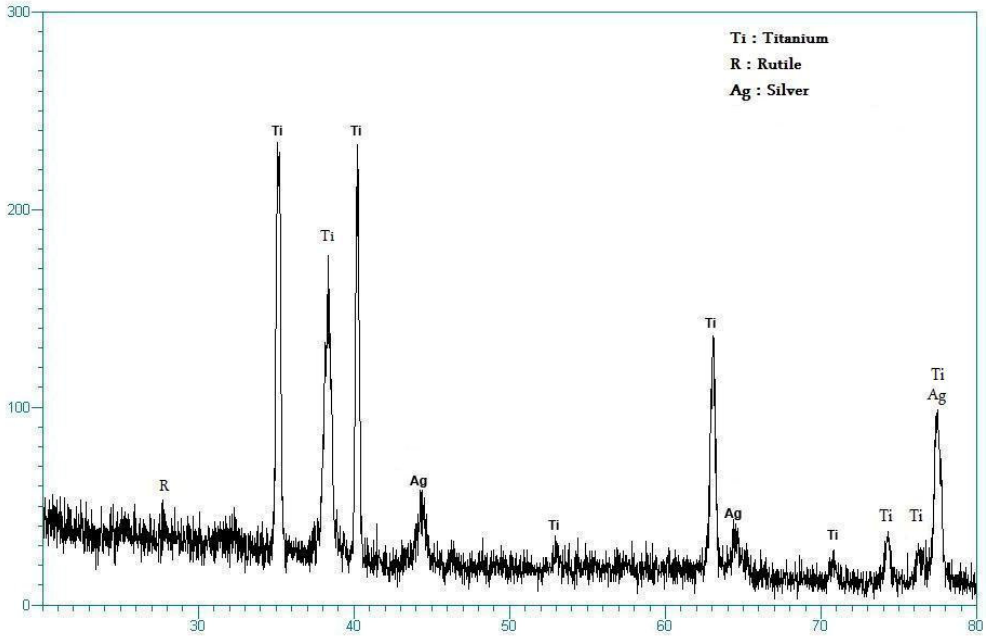

Figure 6.3: XRD pattern of the sample oxidized in 4 g/L $AgNO_3$ containing electrolyte at 350-55V

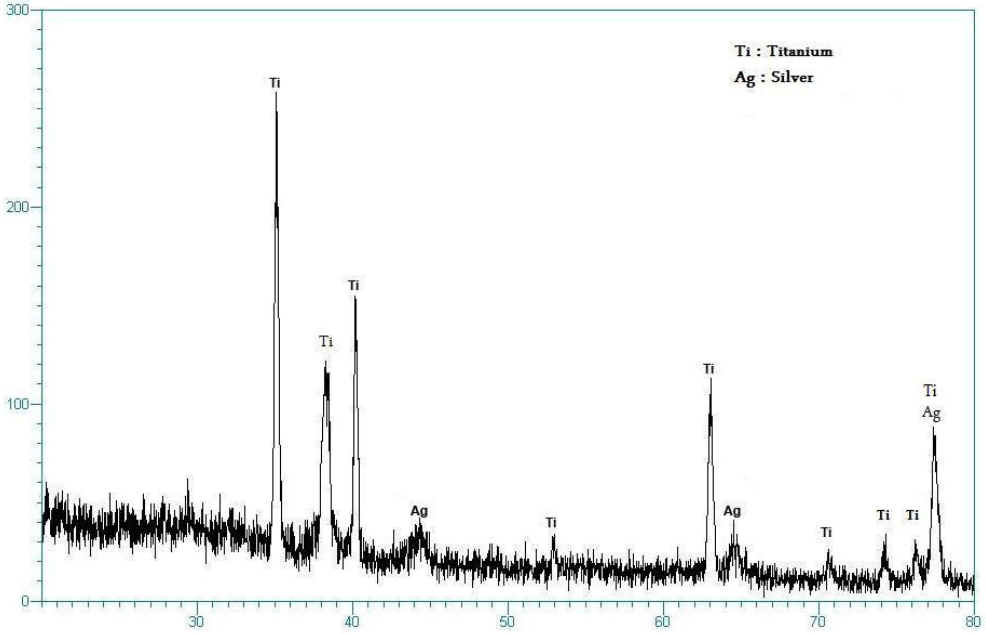

Figure 6.4: XRD pattern of the sample oxidized in 4 g/L $AgNO_3$ containing electrolyte at 400-60V

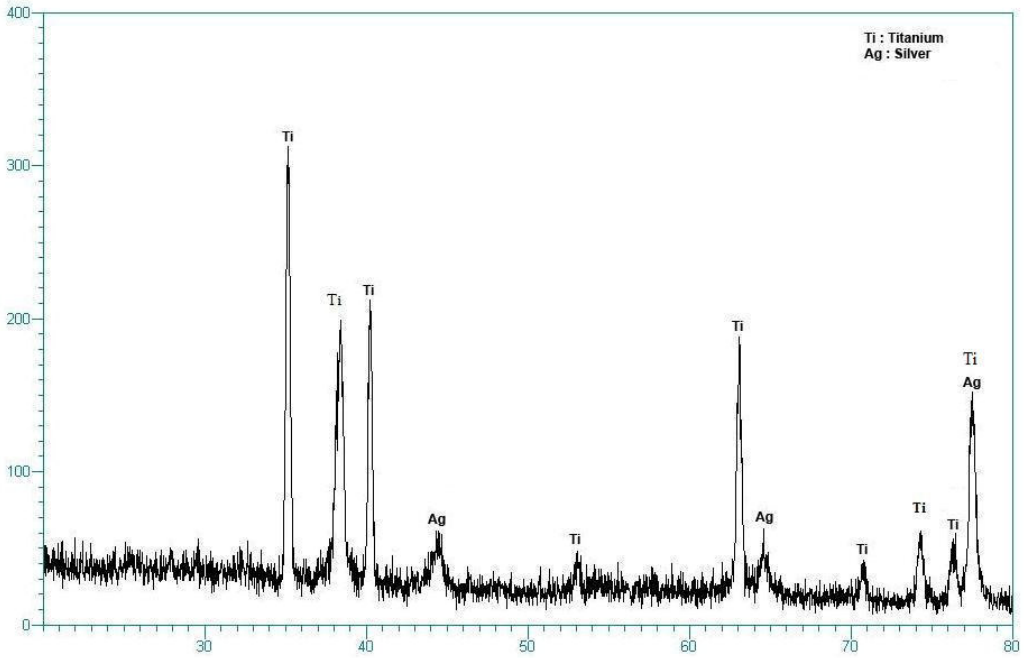

Figure 6.5: XRD pattern of the sample oxidized in 4 g/L $AgNO_3$ containing electrolyte at 450-70V

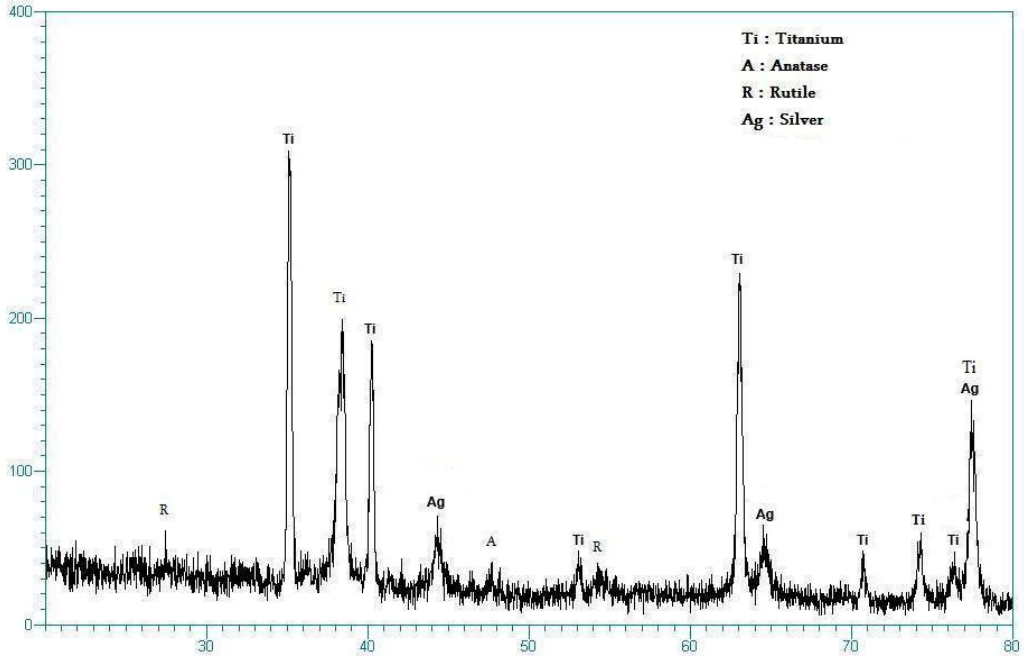

Figure 6.6: XRD pattern of the sample oxidized in 4 g/L $AgNO_3$ containing electrolyte at 500-83V

In Figure 6.7, surface roughness plot is given with respect to the voltage applied. As a general trend, presence of silver nitrate in the electrolyte remarkably increased the average surface roughness (Ra). In 4 g/L silver nitrate containing solution the increase of voltage tended to cause a slight reduction in the surface roughness.

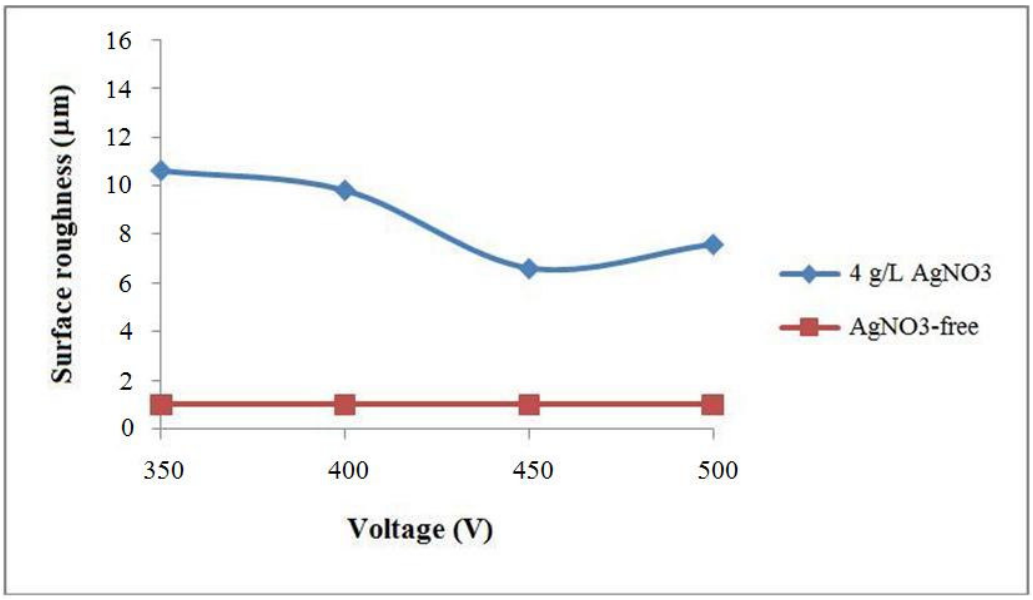

Figure 6.7: Surface roughness-voltage relationhip plot

The reason of the excessive increase of roughness can be attributed to the increase in the conductivity of the electrolyte, which leads an increase in the current. At constant voltage, this enhancement in current, damages the oxide layer because of the decrement of the resistivity of ceramic oxide layer.

The results of the contact angle measurements are listed in Table 6.4. When compared to the untreated surface, MAO process increased the wettability of titanium by decreasing the contact angle from 60^{o} to 13^{o}. Also, MAO conducted in silver nitrate containing electrolyte caused further decrease in the contact angle to a value of 0^{o}, leading to a super hydrophilicity irrespective of the voltage. It may be due to the fact that, MAO and silver nitrate addition increases the roughness, suggesting that the surface energy increases. And it is easy for water to penetrate into the resulted cavities leading to a high wettability. Also, higher surface energy may lead to faster cell adhesion [20].

Table 6.4: Photos of contact angle measurements with distilled water

Untreated CP-Ti (**60^o**)	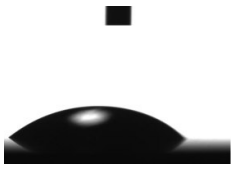
MAO-$AgNO_3$ free (500-83V) (**13^o**)	
MAO- 4 g/L $AgNO_3$ (500-83V) (**0^o**)	
MAO- 4 g/L $AgNO_3$ (450-70V) (**0^o**)	
MAO- 4 g/L $AgNO_3$ (400-60V) (**0^o**)	
MAO- 4 g/L $AgNO_3$ (350-55V) (**0^o**)	

Having a lower contact angle for a biomaterial is a desired property in order to provide better wettability which can improve interaction between biological fluid and implants [55]. Therefore, it has been suggested that hydrophilic surfaces with low contact angle (high wettability) could enhance cell proliferation, adhesion and spreading of osteoblastic cells as well as apatite inducing ability in SBF [55, 56].

The results of bacteria test performed with *E. Coli* is shown in Table 6.5. Cfu, which is a measure of the amount of viable bacteria, is the colony forming unit per mililiter.

Table 6.5: The decrease in the amount of *E.coli* bacteria related to applied voltage for the samples oxidized in 4 g/L $AgNO_3$ containing electrolyte

Voltage (V)	**Time (min)**	**0**	**30**	**60**	**120**
		(Cfu)	(Cfu)	(Cfu)	(Cfu)
350-55		8400000	61100	12634	12956
400-60		8400000	8034	1500	467
450-70		8400000	67	67	67
500-83		8400000	434	0	0

As seen in Table 6.5, the number of the viable bacteria on all the oxidized surfaces decreased with increasing incubation time. After 2h, only the samples, oxidized at 500-83V, exhibited a 100% anti-bacterial activity. Also, the samples oxidized at 350-55V showed a 99.85% anti-bacterial activity, which is the least among all samples. One interesting observation was that, the fastest decrease in the amount of viable bacteria, was detected at 450-70V after 30 minutes, however it did not cause further reduction at prolonging time. Also, 60 minutes were enough for 500-83V process parameter to obtain 100% anti-bacterial activity. For the sample oxidized in the original solution without $AgNO_3$, on the other hand, no decrement was observed in bacteria counts giving the same value (8400000) as prior to the test, which means that anti-bacterial property could not be achieved on those samples.

As a result, at constant $AgNO_3$ concentration (4 g/L), 500-83V was selected as the ideal process parameter for the following experiments due to its 100% anti-bacterial effect.

6.2 Effect of Silver Nitrate Concentration

It was concluded that 500-83V was the ideal MAO process parameter by considering the 100% antibacterial activity obtained in Section 6.1. In this section, the priority was to find out the minimum silver nitrate ($AgNO_3$) concentration, which yields the maximum anti-bacterial activity, at this constant voltage in order to decrease the probability of toxicity of excessive silver concentration, which might affect the performance of other cells, detrimentally.

For this purpose, four different concentrations of silver nitrate were chosen (1 g/L, 2 g/L, 3 g/L and 4 g/L). Additionally, samples were hold in SBF for 30 days to investigate the effect of silver addition on bioactivity.

The pH value of the electrolyte decreased from 10 to 8, as the silver nitrate concentration increased. The resulting surfaces were quite rough, due to the presence of silver nitrate in the electrolyte. This roughness may enhance the adhesion strength between the implant material and the bone. As the roughness increases, the interlocking mechanism is easier to take place between the implant and the bone tissue [3]. However, cell adhesion and proliferation mechanisms must not be damaged because of the excessive roughness and the presence of silver in the coating. Therefore, cell adhesion tests should be conducted.

In Table 6.6, stereo photographs of the coated samples can be seen. It was observed that, sample oxidized in 1 g/L $AgNO_3$ containing electrolyte for 5 minutes showed a changing color at the center of the surface. In order to understand what led this, oxidation times were changed between 1 to 10 minutes in the same electrolyte, which contained 1 g/L $AgNO_3$. Table 6.7 shows that as the process time prolonged from 1 minute to 10 minutes, the different colour observed on the centre of the surface, seemed to become smaller. This may be a hint that, the coating process may not have been finished for 1 g/L silver nitrate containing sample within 5 minutes, and the process time should be prolonged to finish the process.

Table 6.6: Stereo photograhs of micro-arc oxidized samples at different concentrations of $AgNO_3$

Concentration (g/L)	10x	75x
1	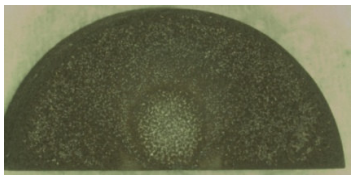	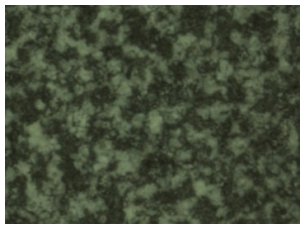
2	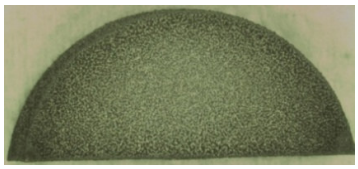	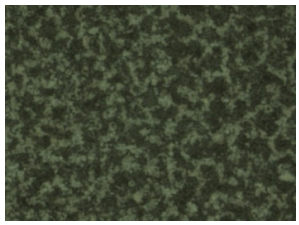
3	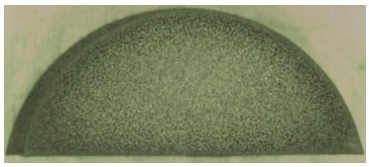	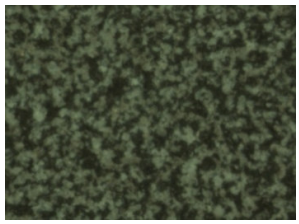
4	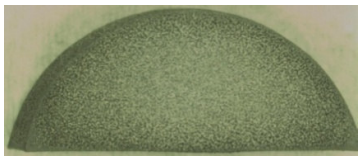	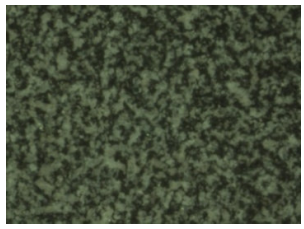

Table 6.7: Stereo photograhs of micro-arc oxidized samples in 1 g/L $AgNO_3$ containing solution for different process times

Process time (min)	10x	50x
1	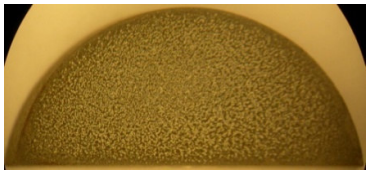	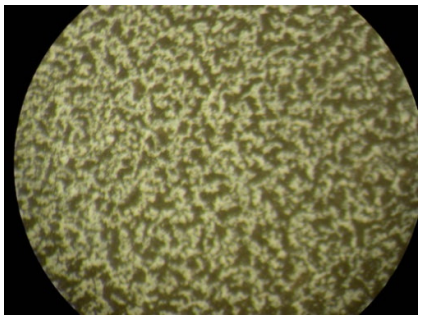
3	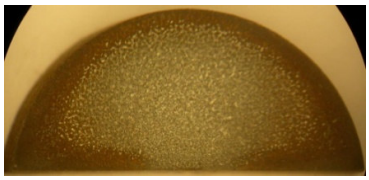	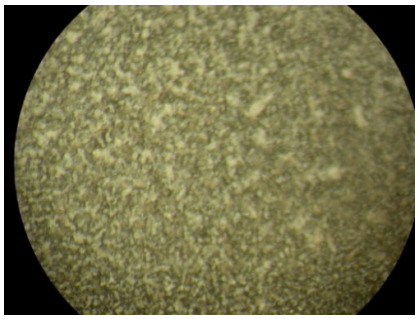
5	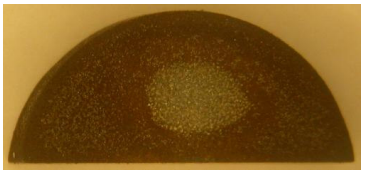	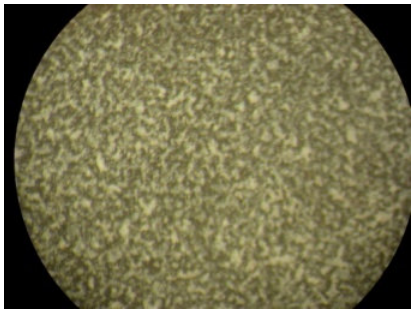
10	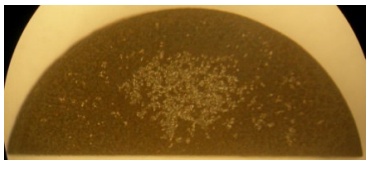	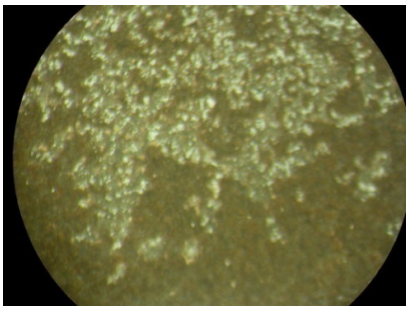

In Table 6.8, the surface morphologies of the oxidized surfaces with different silver nitrate concentrations were given as SEM micrographs. The surface of the sample oxidized in the original solution without $AgNO_3$ exhibited a characteristic surface topography for the micro-arc oxidation process with pores 1-5 μm in size distributed throughout the surface. As seen in Table 6.8, silver nitrate addition increased the surface roughness. And, the macro pores appered on the oxide layer developed in silver nitrate free electrolyte disappeared upon addition of $AgNO_3$. According to Jifeng Sun et al. [18], increasing film roughness shortens the apatite induction time but the effect of the disappearance of pores on apatite formation are not known at this stage. Bioactivity tests may give an idea about that. However, as the silver nitrate concentration decreased to 1 and 2 g/L, additional macro and nano-pores were observed. This might cause shortening the apatite induction time again, as stated by Jifeng Sun et al. [18]. There are studies indicating the nano-sized pores serving as a nucleation site for apatite and enhancing the cell proliferation [19]. But it is different when the increased roughness is considered. Because, increased roughness is thought to decrease the cell proliferation rate, although it increases the ALP activity [9]. General compositions of the oxide layers obtained by EDS analysis during SEM studies are presented in Table 6.9. As seen, no specific effect of silver nitrate addition were observed on Ti concentration. Because it showed a fluctuation with increasing silver nitrate concentration. However, Ag concentration of the oxide layer tended to increase remarkably when the silver nitrate concentration of the electrolyte was over 3 g/L. Oxygen concentration tended to decrease with silver nitrate addition to the electrolyte, however it showed a big jump at 4 g/L silver nitrate concentration. Another important point was that, Ca and P concentrations increased at 1 g/L silver nitrate content and then started to decrease as the content of silver nitrate increased. However, the Ca/P ratio at 4 g/L reached 1.67 from 1.16, which was calculated on the sample without the presence of silver nitrate.

Table 6.8: SEM micrographs of samples oxidized at 500-83V with different concentrations of $AgNO_3$

Concentration (g/L)	100x	High magnification
0 **($AgNO_3$ free solution)**	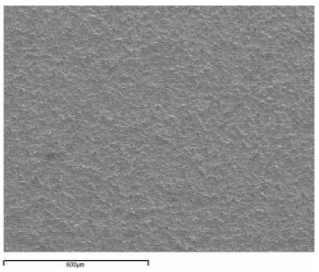	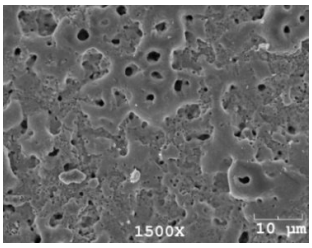
1	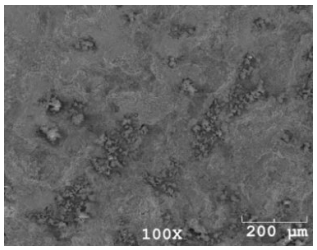	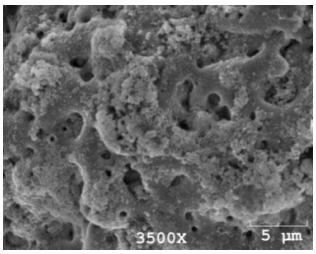
2	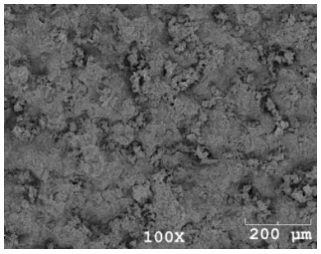	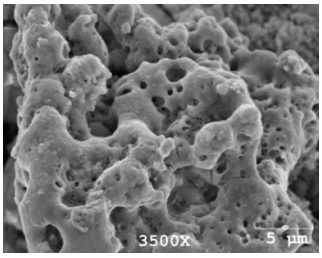
3	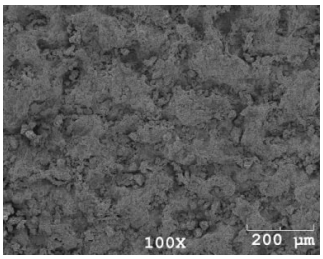	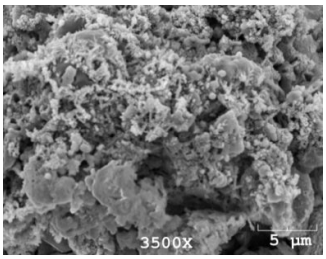
4	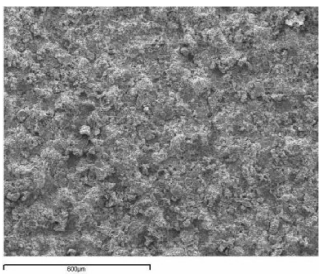	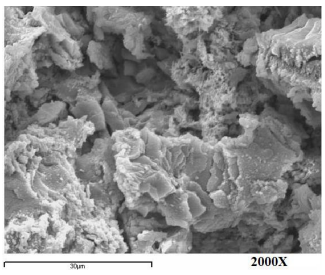

Table 6.9: General surface EDS results of the samples oxidized at 500-83V with different silver nitrate concentrations

Element (at.%)	$AgNO_3$ free solution	1 g/L	2 g/L	3 g/L	4 g/L
Ti	26	18.3	33	43.15	21.8
O	54	45.3	36.5	34	62.1
Ag	-	1.97	9.5	10.78	7.29
Ca	10.25	22	12.33	7.25	4.35
P	8.83	12.34	8.65	4.75	2.60
Ca/P	1.16	1.78	1.42	1.53	1.67

In Figure 6.8, 6.9, 6.10, 6.11 and 6.12, the surface XRD results, which belong to the sample without silver nitrate addition, 1 g/L silver nitrate, 2 g/L silver nitrate, 3 g/L silver nitrate and 4 g/L silver nitrate are shown, respectively.

As seen in Figure 6.8, anatase, rutile, β-$Ca_2P_2O_7$ and $CaTiO_3$, which is claimed to be an apatite inducer, were present on the oxidized layer of the sample without silver addition.

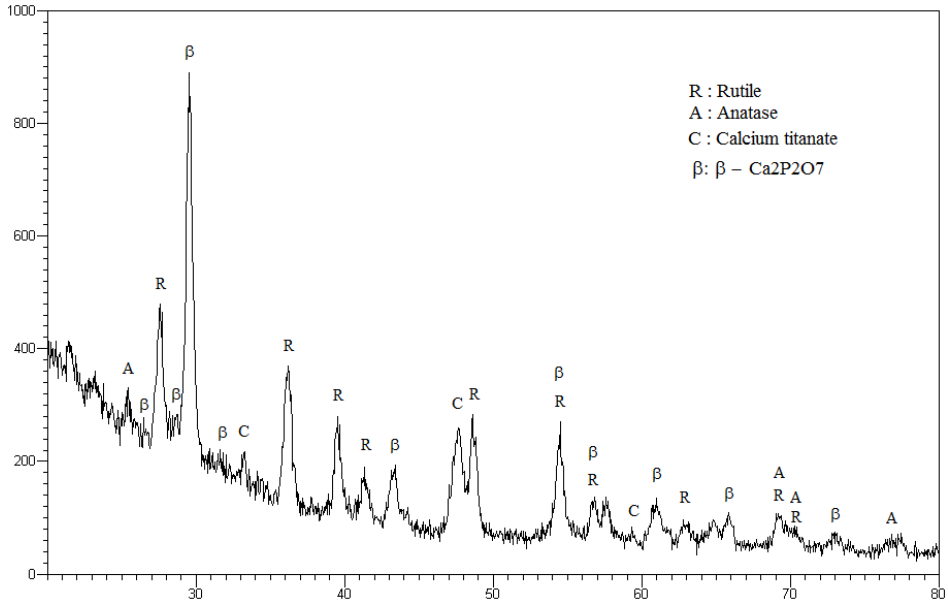

Figure 6.8: XRD pattern of titanium oxidized at 500-83V without silver nitrate addition

With the addition of silver nitrate, titanium and silver peaks were observed. Rutil was the abundant type of TiO_2 in the patterns. And, anatase started to disappear when the concentration of the silver nitrate exceeded 3g/L. So, it was clear that a different mechanism was taking place, which was affecting the formation of titanium oxides. Interestingly, α-$Ca_2P_2O_7$ peaks were observed, only at the concentration of 3g/L silver nitrate.

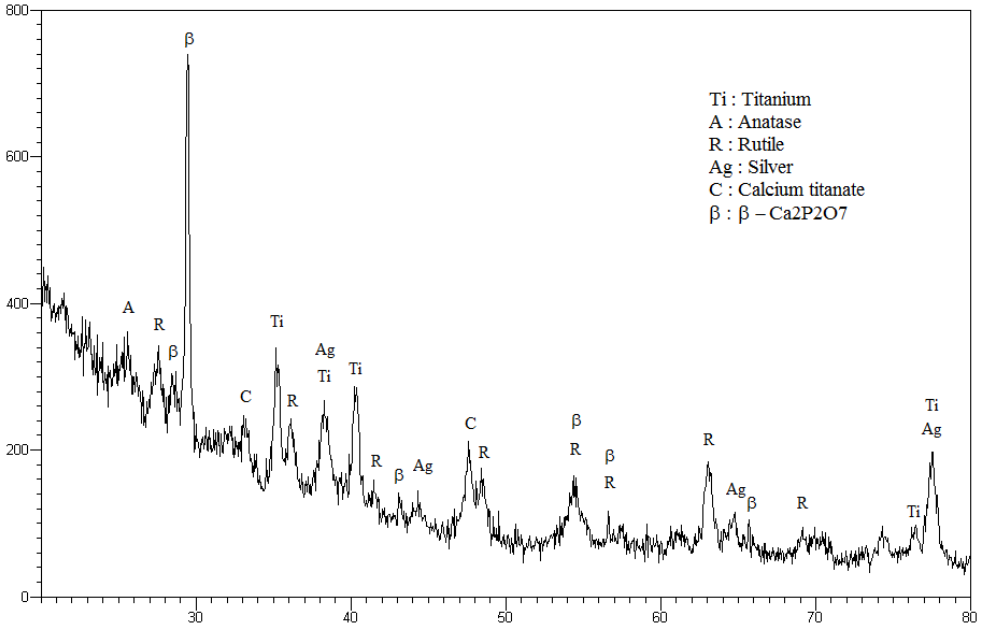

Figure 6.9: XRD pattern of titanium oxidized at 500-83V in 1 g/L $AgNO_3$ containing electrolyte

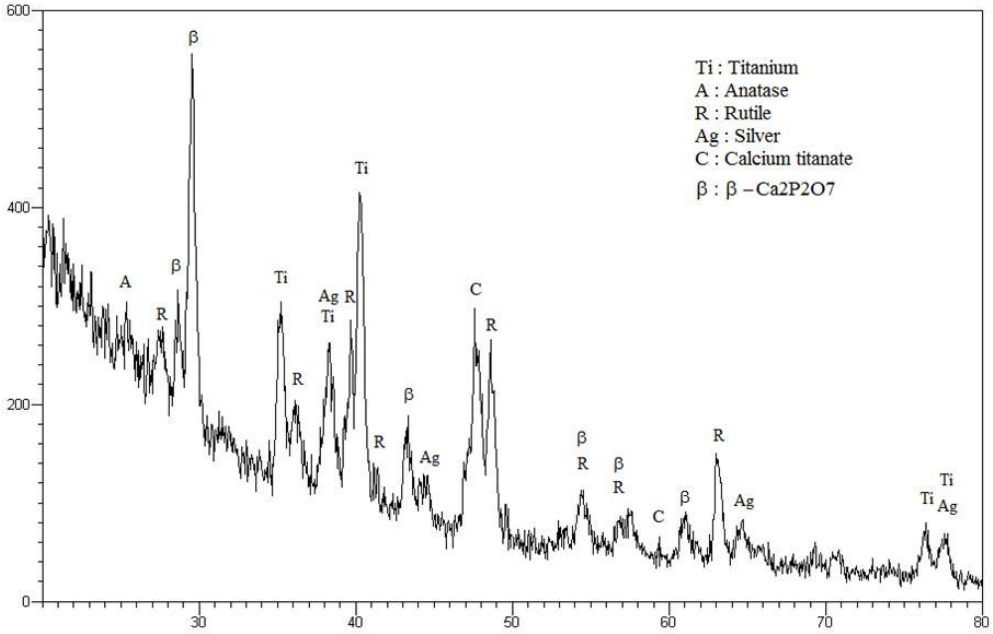

Figure 6.10: XRD pattern of titanium oxidized at 500-83V in 2 g/L $AgNO_3$ containing electrolyte

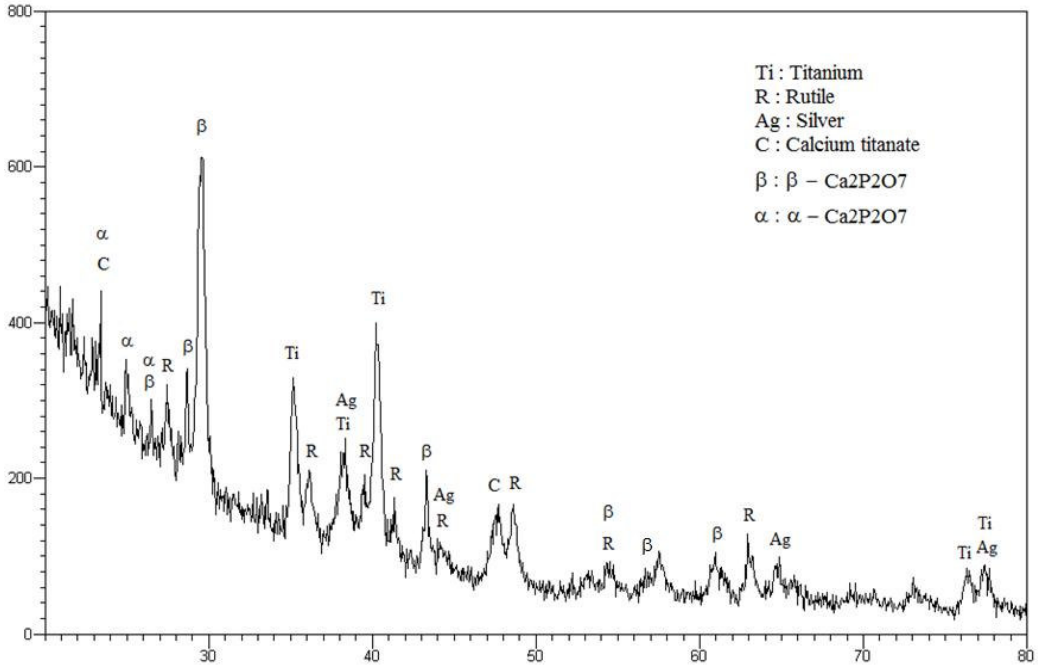

Figure 6.11: XRD pattern of titanium oxidized at 500-83V in 3 g/L $AgNO_3$ containing electrolyte

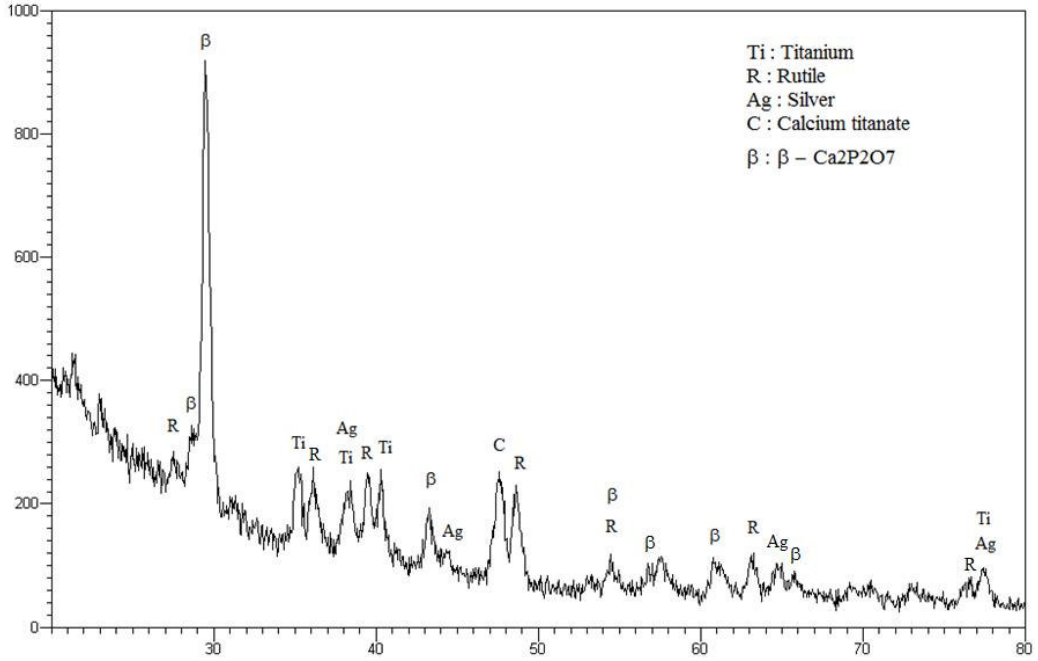

Figure 6.12: XRD pattern of titanium oxidized at 500-83V in 4 g/L $AgNO_3$ containing electrolyte

In Figure 6.13, the effect of silver nitrate addition on the thickness of surface oxide layer is presented. The thickness of the surface oxide layer, formed in $AgNO_3$ free electrolyte, was in the range of 15-17 μm. However, $AgNO_3$ addition into the

electrolyte increased the oxide thickness. It was about 23-25 µm, irrespective of the $AgNO_3$ concentration of the electrolyte. Also, the oxide layers were integrated with the substrate without a distinct interface, which is said to provide a high bonding strength between the substrate and the layer [15].

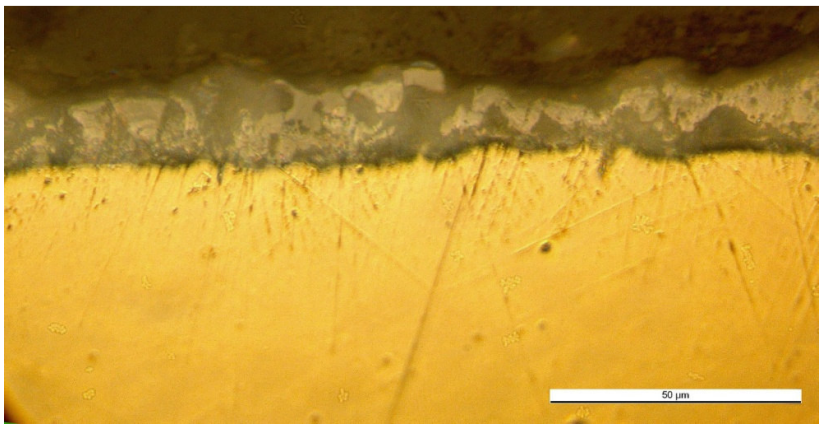

(a)

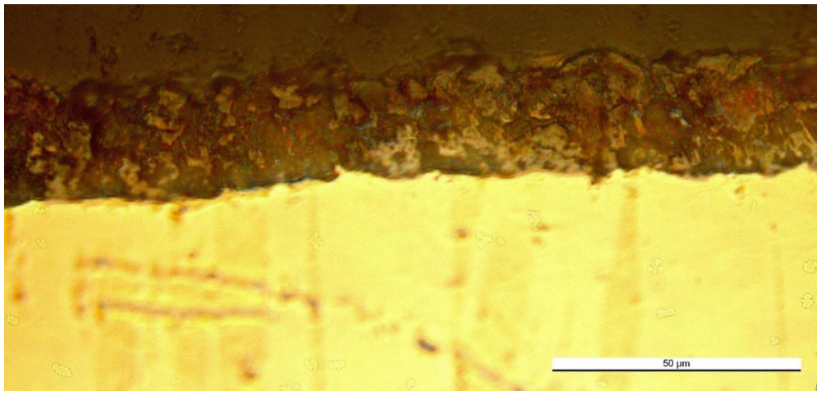

(b)

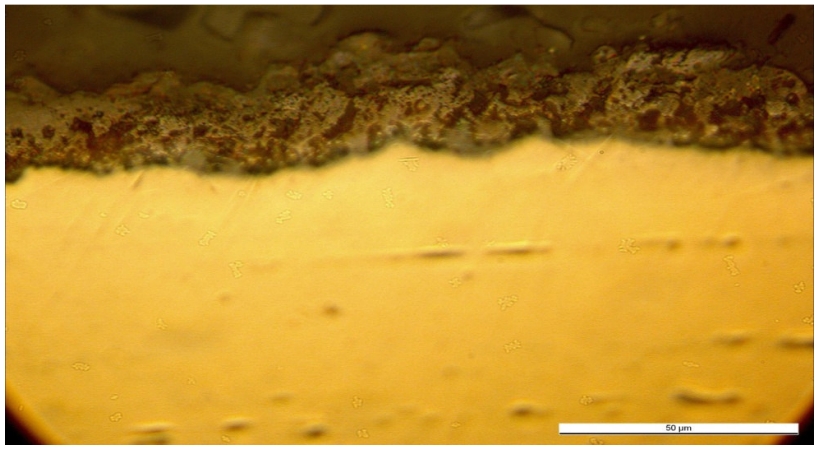

(c)

Figure 6.13: Cross-section views of MAO-treated samples (a) $AgNO_3$ free electrolyte (b) 1 g/L $AgNO_3$ containing electrolyte (c) 2 g/L $AgNO_3$ containing electrolyte

In the Figure 6.14, the effect of silver nitrate concentration of the electrolyte on the average surface roughness (Ra) is plotted. When compared to the silver nitrate free electrolyte, addition of 1 g/L silver nitrate into electrolyte, caused a dramatic increase in the surface roughness of the oxide layer. The surface roughness of the oxide layer obtained from 1 g/L silver nitrate electrolyte was about 12 times higher than that of the oxide layer formed in silver nitrate free electrolyte. Further additions of silver nitrate into the electrolyte caused a slight reduction in the surface roughness.

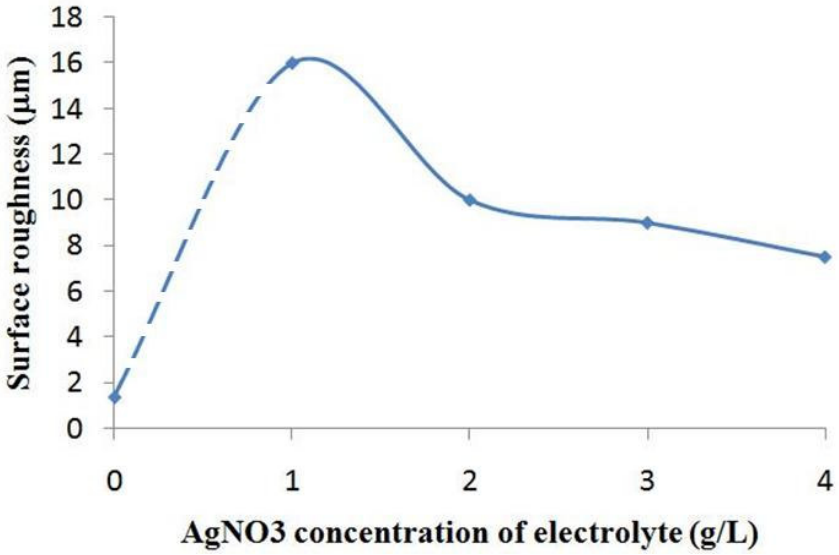

Figure 6.14: The effect of $AgNO_3$ concentration on surface roughness at 500-83V

The contact angle measurements were performed by using both distilled water and SBF. MAO-treated sample without silver nitrate, exhibited a higher wettability with distilled water than SBF. The angle was 13^o for water, meanwhile it was 23^o for SBF. In the case of $AgNO_3$ addition, the results did not show any differences whether it was done by water or SBF. The contact angles were measured 0^o, irrespective of the silver nitrate concentration. It was also observed that, silver nitrate containing samples absorbed SBF faster than distilled water. This may be a hint about the wettability behaviour of the samples in human body, in a positive manner. This absorbability may be utilized in drug delivery systems to send antibiotics or active molecules into the body (tissue) and the healing process after implantation can be accelerated. In Table 6.10, contact angle photos can be seen.

Table 6.10: Photos of contact angle measurements of micro-arc oxidized samples at 500-83V with different concentrations of $AgNO_3$

Concentration (g/L)	Distilled water	SBF
0 ($AgNO_3$ free solution)		
1 g/L		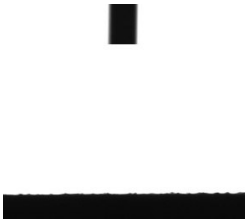
2 g/L		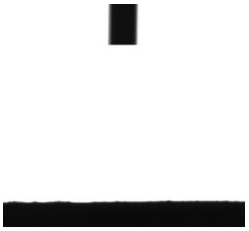
3 g/L		
4 g/L		

To investigate the liquid absorbtion ability of the samples, a weight gain test were performed. After oxidation treatment, samples with changing $AgNO_3$ concentration, a sample oxidized without silver nitrate and an untreated, polished titanium were

dried in an autoclave at 100°C for an hour. Then, the weights of the samples were measured and put in a glass container, containing distilled water. After 15 minutes, the samples were taken out and dried in air in order to measure their weight. Table 6.11 shows the weight gains of the samples after the procedure described above.

Table 6.11: Weight gain measurements of the samples after the test

Sample	**Weight gain (weight%)**
Untreated CP-Ti	0
MAO without $AgNO_3$	0.042
MAO with 1 g/L $AgNO_3$	0.22
MAO with 2 g/L $AgNO_3$	0.072
MAO with 3 g/L $AgNO_3$	0.076
MAO with 4 g/L $AgNO_3$	0.087

From the results shown in Table 6.11, it was clear that MAO treatment contributed to the liquid absorbtion ability. The samples treated with 2, 3, and 4 g/L silver nitrate containing electrolyte showed an increase about two times than that of the sample treated in silver nitrate free electrolyte. However, the weight gain of the sample treated in 1 g/L silver nitrate containing electrolyte, was 2,5 times higher than that of the samples oxidized in higher concentrations of silver nitrate and 5 times higher than that of the sample treated in silver nitrate free electrolyte, which may be attributed to its excessive surface roughness.

Bioactivity tests were performed in SBF for 30 days to investigate the apatite forming ability of micro-arc oxidized samples with and without silver nitrate. For this test, titanium oxidized in 4 g/L silver nitrate containing electrolyte was chosen. After 30 days, SEM analysis was conducted (Table 6.12 and 6.13).

Table 6.12: SEM images of the samples oxidized in $AgNO_3$ free electrolyte before and after SBF

Magnification	Before SBF	After SBF
100x	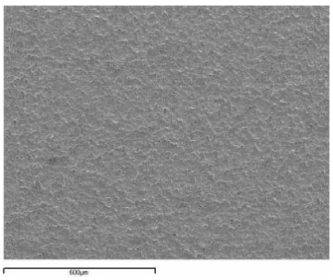	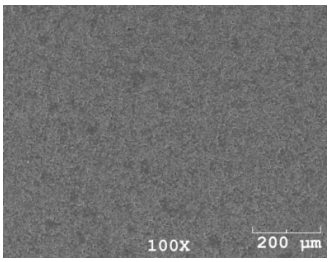
500x	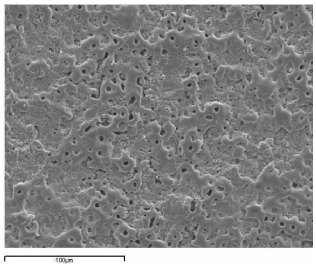	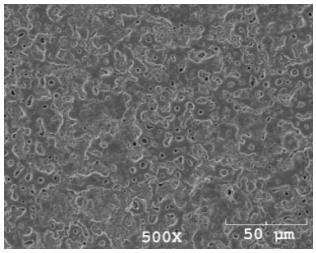
1500x	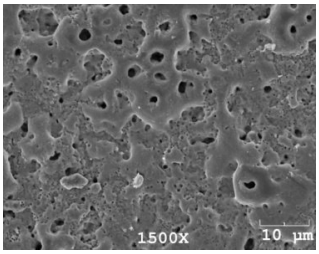	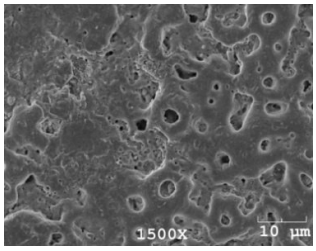
2000-3500x	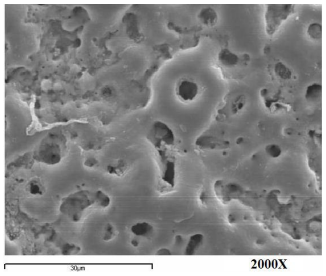	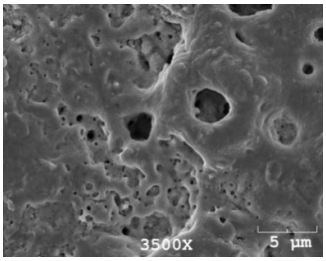

Table 6.12 indicates that, after SBF, pores began to be filled however, it is thought to be insufficient because the apatite particulates were supposed to become larger in size after 30 days but they were not. In the following sections, UV light will be utilized to increase apatite inducing ability and to shorten the immersion time in SBF. In Table 6.13, silver nitrate containing sample was investigated.

Table 6.13: SEM images of the samples oxidized in 4 g/L $AgNO_3$ containing electrolyte before and after SBF

Magnification	Before SBF	After SBF
100x	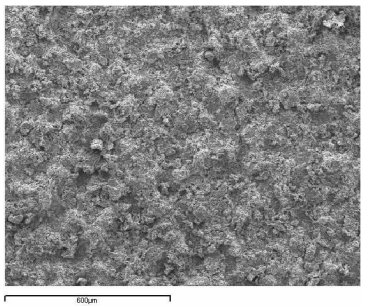	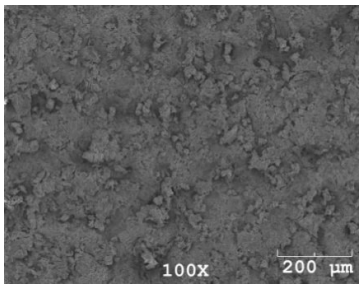
500x	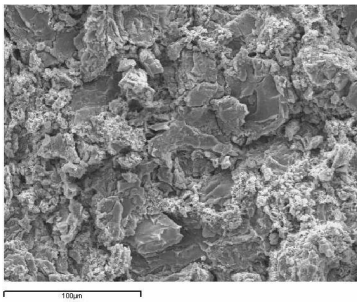	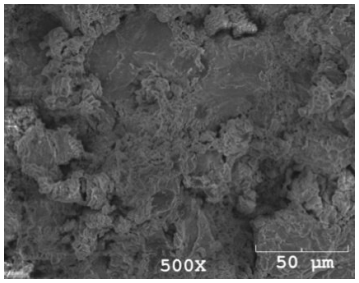
1500x	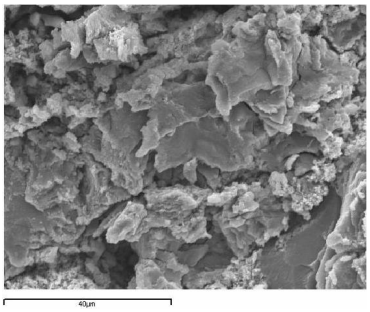	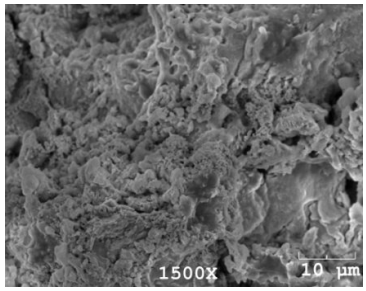
2000-3500x	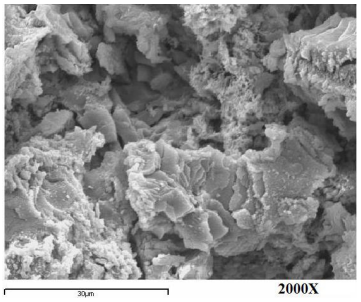	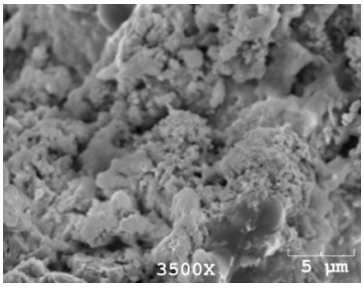

No big differences, such as apatite nucleation, were detected after SBF tests for silver containing sample. However, the sharpness of the edges seen before SBF tests, were

observed as if to be rounded according to Table 6.13. There may be a very thin layer of a kind of bioactive coating. EDS results of the same samples are given in Table 6.14.

Table 6.14: General surface EDS results of the samples before and after SBF immersion for 30 days

	Sample oxidized without $AgNO_3$		**Sample oxidized in 4 g/L $AgNO_3$ containing electrolyte**	
Element (at%)	**Before SBF**	**After SBF**	**Before SBF**	**After SBF**
Ti	26	12.88	21.8	38.82
O	54	77.13	62.1	41.14
Ag	-	-	7.29	6.55
Ca	10.25	6.13	4.35	6.56
P	8.83	3.85	2.60	5.89
Ca/P	1.16	1.59	1.67	1.11

For the sample without silver nitrate, Ca/P ratio increased after SBF immersion reaching to Ca-deficient HA ratio. However, Ca and P content of the layer decreased significantly. Also, Ti/O ratio was observed to decrease. The tiny particles observed on the surface had a Ca/P ratio of 1.62 (Table 6.15) after SBF, which was equivalent to that of HA (1.67). Before SBF, tha Ca/P ratio was 2.1, which was suggested to be $Ca_4P_2O_9$ (tetra calcium phosphate-TTCP) [59].

The behaviour of the samples oxidized in silver nitrate containing electrolyte was completely different, however. Ti/O ratio was observed to increase and Ca/P ratio decreased to 1.11, which may support the formation of bioresorbable phases although, Ca and P incorporated to the layer increased after the immersion, which is said to enhance cell response, especially the ALP activity [9]. The Ca/P ratio of the particles detected on the surface decreased from 1.8 to 0.9 ($CaHPO_4$- dicalcium

phosphate anhidroz or $CaHPO_4.2H_2O$-dicalcium phosphate dihydrate) [59] after 30 days of SBF immersion, indicating that SBF immersion had a negative effect on apatite induction for the samples oxidized in 4 g/L silver nitrate containing electrolyte.

Table 6.15: EDS results of the particles detected on the surfaces of the samples before and after SBF

	Sample oxidized without $AgNO_3$		**Sample oxidized in 4 g/L $AgNO_3$ containing electrolyte**	
	Before SBF	After SBF	Before SBF	After SBF
Ca/P ratio	2.1	1.62	1.8	0.9

The XRD patterns of the samples after SBF tests are displayed in Figure 6.15 - 6.18. After SBF immersion for 30 days, MAO treated sample without silver nitrate, exhibited weak carbonated-hydroxyapatite phases, also calcium titanate and β-$Ca_2P_2O_7$ phases, disappeared after SBF immersion as seen in Figure 6.16. These two phases were thought to undergo hydrolysis in SBF to form apatite.

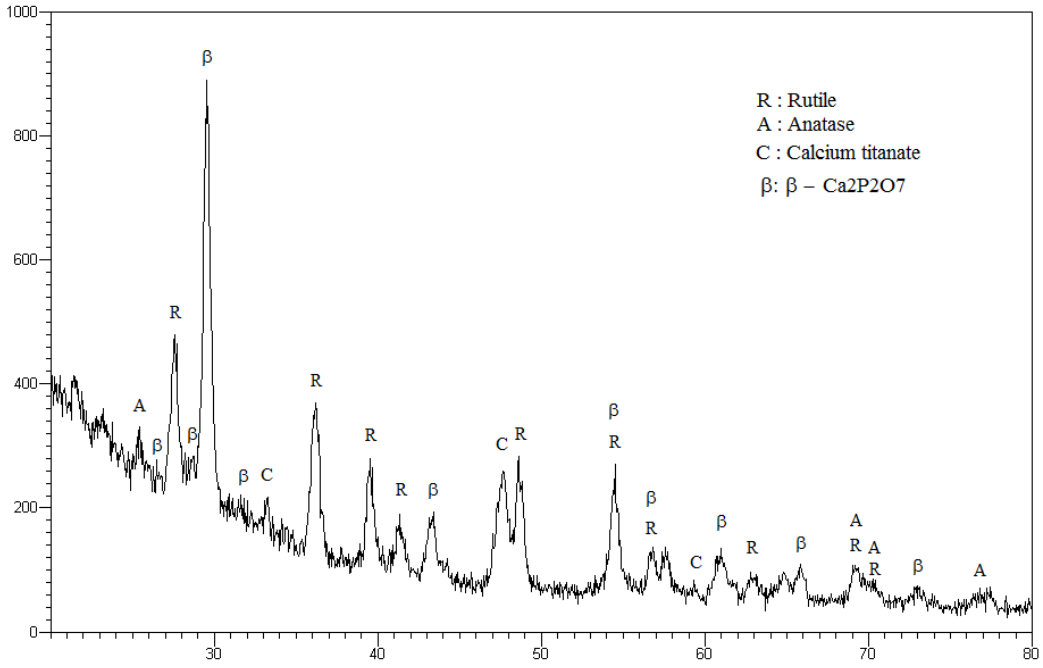

Figure 6.15: XRD pattern of the sample oxidized in $AgNO_3$ free electrolyte before SBF immersion

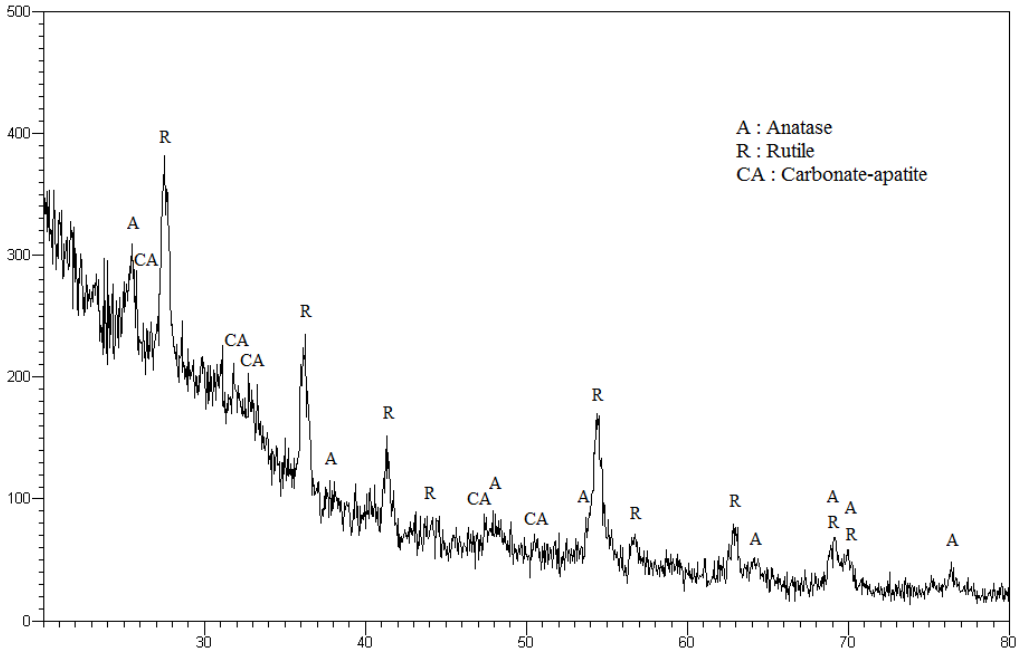

Figure 6.16: XRD pattern of the sample oxidized in $AgNO_3$ free electrolyte after SBF immersion

Han et al. [57] declared that an oxide layer containing, β-$Ca_2P_2O_7$, α-$Ca_3(PO_4)_2$ and $CaTiO_3$ formed on a micro arc oxidized titanium could induce apatite formation after 40 days of immersion in SBF and the surface was fully covered with apatite after 50 days of immersion. Wang et al. [10] reported that preferential carbonated hydroxyapatite was formed on MAO-treated CP-Ti after 30 days of SBF immersion.

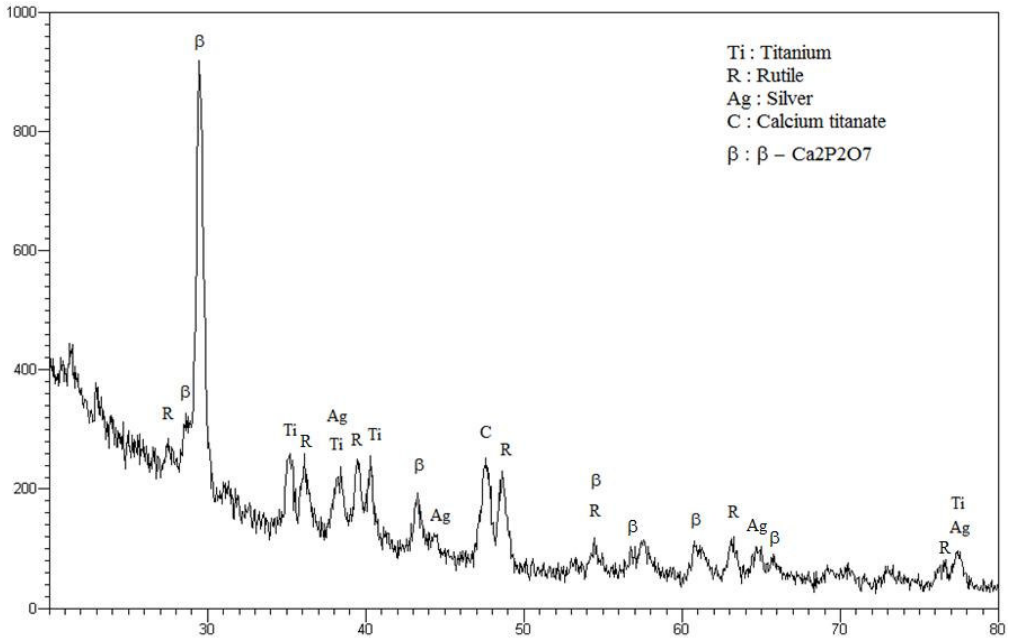

Figure 6.17: XRD pattern of the sample oxidized in 4 g/L $AgNO_3$ containing electrolyte before SBF

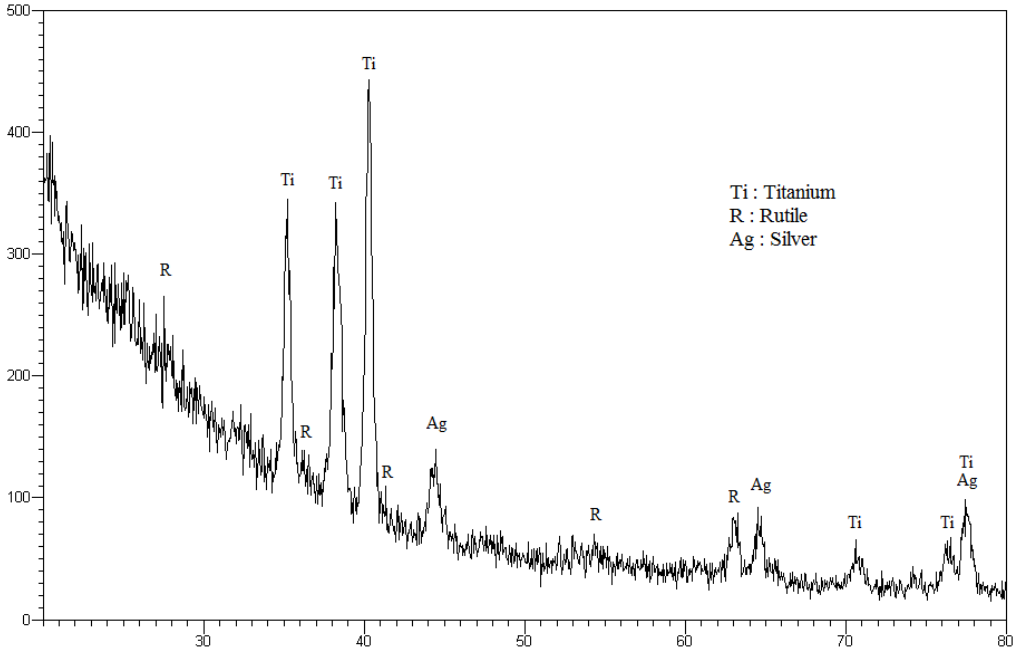

Figure 6.18: XRD pattern of the sample oxidized in 4 g/L $AgNO_3$ containing electrolyte after SBF

In the case of silver nitrate addition, calcium titanate and β-$Ca_2P_2O_7$ phases disappeared after SBF immersion again, however no apatite peaks were observed, as seen in Figure 6.18. Only, titanium, rutile and silver peaks were present, which suggested that silver nitrate addition into the electrolyte could have a negative effect on apatite formation.

Corrosion test, in a lactic acid and NaCl containing solution, was performed for 30 days to investigate the effect of silver, present in the coating. After the test, samples were taken out to measure the weight loss and examine the surfaces. Table 6.16 displays the weight loss percentage of the samples.

Table 6.16: Weight loss of the samples after corrosion test

Sample	Weight loss (%)
Untreated CP-Ti	0.064
MAO without $AgNO_3$	0.186
MAO with 1 g/L $AgNO_3$	0.475
MAO with 2 g/L $AgNO_3$	0.364
MAO with 3 g/L $AgNO_3$	0.311
MAO with 4 g/L $AgNO_3$	0.398

It was concluded that MAO treatment resulted a decrease in corrosion resistance of CP-Ti, which may be attributed to the modification of the continuous bioinert oxide layer to form a porous bioactive layer. Also, it was observed that silver nitrate

addition to the electrolyte decreased the corrosion resistance of the oxide layer formed by MAO process, compared to untreated CP-Ti, which exhibited the highest corrosion resistance. Table 6.17 and 6.18 exhibits the surface stereo photographs before and after corrosion test, 6x and 50x respectively.

Table 6.17: Surface stereo photographs before and after corrosion test (6x)

Sample	Before test	After test
Untreated CP-Ti	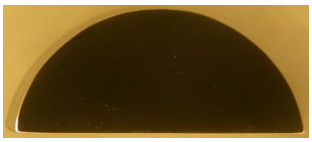	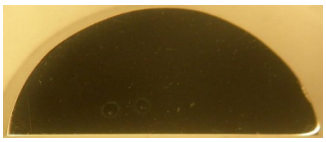
MAO ($AgNO_3$ free electrolyte)	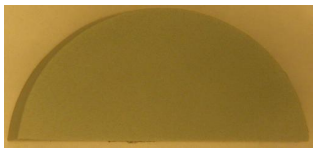	
MAO-1 g/L $AgNO_3$	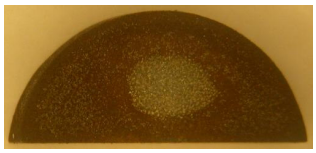	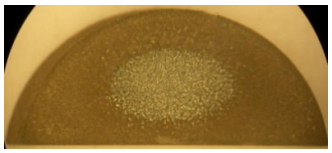
MAO-2 g/L $AgNO_3$		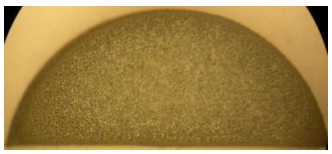
MAO-3 g/L $AgNO_3$		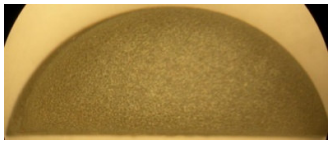
MAO-4 g/L $AgNO_3$	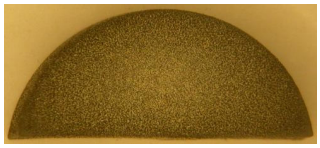	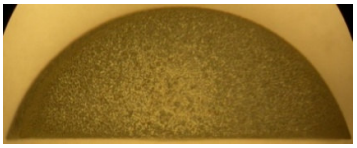

Table 6.18: Surface stereo photographs before and after corrosion test (50x)

Sample	Before test	After test
Untreated CP-Ti	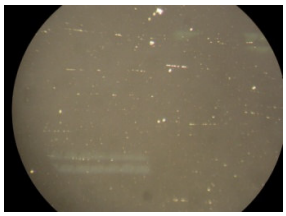	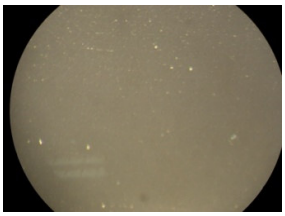
MAO ($AgNO_3$ free electrolyte)	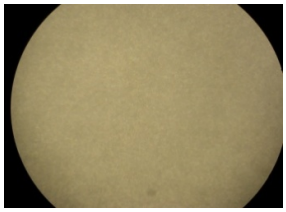	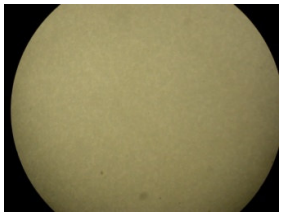
MAO-1 g/L $AgNO_3$	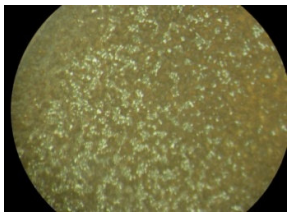	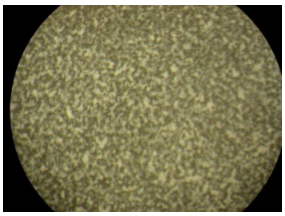
MAO-2 g/L $AgNO_3$	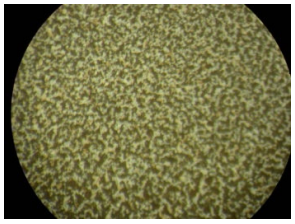	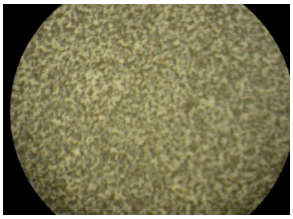
MAO-3 g/L $AgNO_3$	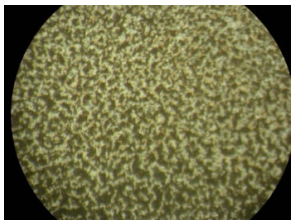	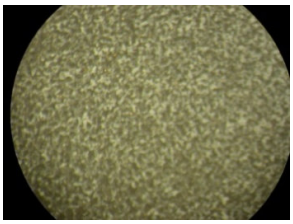
MAO-4 g/L $AgNO_3$	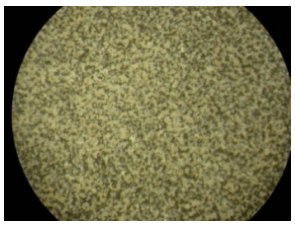	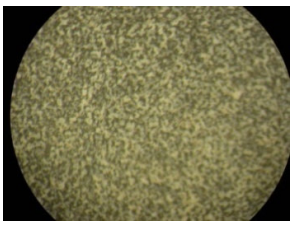

To evaluate the adhesion performance of the coatings, Rockwell C adhesion test was conducted. A 150 kg load with a diamond tip was applied on the surface of the samples and the imprints formed on the coatings were detected if any delaminations or any cracks occured. It should be noted that 150 kg is quite a large load if the material is thought to be used as a dental implant. Table 6.19 displays the surface photos taken after the test.

Table 6.19: Photos of the MAO treated samples after Rockwell C load

Concentration (g/L)	Top view	Profile view
0 ($AgNO_3$ free electrolyte)	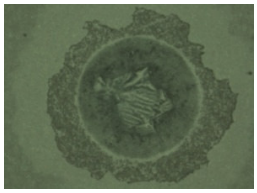	
1	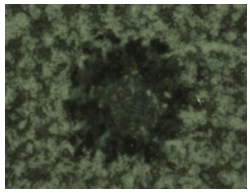	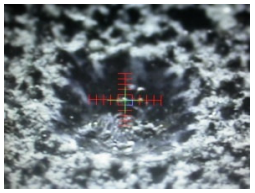
2	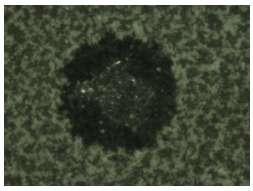	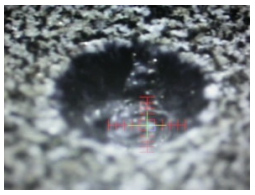
3	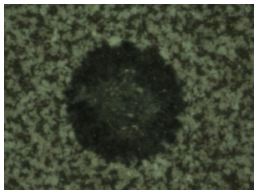	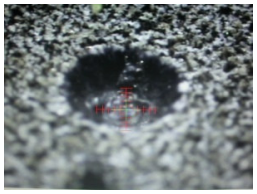
4	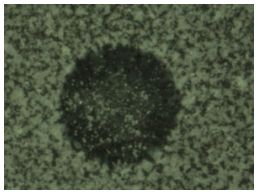	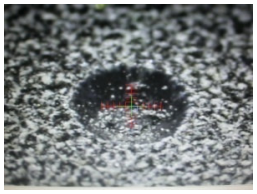

From Table 6.19, it was seen that MAO-treated titanium in silver nitrate free electrolyte, showed a delamination around the imprint. However there were not any cracks, which might cause the progression of the failure along the whole surface. Meanwhile, there were not any delaminations on the surface of the MAO-treated samples in silver nitrate containing electrolyte, irrespective of the concentration of silver nitrate. It is assumed that silver nitrate addition to the electrolyte improved the adhesion strength of the coating to the substrate.

Finally, the bacteria tests were performed with (Gr+) bacteria *S.aureus* and *S.epidermidis* and a (Gr-) *P.aeruginosa* in order to find the minimum concentration of silver nitrate, which gives the best anti-bacterial activity. The results are listed in Table 6.20 - 6.22.

Table 6.20: The decrease in the amount of viable *S.aureus* bacteria related to $AgNO_3$ concentration

	Time (min)	**0**	**60**	**120**
Concentration (g/L)		(Cfu)	(Cfu)	(Cfu)
1		8400000	8600	3856
2		8400000	3350	1567
3		8400000	2500	1100
4		8400000	9367	5800

Table 6.21: The decrease in the amount of viable *S.epidermidis* bacteria related to $AgNO_3$ concentration

	Time (min)	**0**	**60**	**120**
Concentration (g/L)		(Cfu)	(Cfu)	(Cfu)
1		8400000	11733	5033
2		8400000	5466	2700
3		8400000	2600	1400
4		8400000	16566	7967

Table 6.22: The decrease in the amount of viable *P.aeruginosa* bacteria related to $AgNO_3$ concentration

	Time (min)	**0**	**60**	**120**
Concentration (g/L)		(Cfu)	(Cfu)	(Cfu)
1		8400000	19667	10233
2		8400000	17667	7367
3		8400000	13067	5167
4		8400000	22900	12733

According to Table 6.20, 6.21 and 6.22, remarkable antibacterial activity was achieved against all three types of bacteria upon silver nitrate addition into the electrolyte. The best results were obtained from the electrolyte with the 3 g/L silver nitrate concentration. The bacteria test performed with *E. Coli* (Section 6.1), had shown that the concentration of 4 g/L at 500-83V had given a 100% antibacterial activity, however in the case of *S.aureus*, *S.epidermis* and *P.aeruginosa*, 4 g/L was the worst. However, according to Table 6.9, 1 g/L silver nitrate containing sample would have been expected to have the worst antibacterial effect because it showed the minimum atomic Ag content (1.97). Therefore, Ag concentration of the electrolyte is not the only parameter influencing the anti-bacterial activity of the oxide layer. But it is thought that, if the test duration had been prolonged, the anti-bacterial activities might have reached to 100% for all the samples. In the literature, there are bacteria tests conducted for longer than 24 hours. As the result of this section, 3 g/L $AgNO_3$ containing electrolyte was chosen as the ideal electrolyte concentration.

6.3 Ultraviolet Irradiation

In the previous sections, for MAO of CP-Ti, the ideal process voltage and $AgNO_3$ concentration of the electrolyte were determined as 500-83V and 3 g/L, respectively. However, the bioactivity results were not satisfactory. The apatite nucleation was insufficient even after immersion in SBF for 30 days.

In order to obtain a stronger bioactivity and to shorten the apatite induction time, the samples were irradiated by UV in distilled water. It has been reported that UV irradiation in water facilitates more basic Ti-OH generation than in air [5]. As investigated in the literature survey, Ti-OH groups are responsible for apatite induction. In this section, SEM observations and XRD analysis were performed before and after SBF to evaluate the results.

No effect of UV irradiation were observed on morphology and surface roughness of the micro-arc oxidized samples. However, in contact angle measurements, even the edges of the samples were wetted with a 8 µl drop of distilled water and SBF, which may indicate the enhancement of the hydrophilicity of the samples.

SEM micrographs of MAO-treated and UV irradiated samples are shown in Table 6.22 and 6.23. The photos were taken in 14th and 34th days of SBF immersion.

Table 6.23: SEM analysis of MAO treated and UV irradiated samples before and after SBF ($AgNO_3$ free electrolyte)

	1500X	**2000X-3500X**
Before SBF	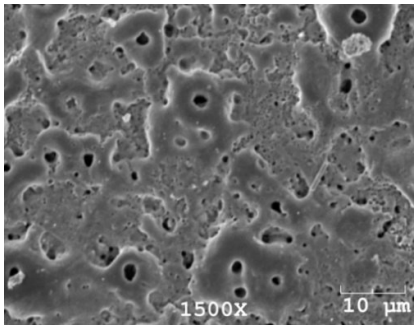	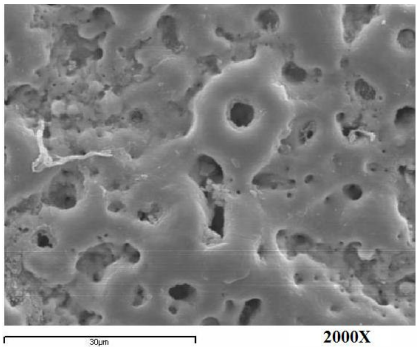
14 d	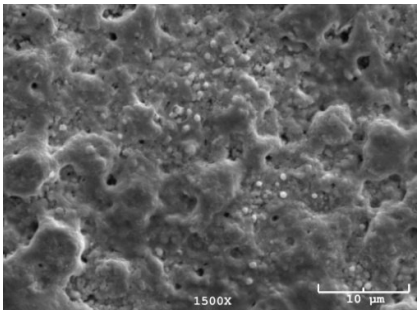	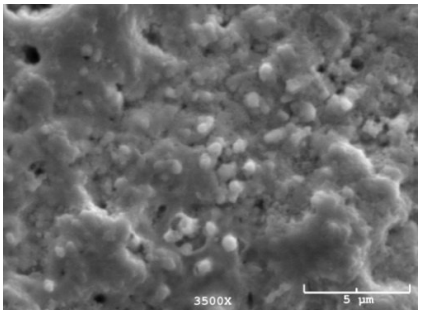
34 d	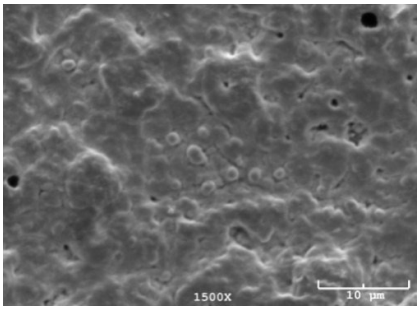	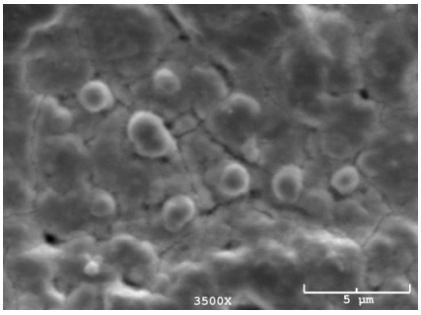

The porous structure of oxide layer before SBF immersion, is clearly seen in Table 6.22. After 14 days of SBF immersion, the pores started to disappear by formation of a layer, which is probably an apatite layer and there were small white particulates, which were thought to be apatite particulates. In literature, these are called secondary apatite nucleations. At 34th day, nearly all the surface was covered and the number of the pores decreased drastically. Also, the growth of the small white particulates were

observed. There were also small cracks on the surface of the apatite layers below the particulates, as seen at high magnifications.

Table 6.24: SEM analysis of MAO treated and UV irradiated samples before and after SBF (3 g/L $AgNO_3$ containing electrolyte)

	1500X	**3500X**
Before SBF	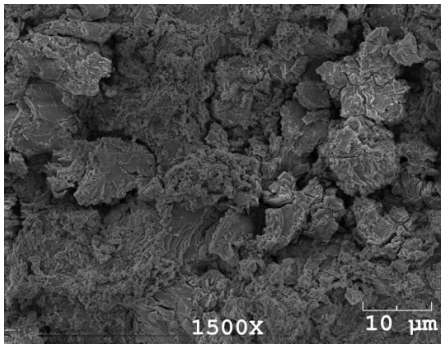	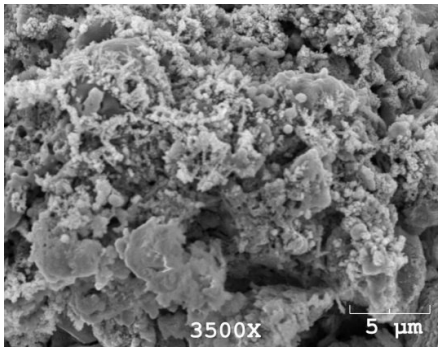
14 d	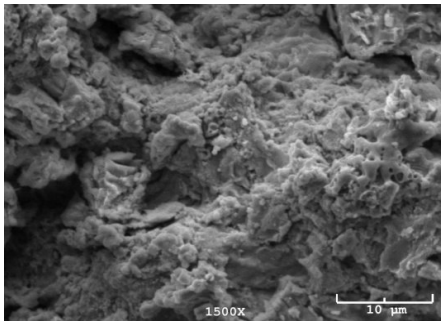	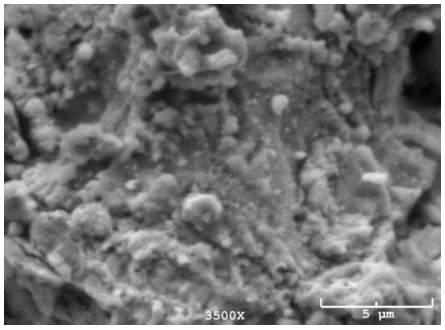
34 d	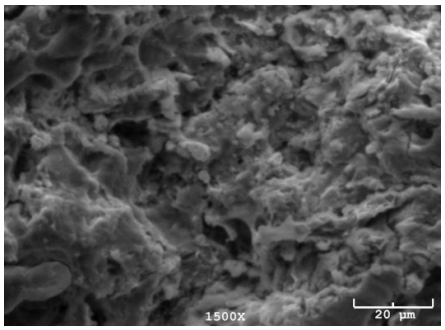	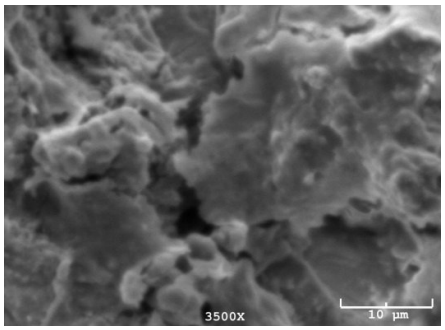

In Table 6.23, the highly roughened surface of the sample oxidized in 3 g/L $AgNO_3$ containing electrolyte can be observed. After 14 days in SBF solution, the roughness seemed to decrease and the sharp edges of the surface structure started to disappear as if there occured a surface layer. Again, small particulates started to be observed, however their amount was not as much as that of the surface formed in silver nitrate free solution. At 34^{th} day, there was a layered structure, clearly seen. But, no

secondary apatite nucleation were observed or they were very weak. EDS results of MAO-treated and UV irradiated samples, taken before and after SBF, are given in Table 6.24.

Table 6.25: EDS analysis of the UV-treated samples after different periods of SBF immersion

	MAO + UV (without $AgNO_3$)				MAO + UV (with 3 g/L $AgNO_3$)			
Element (at.%)	**Before SBF**	**14 d**	**34 d**	**54 d**	**Before SBF**	**14 d**	**34 d**	**54 d**
Ti	26	9.94	1.02	5.69	43.15	16.5	10.45	11.9
O	54	77.8	76.8	80	34	78.7	77.7	79.3
Ag	-	-	-	-	10.78	0.5	2.25	0.4
Ca	10.25	6.37	8.34	6.78	7.25	1.52	3.25	2.8
P	8.83	5.11	11.57	5.38	4.75	1.51	4.76	3.8
Ca/P	1.16	1.24	0.72	1.26	1.53	1	0.7	0.74

When the MAO-treated and UV-irradiated surface is considered, it was seen that Ti content decreased and O content increased drastically with SBF immersion. Also Ca and P content decreased after the SBF tests. Interestingly, at 34^{th} day, Ti concentration made a minimum and then increased, while Ca and P increased and from then on, they decreased again. Although Ca and P increased at 34^{th} day, the Ca/P ratio was 0.72. But eventually, it was 1.26 at 54^{th} day.

Meanwhile, samples oxidized in silver nitrate containing electrolyte exhibited a decreasing trend of Ca/P ratio from 1.53 to 0.74 after SBF test. Ti/O ratio decreased similar to other samples. Again Ca and P content decreased, however at 34^{th} day, it made a peak as the sample without silver. The same thing also happened for Ag content. It decreased from 10.78 to 0.4. The results were far from the Ca/P ratio (1.67) of hydroxyapatite. But it should be noted that the results were changing

locally. According to Won Hoon Song et al. [24], Ca/P ratio was decreasing over 450V and it was difficult to determine it at 500V because it varied from place to place due to the compound formation across the oxide film [2]. Table 6.25 shows the Ca/P ratio of the particles detected on the surface of the samples. There is an important reduction in the Ca/P ratios of the particles detected on the surface of the UV-treated samples. These particles are supposed to be $CaHPO_4$ (dicalcium phosphate anhidroz) or $CaHPO_4.2H_2O$ (dicalcium phosphate dihydrate) [59]. However, the Ca/P ratio of the particles detected on the oxide layer formed in $AgNO_3$ free electrolyte had not shown such a big reduction and it had reached to 1.62 (Table 6.15) after 30 days of SBF immersion.

Table 6.26: EDS results of the particles detected on the surfaces of the UV-treated samples before and after SBF

	Sample oxidized without $AgNO_3$		**Sample oxidized in 3 g/L $AgNO_3$ containing electrolyte**	
	Before SBF	After SBF	Before SBF	After SBF
Ca/P ratio	2.1	1	1.8	0.85

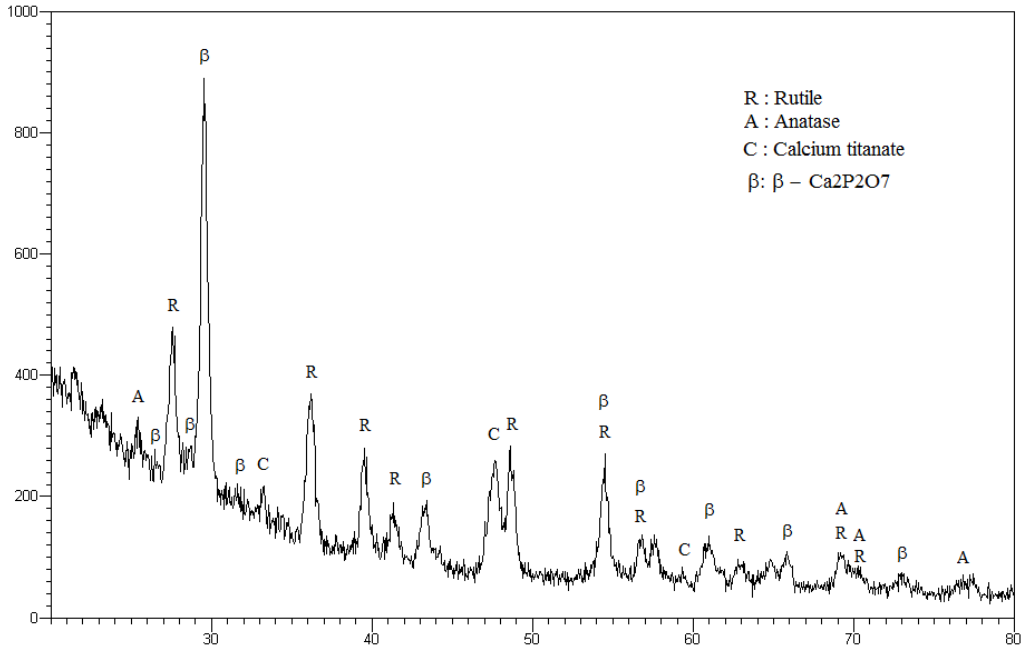

Figure 6.19: XRD pattern of MAO-treated sample in silver nitrate free electrolyte before SBF

Figure 6.19 indicates the phases for the sample oxidized in silver nitrate free electrolyte before SBF immersion. Figure 6.20, 6.21 and 6.22 show the XRD patterns of MAO and UV-treated samples without silver nitrate after 14, 34 and 54 days of SBF immersion.

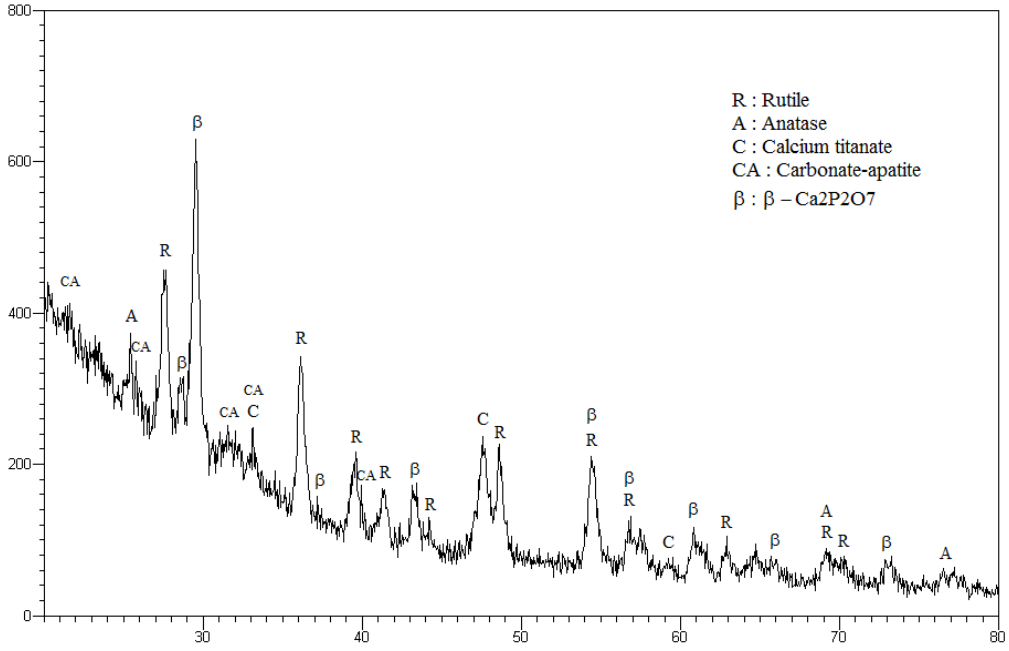

Figure 6.20: XRD pattern of MAO and UV-treated sample without silver nitrate after 14 days SBF

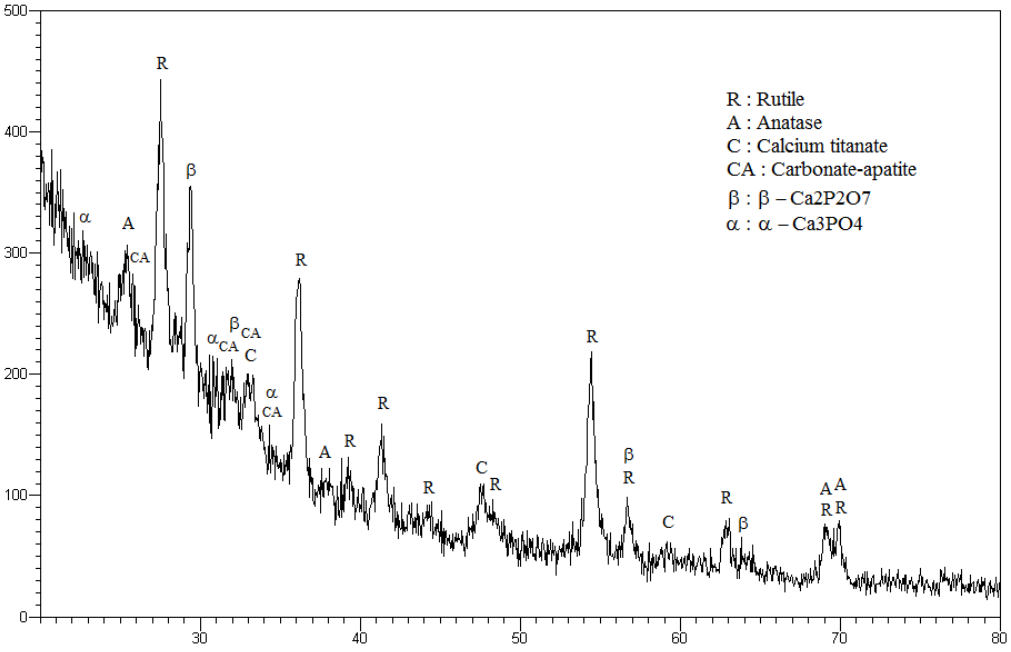

Figure 6.21: XRD pattern of MAO and UV-treated sample without silver nitrate after 34 days SBF

As seen from the XRD patterns shown above, carbonated-hydroxyapatite phases formed at the 14th day of SBF immersion with the effect of UV-irradiation. However, the intensities of the apatite peaks did not change with prolonging immersion times. It could be due to the low crystallinity of theses phases. Additionally, β-$Ca_2P_2O_7$ and α-$Ca_3(PO_4)_2$ phases formed. They are well-known bioresorbable phases, being obtained above 450V and having a positive effect on HA inducing [19-24]. It has been reported that biphasic calcium phosphate porous ceramics such as HA+$Ca_3(PO_4)_2$ have higher bioactivity and osteoinduction relative to HA [19-26]. Calcium titanate phases did not disappear, which suggested that carbonated-hydroxyapatite formed with the effect of UV instead of $CaTiO_3$ hydrolysis.

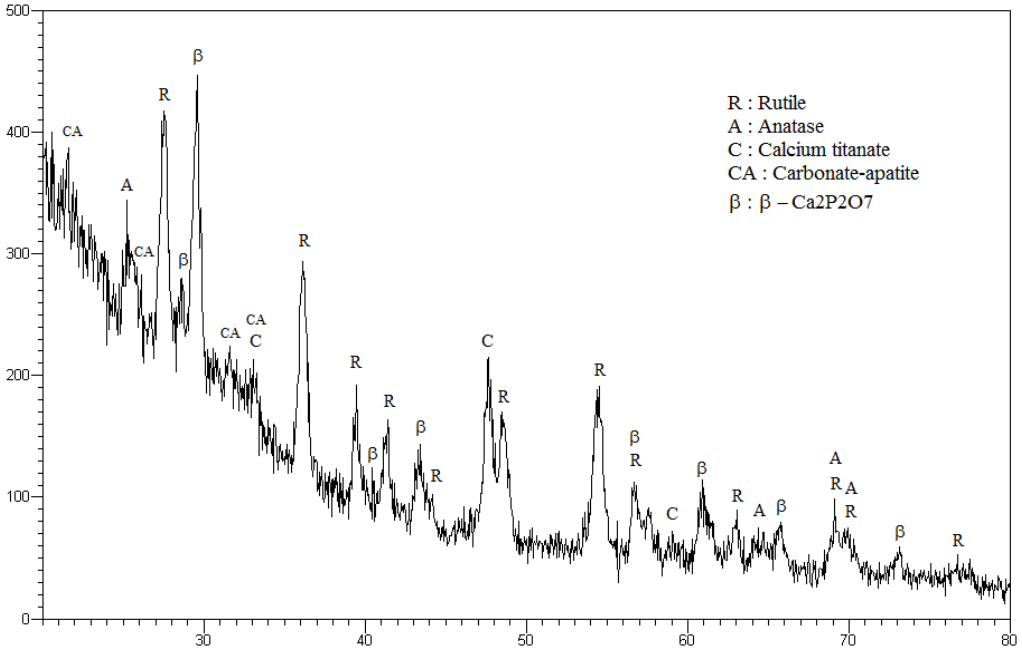

Figure 6.22: XRD pattern of MAO and UV-treated sample without silver nitrate after 54 days SBF

According to Jian Zhi Chen et al. [23], the structure of the oxide layer has an important effect on calcium phosphate precipitates. The highest nucleation ability is shown by anatase [23-30], whereas amorphous oxides do not have this ability at all. It is said that rutile has a closer packed structure inhibiting atom and ion diffusion as compared to anatase [23]. In our case, rutile is the abundant titanium oxide phase, and this may have negative effects on the formation of calcium phosphate phases, including HA. Furthermore, this may be the reason why the apatite peaks were so weak in the XRD patterns. However, rutile is said to improve the dissolution resistance of the forming oxide [23]. And our process voltage (500-83) is giving rise

to the formation of rutile type oxide, which is stable at higher MAO voltages, as mentioned by Won Hoon Song et al. [24]. Figure 6.23 displays the XRD pattern of MAO-treated samples in 3 g/L silver nitrate containing electrolyte before SBF immersion.

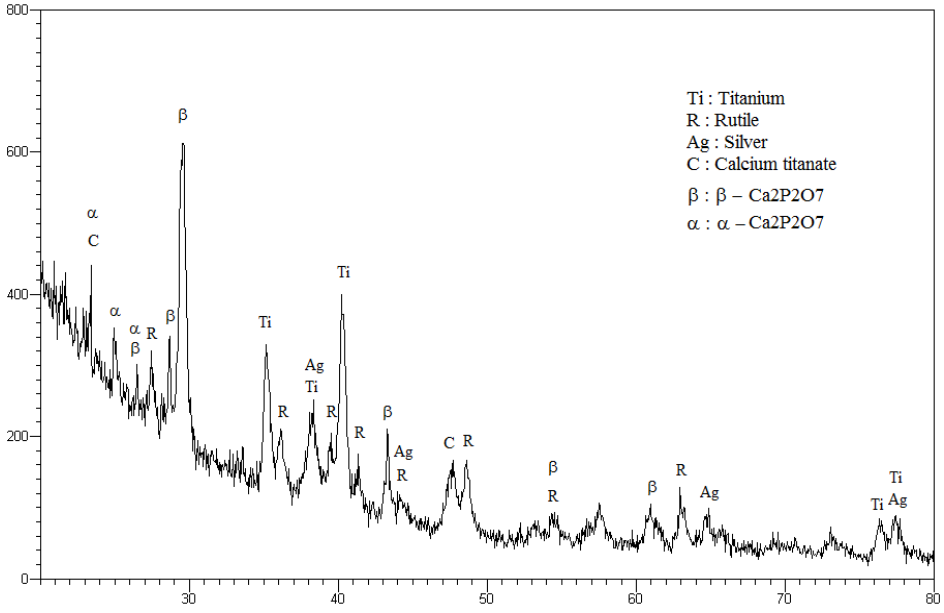

Figure 6.23: XRD pattern of MAO-treated sample in 3 g/L $AgNO_3$ containing electrolyte before SBF

Figure 6.24 - 6.26 show the XRD patterns of MAO and UV-treated samples in 3 g/L silver nitrate containing electrolyte after 14, 34 and 54 days of SBF immersion.

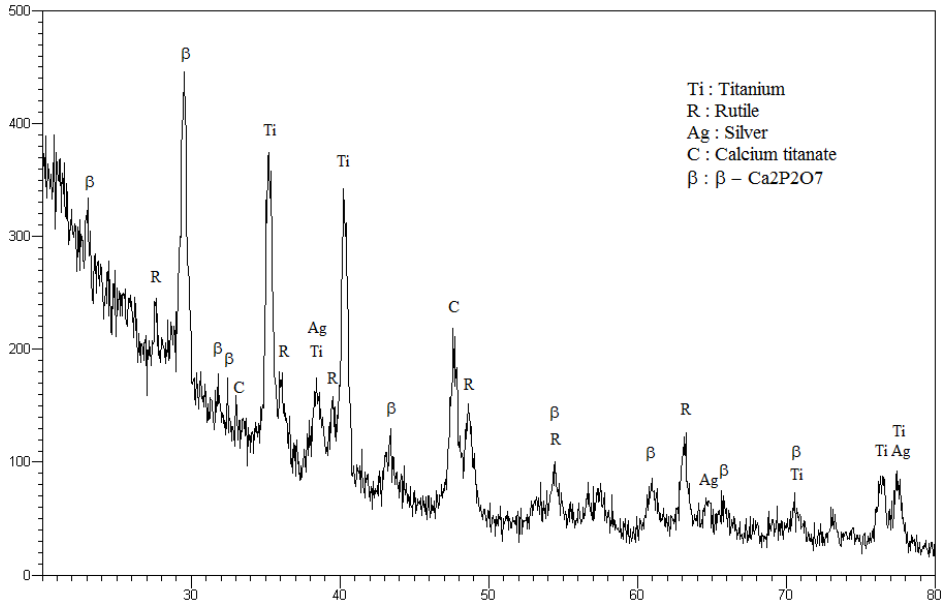

Figure 6.24: XRD pattern of MAO and UV-treated sample in 3 g/L $AgNO_3$ containing electrolyte after 14 days SBF

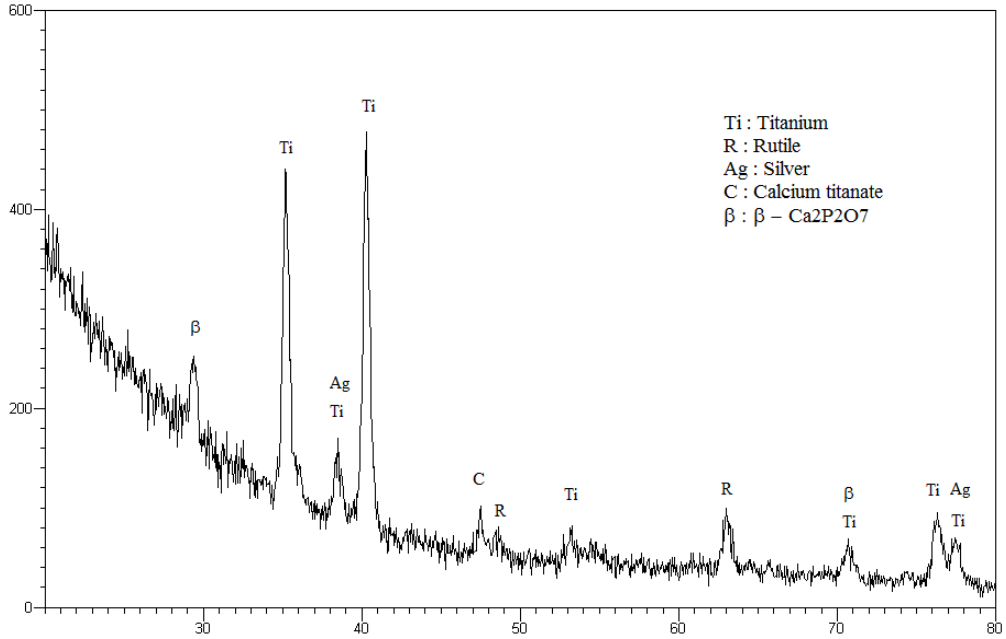

Figure 6.25: XRD pattern of MAO and UV-treated sample in 3 g/L $AgNO_3$ containing electrolyte after 34 days SBF

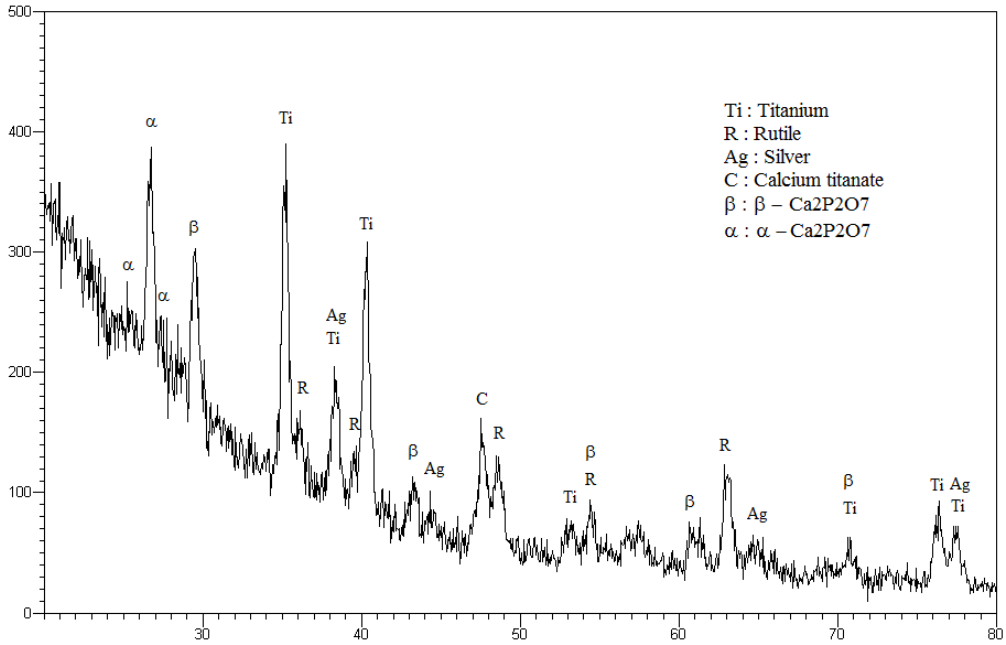

Figure 6.26: XRD pattern of MAO and UV-treated sample in 3 g/L $AgNO_3$ containing electrolyte after 54 days SBF

In the case of silver nitrate addition, UV irradiation did not promote the formation of hydroxyapatite but other bioresorbable Ca-P phases, such as α-$Ca_2P_2O_7$ and β-$Ca_2P_2O_7$, formed at the 14th day of SBF immersion and did not disappear as the SBF immersion time increased.

As a result, the basic Ti-OH groups, formed on the surface after UV exposure, are said to be responsible for the formation of calcium phosphate phases because the negativity of Ti-OH groups attracts positive Ca and P ions from the SBF solution [4-5]. These duplex coatings consisting of TiO_2 and calcium phosphate phases are said to be highly bioactive by Han et al. [57], Huang et al. [58] and Yong et al. [19]. And we were able to obtain these phases within 14 days with the co-operation of UV exposure. When talking about hydrothermal treatment, it was said that the number of HA crystals precipitating, gradually increased with increasing pH of the solution. So, increasing the pH of our electrolyte may be effective in obtaining stronger bio-activity. Especially, in $AgNO_3$ added electrolyte, pH increases from 8 to 10 as the silver nitrate concentration is reduced to 1 g/L. If we obtain enough anti-bacterial activity, we can decrease the silver nitrate concentration to obtain cyrstalline HA, which yields higher rates of cell proliferation.

Interestingly, Amparo et al. [6] stated that UV irradiation reduced not only the initial bacterial adhesion but also the retention ability of them on the surface of Ti6Al4V alloy. The same observation may be performed with Cp-Ti.

7. CONCLUSIONS

Following conclusions can be drawn according to the results of this study:

1. 4 g/L $AgNO_3$ addition into the electrolyte considerably improved the antibacterial activity of MAO-treated CP-Ti. The presence of silver nitrate in the electrolyte also altered the morphology of the oxide layer. The classical porous structure obtained in $AgNO_3$ free electrolyte disappeared and a rough oxide layer developed. The average surface roughness of MAO-treated CP-Ti increased from 1,36 μm to 7,6 μm upon $AgNO_3$ addition into the electrolyte. Further increase in average surface roughness was obtained by decreasing the process voltage. The addition of silver nitrate into the electrolyte enhanced the wettability of the samples, leading to a 0^o contact angle. Silver was found in the metallic state in the layer, irrespective of the voltage applied. Silver nitrate addition into the electrolyte caused remarkable antibacterial activity. A 100% antibacterial activity against *E.coli* was obtained for the sample oxidized at 500-83V after an incubation time of 1 hour. Decreasing the process voltage caused a reduction in antibacterial activity.
2. MAO at 500-83V in electrolytes containing different amounts of $AgNO_3$ improved the antibacterial activity. The oxide layers were rough again, for all $AgNO_3$ concentrations. However, micro and additional nano pores were observed on the samples oxidized in 1 g/L and 2 g/L $AgNO_3$ containing electrolytes. The maximum surface roughness (16 μm) was obtained on the sample oxidized in 1 g/L $AgNO_3$ containing electrolyte. The contact angles were 0^o after the tests performed with both distilled water and SBF, irrespective of the $AgNO_3$ concentration of the electrolyte. Silver nitrate addition to the electrolyte, also increased the thickness of the oxide layer. After the bacteria tests performed with *S.aureus*, *S.epidermidis* and

P.aeruginosa, the best results were obtained on the samples oxidized in 3 g/L $AgNO_3$ containing electrolyte at 500-83V.

3. After SBF tests, carbonated-hydroxyapatite phases were detected on the sample oxidized in $AgNO_3$ free electrolyte however no apatite phases were detected on the sample oxidized in $AgNO_3$ containing electrolyte. UV irradiation of the MAO-treated samples did not cause remarkable changes on morphology and roughness of the oxide layer. But the wettability of the $AgNO_3$ free samples increased, leading to a 0^o contact angle. However, immersion in SBF solution for 14 days caused precipitations of calcium phosphate layers and sphere-like particles on the surface, which were fully covered after 54 days. On the XRD patterns of the sample oxidized in silver nitrate free electrolyte, carbonated-hydroxyapatite and β-$Ca_2P_2O_7$ phases were detected. The sample, oxidized in 3 g/L $AgNO_3$ containing electrolyte, exhibited calcium phosphate precipitations such as α-$Ca_2P_2O_7$ and β-$Ca_2P_2O_7$ but there were not any apatite phases. Thus, UV irradiation shortened the time for the induction of the calcium-phosphate layers on the oxide layer.

REFERENCES

[1] **Yong, H., Yingjun, W., Chengyun, N., Kaihui, N. and Yong H.**, 2007. Hydroxyapatite coatings produced on commercially pure titanium by micro-arc oxidation, *Biomedical Materials*, **2**, 196-201.

[2] **Fu, L., Ying, S., Fuping, W., Tadao, S., Kaoru, I. and Liancheng, Z.**, 2005. Formation Characterization of Hydroxyapatite on Titanium by Microarc Oxidation and Hydrothermal Treatment, *Journal of Bioscience and Bioengineering*, **100**, 100-104.

[3] **Leyens, C. and Peters, M.**, 2003. Titanium and Titanium Alloys, Wiley-Wch, Weinheim.

[4] **Min, K., Jae, R. and Yun, M.**, 2007. One-step approach for nano-crystalline hydroxyapatite coating on titanium via micro-arc oxidation, *Electrochemistry Communications*, **9**, 1886-1891.

[5] **Yong, H., Donghui, C., Jifeng, S., Yumei, Z.and Kewei, Xu.**, 2008. UV-enhanced bioactivity and cell response of micro-arc oxidized titania coatings, *Acta Biomaterialia*, **4**, 1518-1529.

[6] **Amparo, M., Miguel, A., Laura, S., Jose, M., Nuria, V. and Luisa, G.**, 2008. In vitro biocompatibility and bacterial adhesion of physico-chemically modified Ti6Al4V surface by means of UV irradiation, *Acta Biomaterialia*, doi:10.1016/j.actbio.2008.07.028.

[7] **Jeyachandran, Y., Narayandass, S., Mangalaraj, D., Bao, C., Li, w., Liao, Y., Zhang, C., Xiao, L. and Chen, W.**, 2006. A study on bacterial attachment on titanium and hydroxyapatite based films, *Surface Coatings and Technology*, **201**, 3462-3474.

[8] **Anchun, M., Juan, L., Wei, X., Suqin, X., Yubao, L. and Shi, B.**, 2008. Preparation and antibacterial effect of silver–hydroxyapatite/titania nanocomposite thin film on titanium, *Applied Surface Science*, **255**, 435-438.

[9] **Long, H., Young, M., Hae, K., Young, K., Hyoun, K., Seong, H. and Jai, K.**, 2004. Improved biological performance of Ti implants due to surface modification by micro-arc oxidation, *Biomaterials*, **25,** 2867- 2875.

[10] **Wang, E., Nan, K., Chen, X., Ning, C., Wang, L. and Zhao, N.**, 2006. Characterization of bioactive ceramic coatings prepared on titanium implants by micro-arc oxidation, *Rare Metals*, **25**, 84-89.

[11] **Young, S.**, 2003. The significance of the surface properties of oxidized titanium to the bone response: special emphasis on potential biochemical bonding of oxidized titanium implant, *Biomaterials*, **24**, 3893-3907.

[12] **Xuanyong, L., Paul, K. and Chuanxian, D.**, 2004. Surface modification of titanium, titanium alloys, and related materials for biomedical applications, *Materials Science and Engineering*, **47**, 49-121.

[13] **Wenbin, X., Chao, W., Zhiwei, D. and Tonghe, Z**., 2002. Characterization of Oxide Coatings Deposited on Pure Titanium by Alternating-current Microarc Discharge in Electrolyte, *ISIJ International*, **42**, 651-655.

[14] **Yaming, W., Tingquan, L., Bailing, J. and Lixin, G**., 2004. Growth, microstructure and mechanical properties of microarc oxidation coatings on titanium alloy in phosphate-containing solution, *Applied Surface Science*, **233**, 258-267.

[15] **Ping, H,. Yong, Z., Kewei, X. and Yong, H**., 2004. Surface Modification of Titanium Implant by Microarc Oxidation and Hydrothermal Treatment, *Biomedical Materials*, **70**, 187-190.

[16] **Gunyuz, M.,** 2007. Coating of titanium and its alloys by micro-arc oxidation, *M.Sc. Thesis*, ITU, Institute of Science and Technology, Istanbul.

[17] **Yan, L., In, L., Fu, C. and Seong, C**., 2008. The biocompatibility of nanostructured calcium phosphate coated on micro-arc oxidized titanium, *Biomaterials*, **29**, 2025-2032.

[18] **Jifeng, S., Yong, H. andKai, C**., 2008. Microstructure and apatite-forming ability of the MAO-treated porous titanium, *Surface and Coatings Technology*, **202**, 4248-4256.

[19] **Yong, H., Seong, H. and Kewei, X.,** 2003. Structure and in vitro bioactivity of titania-based films by micro-arc oxidation, *Surface and Coatings Technology*, **168**, 249-258.

[20] **Zhang, Y., Bataillon, P., Huang, P., Zhao, Y., Han, Y., Traisnel, M., Xu, K. and Hildebrand, H**., 2003, Surface analyses of micro-arc oxidized and hydrothermally treated titanium and effect on osteoblast behavior, *Biomaterials*, **78**, 383-391.

[21] **Huang, Y., Wang, Y., Ning, C., Nan, K. and Han, Y.**, 2008. Preparation and properties of a cerium-containing hydroxyapatite coating on commercially pure titanium by micro-arc oxidation, *Rare Metals*, **27**, 257-260.

[22] **Won, S., Hyun, R. and Seong, H.**, 2005. Apatite Induction on Ca-Containing Titania Formed by Micro-Arc Oxidation, *J. Am. Ceramic Society*, **88**, 2642-2644.

[23] **Jian, C., Yu, S., Lei, W., Feng, Y. and Fu, Z.**, 2006. Preparation and properties of hydroxyapatite-containing titania coating by micro-arc oxidation, *Materials Letters*, **60**, 2538-2543.

[24] **Won, S., Youn. J.,Yong, H. and Seong, H.**, 2004. Biomimetic apatite coatings on micro-arc oxidized titania, *Biomaterials*, **25**, 3341-3349.

[25] **Jifeng, S., Yong, H. and Xin, H.**, 2007. Hydroxyapatite coatings prepared by micro-arc oxidation in Ca- and P-containing electrolyte, *Surface and Coatings Technology*, **201**, 5655-5658.

[26] **Yong, H., Jifeng, S. and Xin, H.**, 2008. Formation mechanism of HA-based coatings by micro-arc oxidation, *Electrochemistry Communications*, **10**, 510-513.

[27] **Young, S., Carina, J., Eungsun, B. and Tomas, A.**, 2005. The bone response of oxidized bioactive and non-bioactive titanium implants, *Biomaterials*, **26**, 6720-6730.

[28] **Filho, J.T., Lidízio, L.R., Sena, L., Damasceno, J. and Achete, C**., 2006. Titanium oxide films produced by micro-arc oxidation for high performance Titanium Implants, *18.Imeko World Congress*, Rio de Janeiro, Brazil, September, 17–22.

[29] **Li, P., Ohtsuki, C., Kokubo, T., Nakanishi, K., Soga, N., and De Groot, K.**, 1994. A role of hydrated silica, titania and alumina in forming biologically active bone-like apatite on implant, *J. Biomed. Mater. Res.*, **28**, 7–15.

[30] **Yang, B. C., Uchida, M., Kim, H.-M., Zhang, X. D., and Kokubo, T**., 2004. Preparation of bioactive titanium metal via anodic oxidation treatment, *Biomaterials,* **25**, 1003–1010.

[31] **Hamada, K., Kon, M., Hanawa, T., Yokoyama, K., Miyamoto, Y. and Asaoka, K.**, 2002. Hydrothermal Modification of Titanium Surface in Calcium Solutions, *Biomaterials*, **23**, 2265–2272.

[32] **Bloebaum, R., Mihalopolulus, N., Jensen, J. and Dorn L**., 1997. Post mortem analysis of bone growth into porous-coated acetabular components, *J. Bone Joint Surg.*, **79**, 1013–1022.

[33] **Moroni, A., Caja, V., Egger, E., Trinchese, L. and Chao, E.**, 1994. Histomorphometry of hydroxyapatite coated and uncoated porous titanium bone implants, *Biomaterials*, **15**, 926-930.

[34] **Huang, P., Wang, F., Xu, K. and Han, Y.**, 2004. Surface modification of titanium implant by microarc oxidation and hydrothermal synthesis, *J. Biomed. Mater. Res.*, **70**, 90-187.

[35] **Wang, R., Sakai, N., Fujishima, A., Watanabe, T. and Hashimoto, K.**, 1999. Studies of surface wettability conversion on TiO_2 single-crystal surfaces, *J. Phys. Chem*. **103**, 94-188.

[36] **Baikun, L. and Bruce, E.**, 2005. The impact of ultraviolet light on bacterial adhesion to glass and metal oxide-coated surface, *Colloids and Surfaces*, **41**, 153-161.

[37] **Xuanyong, L., Xiaobing, Z., Baoe, L., Cong, C., Yuqi, D., Chuanxian, D. and Paul, C.,** 2008. UV-irradiation-induced bioactivity on TiO_2 coatings with nanostructural surface, *Acta Biomaterialia*, **4**, 544-552.

[38] **Yong, H., Yuanyuan, Y. and Chunguo, L.**, 2008. Ultraviolet-enhanced bioactivity of ZrO2 films prepared by micro-arc oxidation, *Thin Solid Films,* doi:10.1016/j.tsf.2008.09.064.

[39] **Yoshinari, M., Oda, Y., Kato, T. and Okuda, K.**, 2001. Influence of surface modifications to titanium on antibacterial activity in vitro, *Biomaterials*, **22**, 2043-2048.

[40] **Thiel, J., Pakstis, L., Buzby, S., Raffi, M., Ni, C., Pochan, D, and Ismat, S.**, 2006. Antibacterial Properties of Silver-Doped Titania, *Small*, **5**, 799-803.

[41] **Mahendra, R., Alka, Y. and Aniket, G.**, 2008. Silver nanoparticles as a new generation of antimicrobials, *Biotechnology Advances*, doi:10.1016j.biotechadv.2008.09.002.

[42] **Manish, M., Hemant, K. and Kamlakar, T.**, 2008. Diabetic delayed wound healing and the role of silver nanoparticles, *Digest Journal of Nanomaterials and Biostructures*, **3**, 49-54.

[43] **Brook, L., Evans, P., Foster, H., Pemble, M., Steele, A., Sheel, D. and Yates, H.,** 2007. Highly bioactive silver and silver/titania composite films grown by chemical vapour deposition, *Journal of Photochemistry and Photobiology*, **187**, 53-63.

[44] **Tang, H., Liu, T., Liu, X., Gu, H. and Zhao, J.,** 2007. A study on biocompatibility and bactericidal properties of pyrolytic carbon by silver ion implantation, *Nuclear Instruments and Methods in Physics*, **255**, 304-308.

[45] **Chi, G., Yao, S., Fan, J., Zhang, W. and Wang, H.,** 2002. Antibacterial activity of anodized aluminum with deposited silver, *Surface and Coatings Technology*, **157**, 162-165.

[46] **Chun, H., Jian, G., Jiuhui, Q. and Xuexiang, H.**, 2007. Efficient destruction of bacteria with Ti(IV) and antibacterial ions in co-substituted hydroxyapatite films, *Applied Catalysis*, **73**, 345-353.

[47] **Stigter, M., Bezemer, J., Groot, K. and Layrolle, P.**, 2004. Incorporation of different antibiotics into carbonated hydroxyapatite coatings on titanium implants, release and antibiotic efficacy, *Journal of Controlled Release*, **99**, 127-137.

[48] **Zhang, F., Wolf, G., Xianghui, W., and Xianghuai, L.**, 2001. Surface properties of silver doped titanium oxide films, *Surface and Coatings Technology*, **148**, 65-70.

[49] **Bishara, S., Costagliola, M., Shady, N. and Saad, A.**, 2006. Effect of silver on burn wound infection control and healing: Review of the literature, *Burns*, **33**, 139-148.

[50] **Singh, M., Singh, S., Prasad,S.and Gambhir, I.**, 2008. Nanotechnology in medicine and antibacterial effect of silver nanoparticles, *Digest Journal of Nanomaterials and Biostructures*, **3**, 115-122.

[51] **Berger, T., Spadaro, J., Chapin, S. and Becker, R.**, 1976. Electrically Generated Silver Ions: Quantitative Effects on Bacterial and Mammalian Cells, *Antimicrobial Agents and Chemotherapy*, **9**, 357-358.

[52] **Chai, L., Shun, W., Peng, B. and Zhu, L.**, 2008. Effect of thermal treating temperature on characteristics of silver-doped titania, *Transactions of Nonferrous Metals Society of China*, **18**, 980-985.

[53] **Chen, X. and Schluesener, H.**, 2008. Nanosilver: A nanoproduct in medical application, *Toxicology Letters*, **176,** 1-12.

[54] **Balaban, N.**, 2007. Investigation of the biocompatibilities of titanium and its alloys, *M.Sc. Thesis*, ITU, Institute of Science and Technology, Istanbul.

[55] **Ou, K-L.**, 2008. Preparation of bioactive amorphous-like titanium oxide layer on titanium by plasma oxidation treatment, *Applied Surface Science*, doi:1016/j.apsusc.2008.06.189.

[56] **Guehennec, L.**, 2008. Osteoblastic cell behaviour on different titanium implant surfaces, *Acta Biomaterialia*, **4**, 535-543.

[57] **Han, Y., Hong, S. and Xu, K.**, 2003. Structure and in vitro bioactivity of titania based coatings by micro-arc oxidation, *Surface Coatings Technology*, **168**, 249–258.

[58] **Huang, P., Xu, K. and Han, Y.**, 2005. Preparation and apatite layer formation by plasma electrolytic oxidation on titanium for biomedical application, *Materials Letters*, **59**, 185–189.

[59] **Ozler, F.B.**, 2007. Surface modification of titanium and its alloys by sol-gel dip coating method, *M.Sc. Thesis*, ITU, Institute of Science and Technology, Istanbul.

CURRICULUM VITA

Candidate's Full Name : Cemil Işıksaçan

Place and date of birth : İstanbul / 08.10.1983

Permanent Address **:** Altıntepe Mah. Poyraz Sok. Şahin Apt. No:1 D:5 Maltepe/İstanbul

Bachelor's Degree **:** Yıldız Technical University (2006)
Metallurgical and Materials Engineer